

# Phase Diagrams with FACTSage

## Speaking different Languages for Thermochemical Properties

*Michael Auinger*



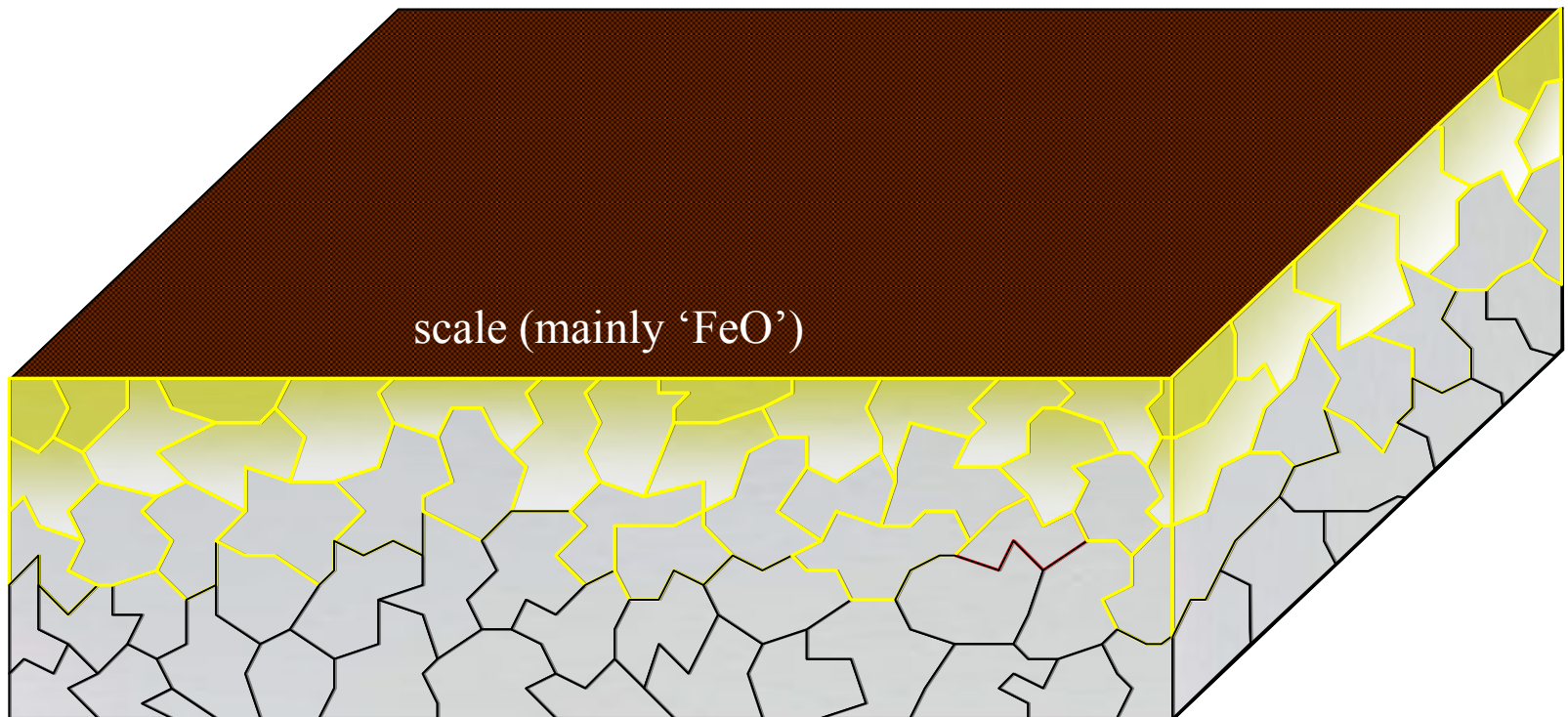
**Max-Planck-Institut  
für Eisenforschung GmbH**

GTT-Technologies Annual Workshop and User's Meeting  
Herzogenrath-Kohlscheid (Aachen, Germany)

5<sup>th</sup> July, 2013

- Motivation
- Thermochemical Properties in Oxides
  - Ellingham-Richardson Diagrams
  - Stability Diagrams
- Thermochemistry of Oxides and Nitrides
  - Nitrides in the System Iron - Chromium - Carbon
  - Nitrogen and Oxygen in Iron - Silicon
- Summary

# Oxidation Processes in Steels



# Grain Boundary Oxidation

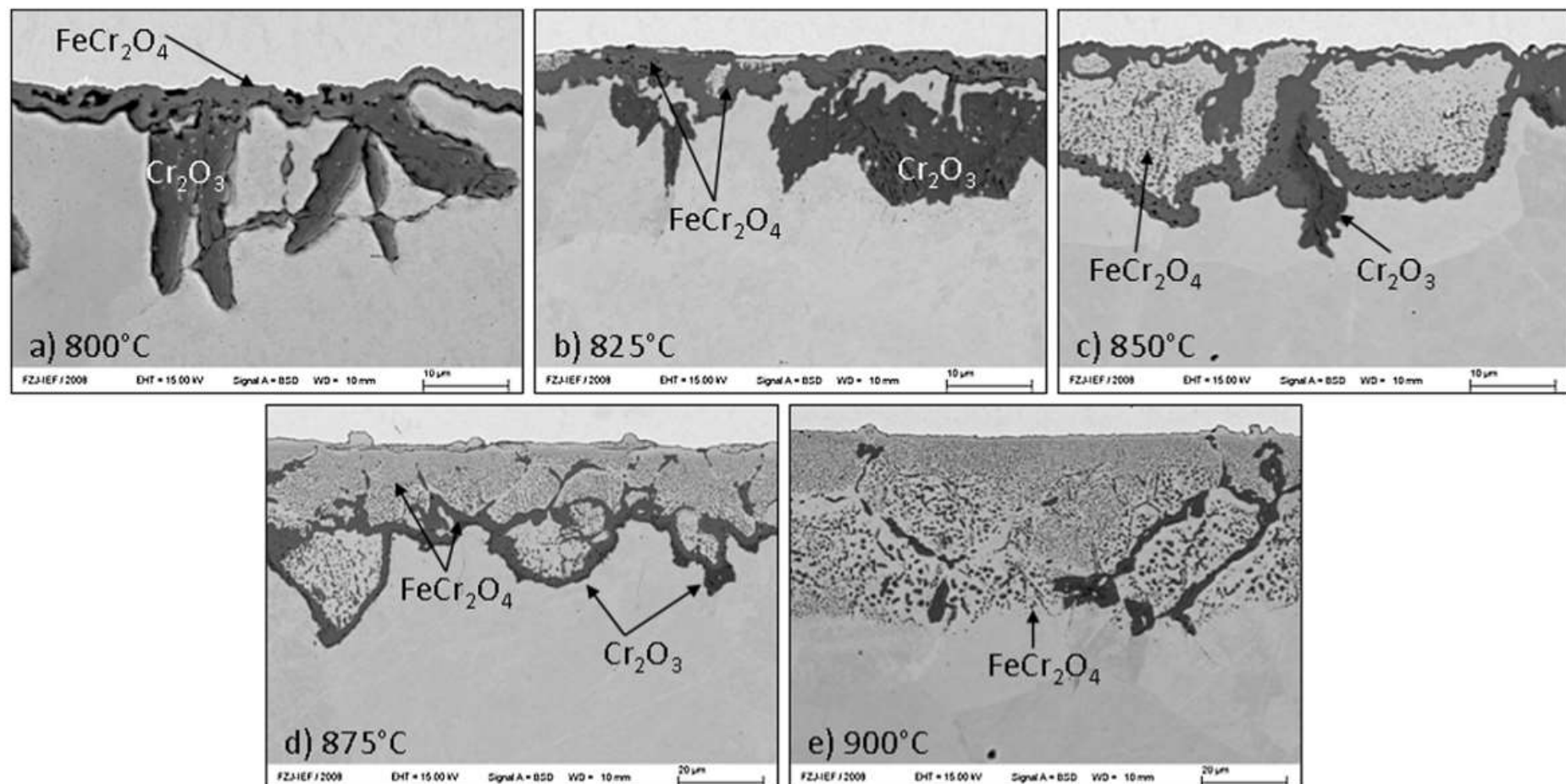
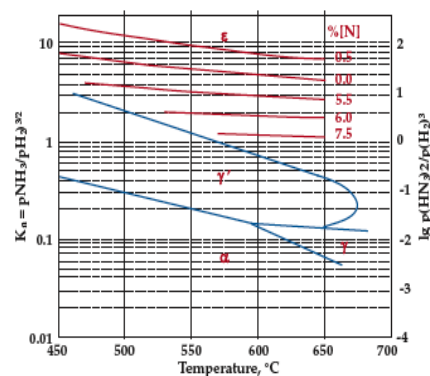
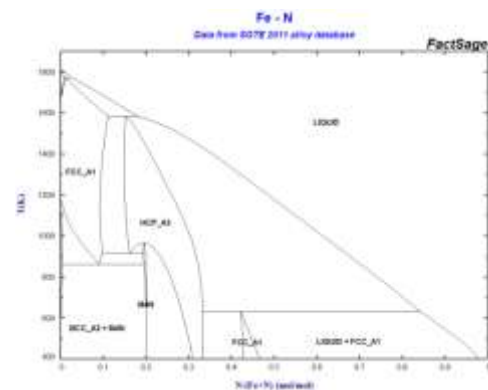
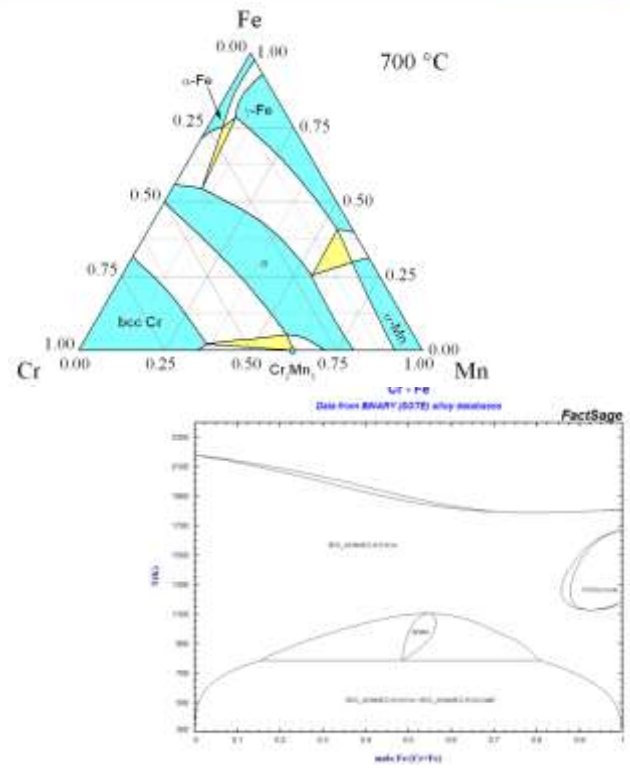
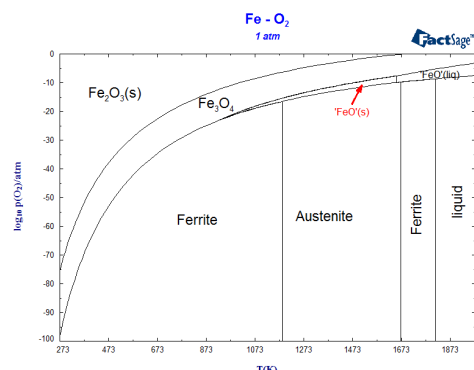
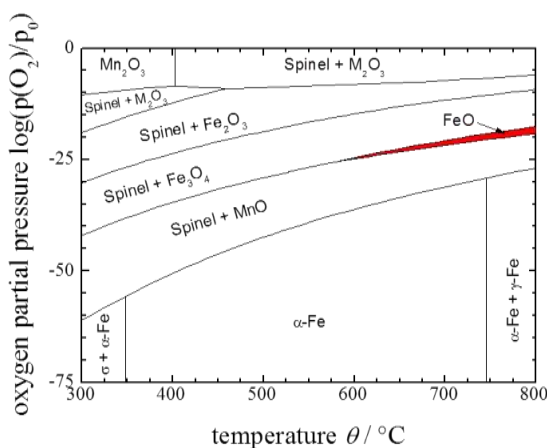
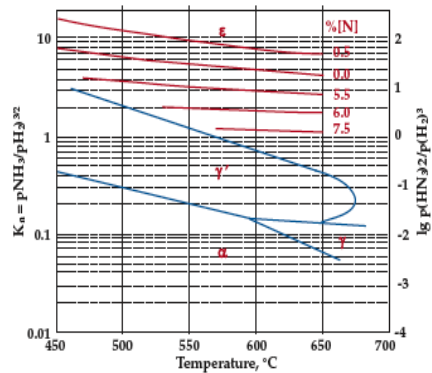
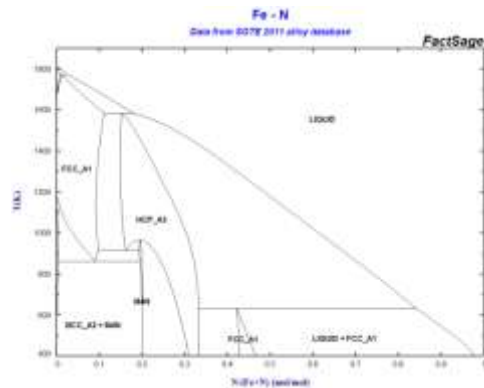
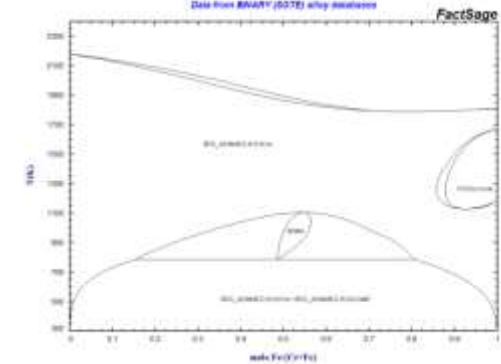
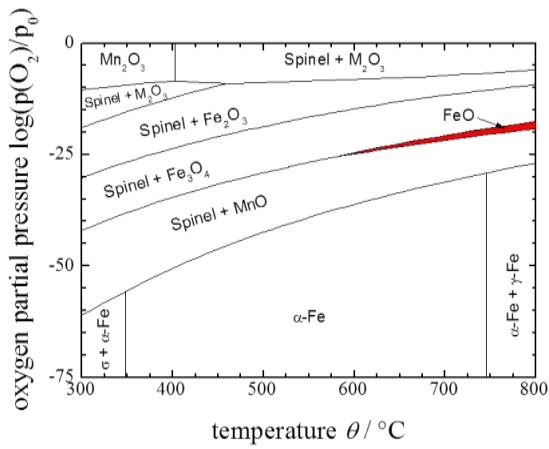
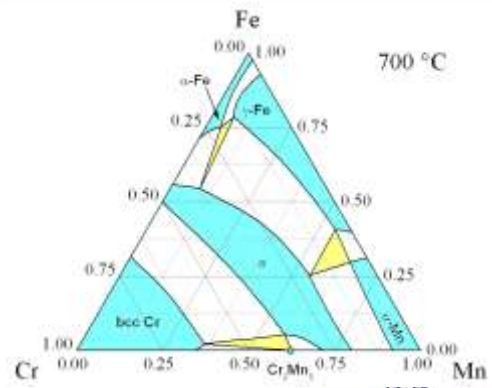
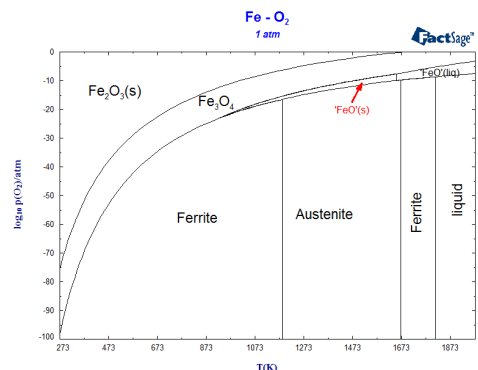
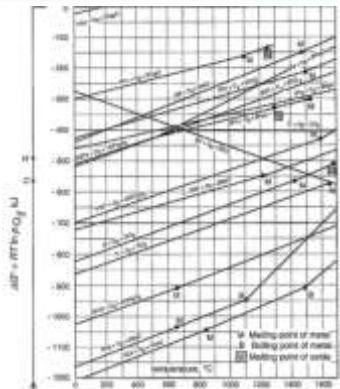


**Figure 18.** Cross-section SEM micrographs of Fe-10Cr after isothermal oxidation for 72 h at temperatures between 800 and 900 °C in Ar-4%H<sub>2</sub>-2%H<sub>2</sub>O

# The Problem



# The Problem



# Lost in Translation?

„ଆମি ତାପଗତିବିଦ୍ୟା  
ପଚଳ“

„Мне нравится  
термодинамики“

„أنا أحب الديناميكا  
الحرارية“



„我喜歡熱力學“

„Μου αρέσει  
θερμοδυναμική“

„나는 열역학을  
좋아“

„ଆমি তাপগতিবিদ্যা  
পছন্দ“

„أنا أحب الديناميكا  
الحرارية“

„Мне нравится  
термодинамики“



„我喜歡熱力學“

„Μου αρέσει  
θερμοδυναμική“

„나는 열역학을  
좋아“

# An Effective Solution

„ଆমি তাপগতিবিদ্যা  
পছন্দ“

„أنا أحب الديناميكا  
الحرارية“

„Μου αρέσει  
θερμοδυναμική“

„Мне нравится  
термодинамики“

„I like thermo-  
dynamics“



„我喜歡熱力學“

„나는 열역학을  
좋아“

# Part I

## Thermochemical Properties of Oxides

# Ellingham Diagram

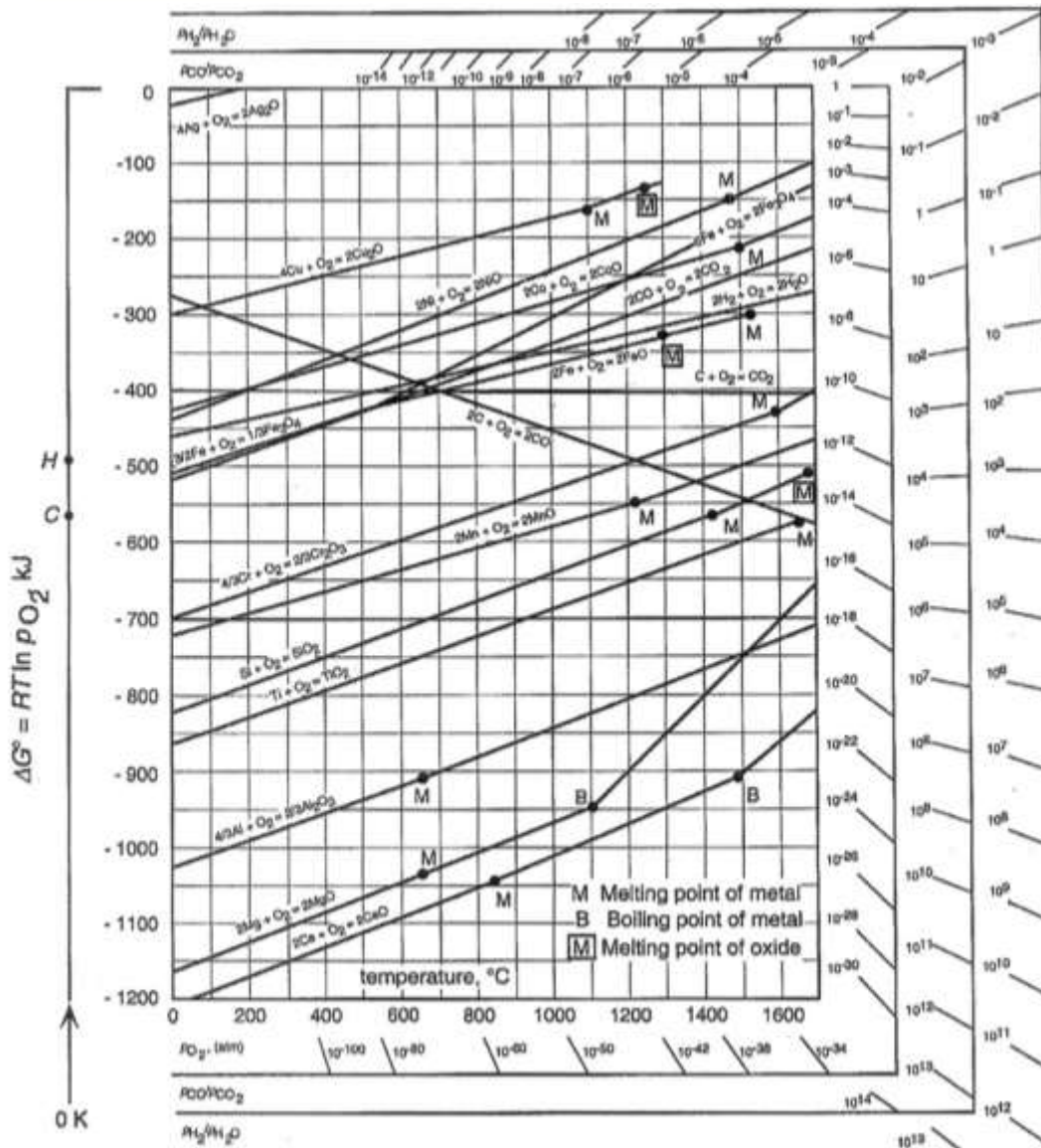
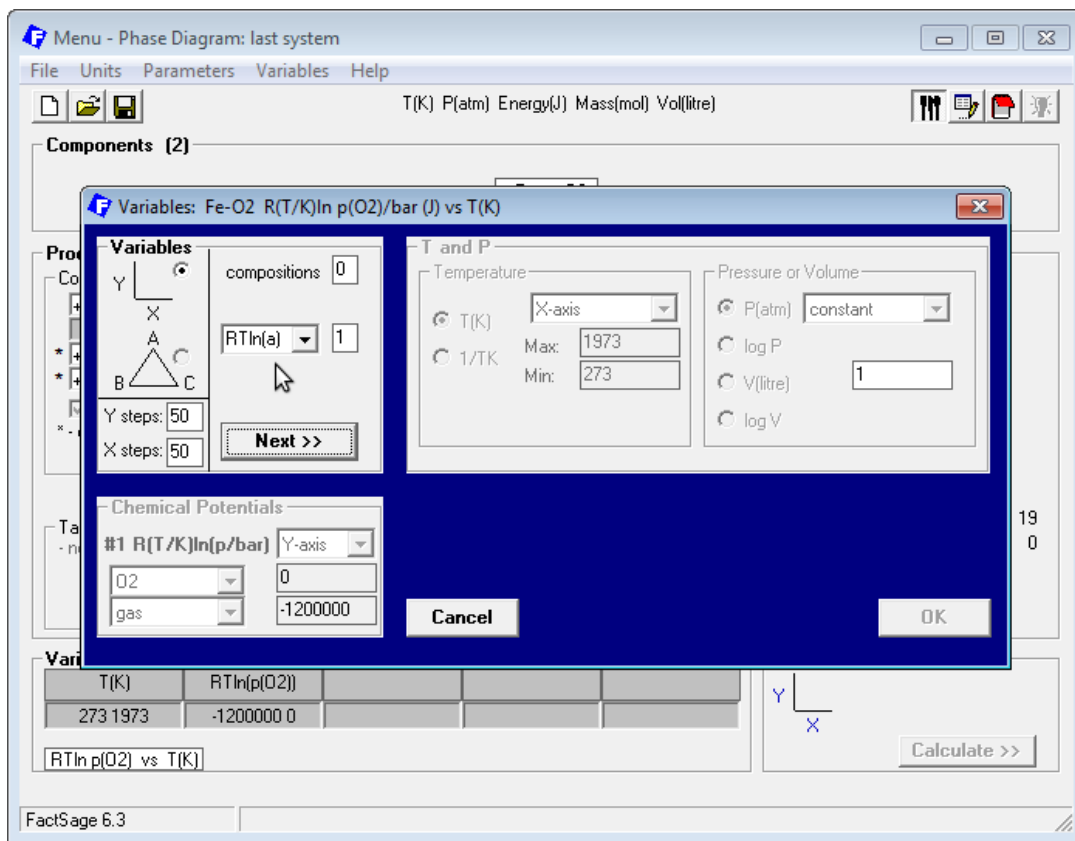
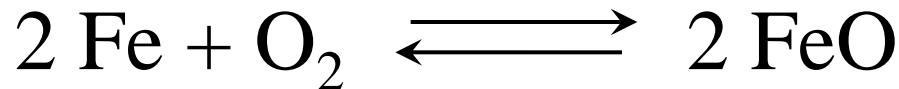


Figure 12.13 The Ellingham diagram for selected oxides.



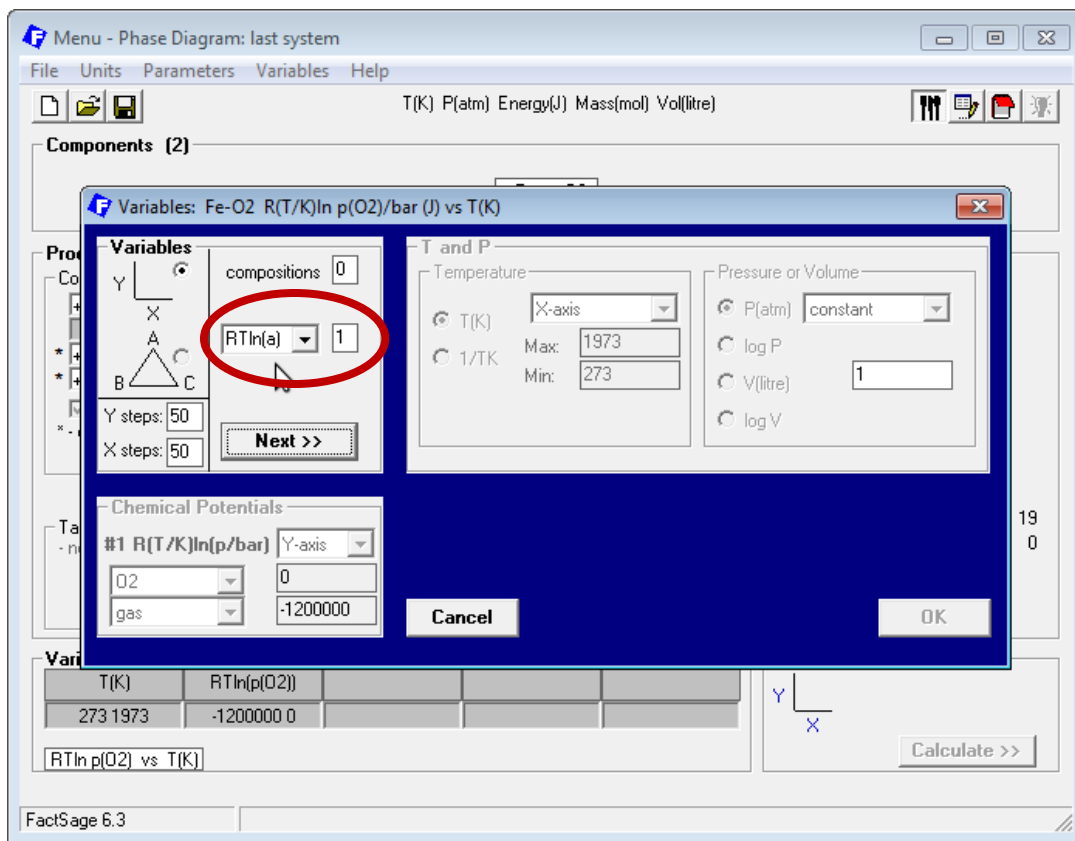
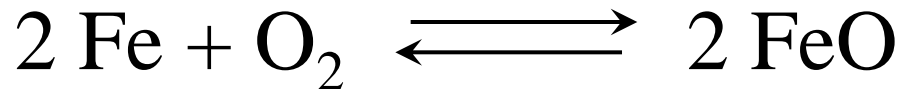
# Ellingham Diagram with FACTSage



$$-2 G_{(T)}^{o, \text{FeO}} + 2 G_{(T)}^{o, \text{Fe}} + G_{(T)}^{o, \text{O}_2} = -R \ln\left(\frac{p_{\text{O}_2}}{p_o}\right) T$$

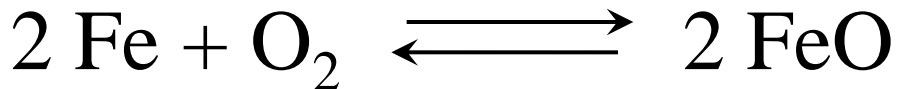


# Ellingham Diagram with FACTSage

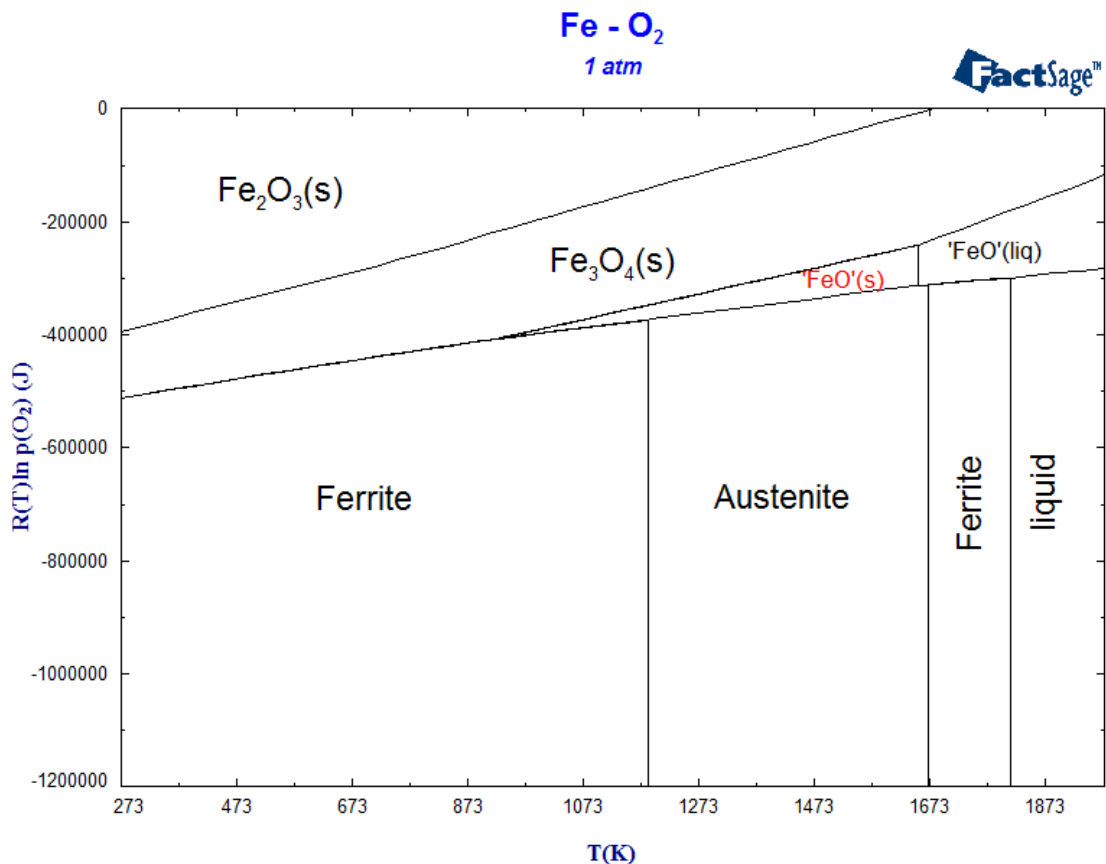
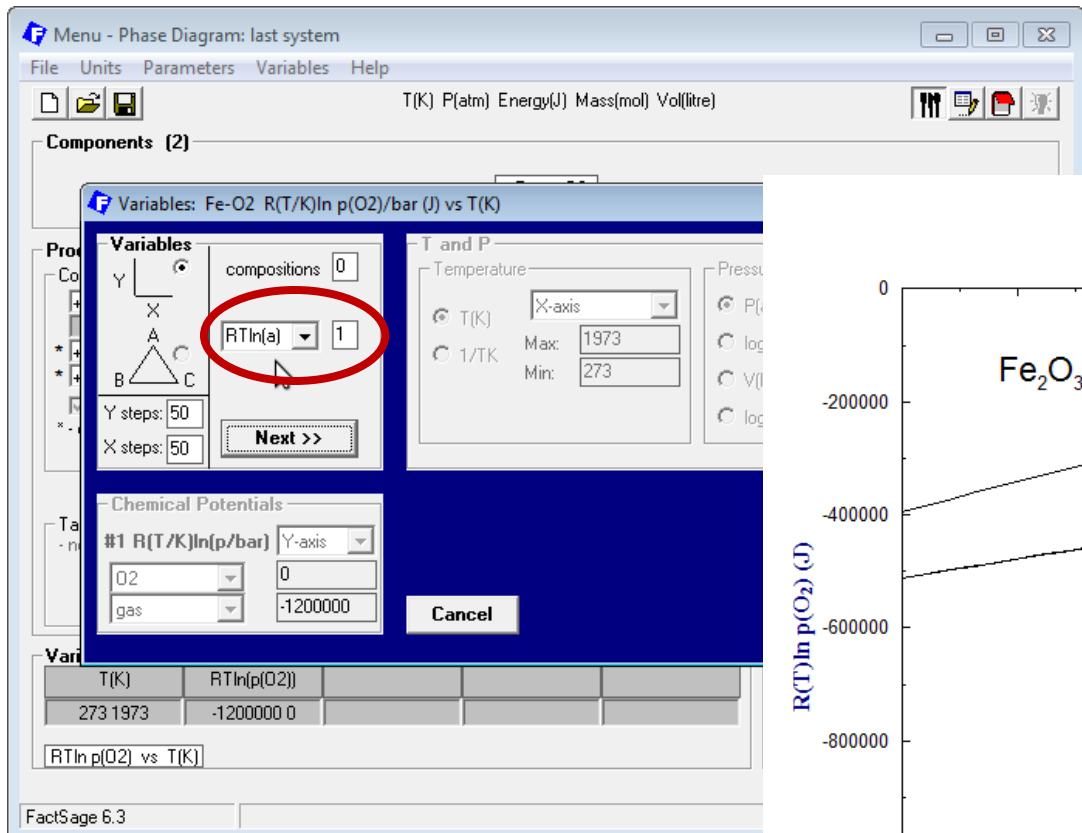


$$-2 G_{(T)}^{o, \text{FeO}} + 2 G_{(T)}^{o, \text{Fe}} + G_{(T)}^{o, \text{O}_2} = -R \ln\left(\frac{p_{\text{O}_2}}{p_o}\right) T$$

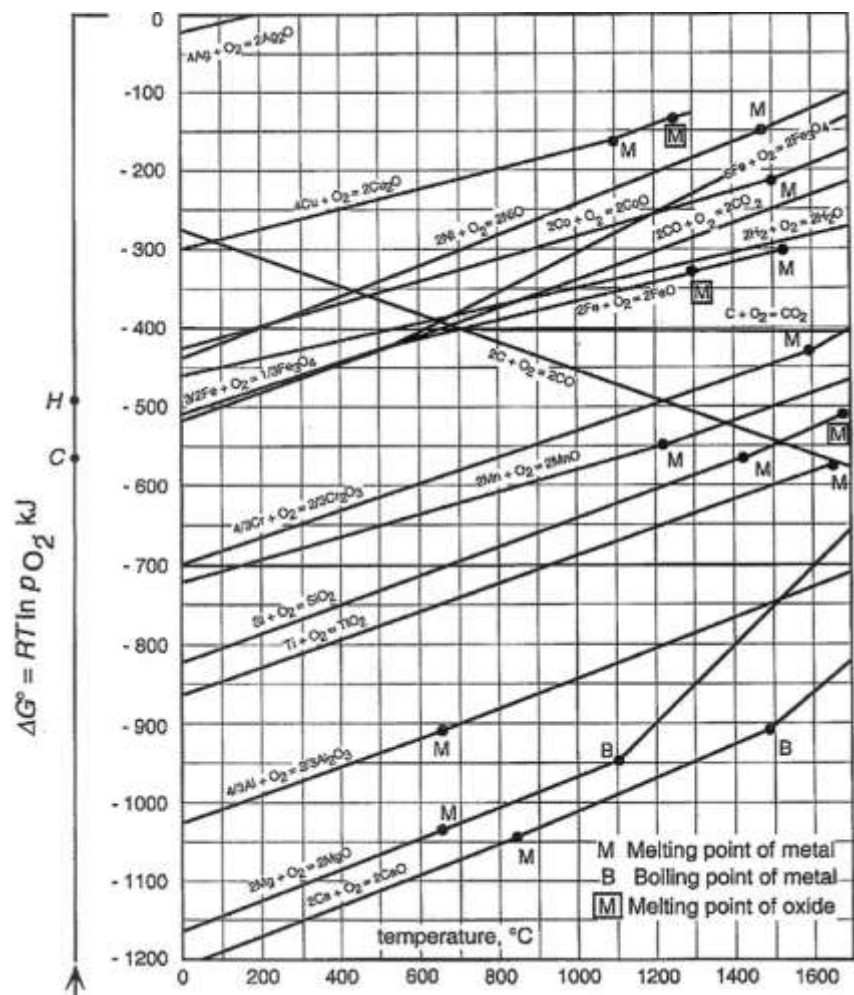
# Ellingham Diagram with FACTSage



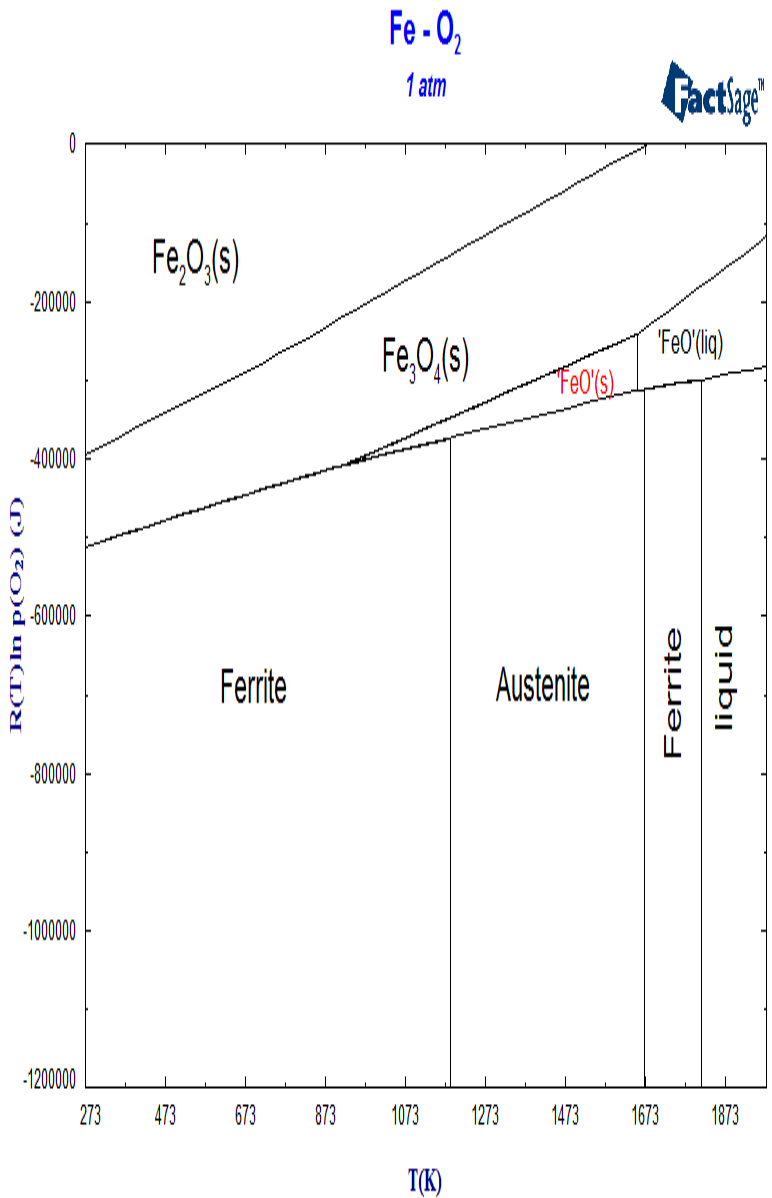
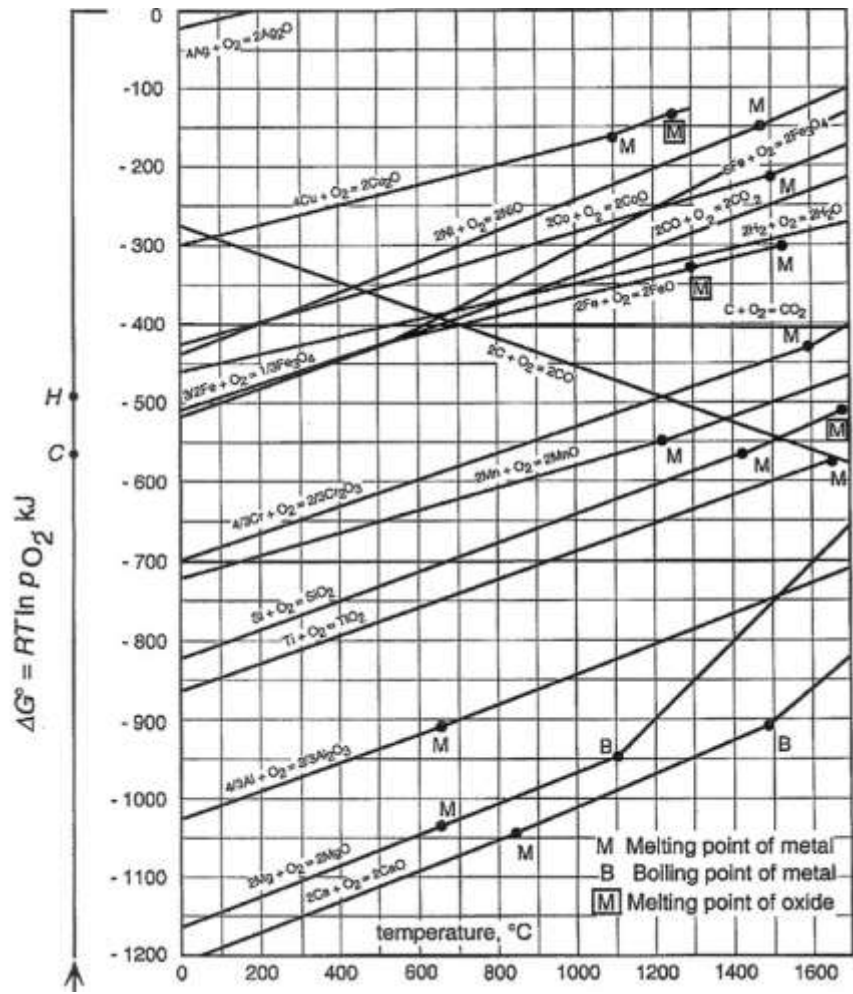
$$-2 G_{(T)}^{o, \text{FeO}} + 2 G_{(T)}^{o, \text{Fe}} + G_{(T)}^{o, \text{O}_2} = -R \ln\left(\frac{p_{\text{O}_2}}{p_o}\right) T$$



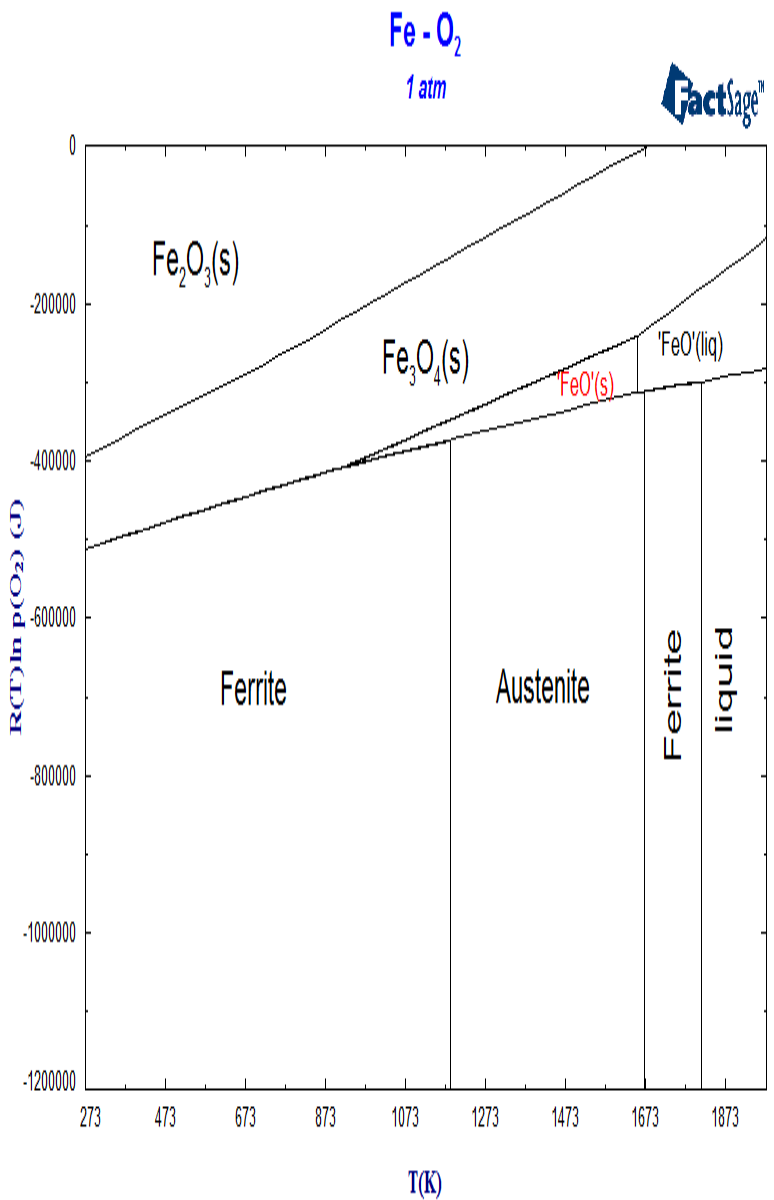
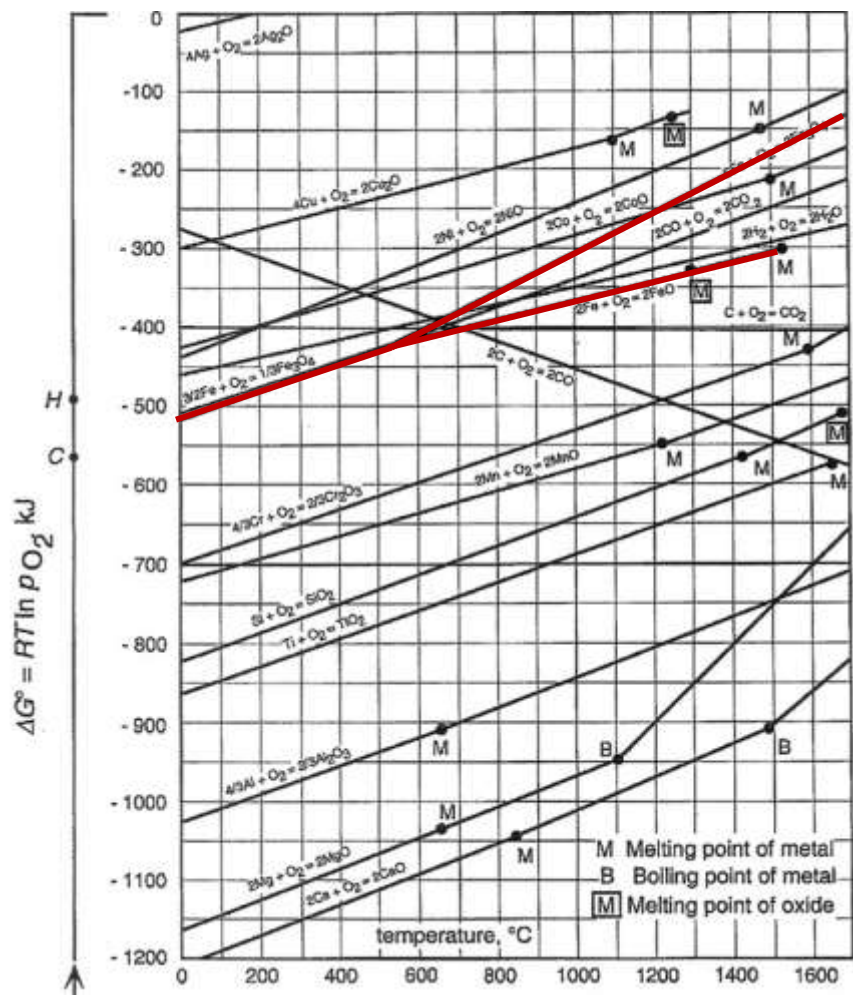
# Ellingham Diagrams for Oxide Formation



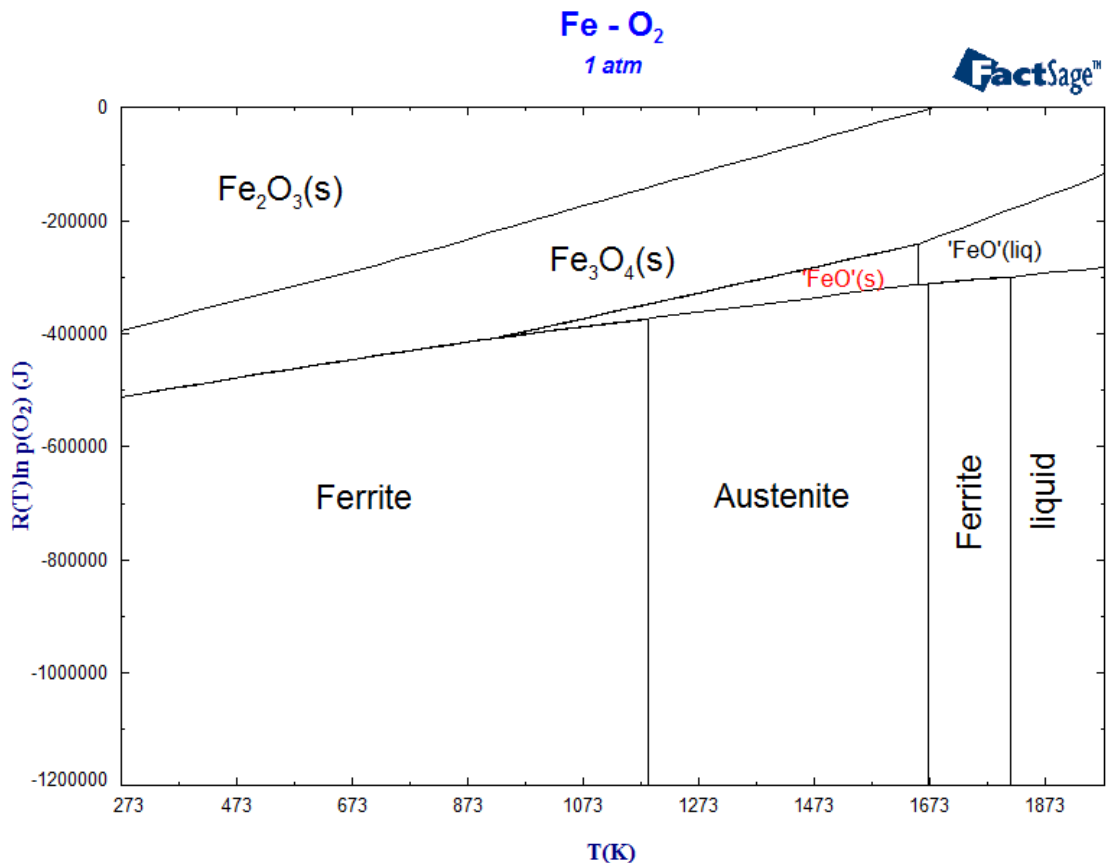
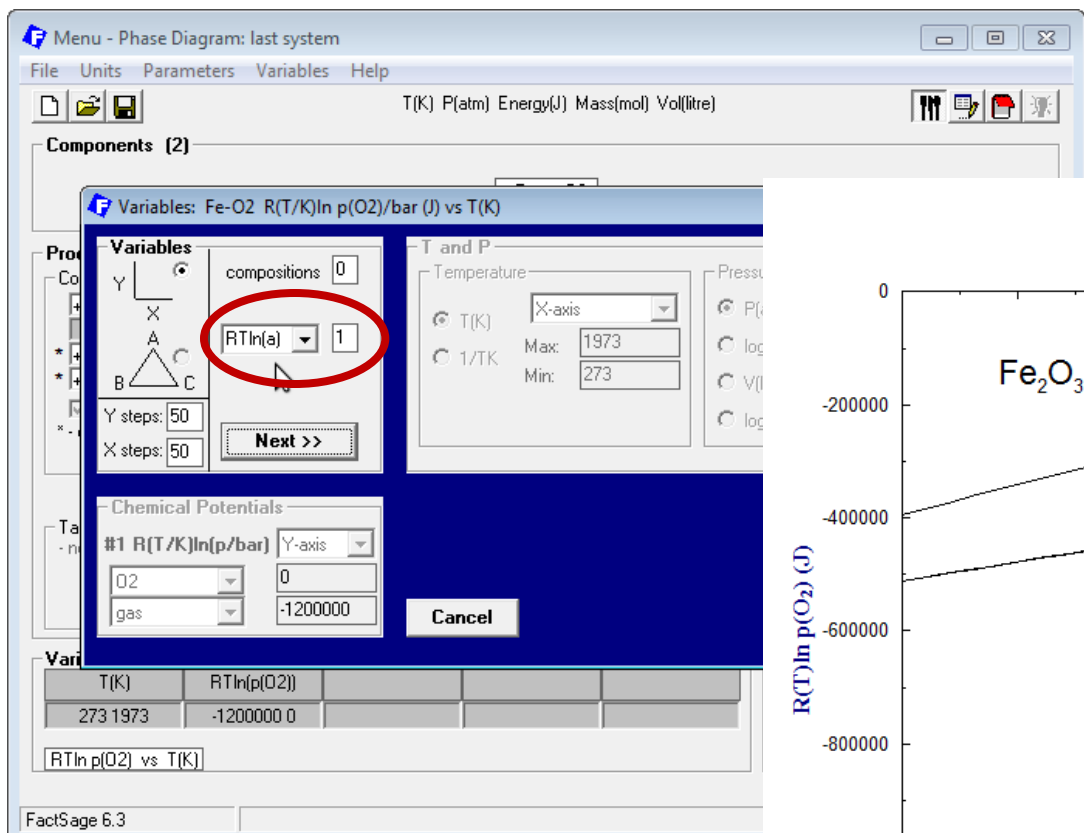
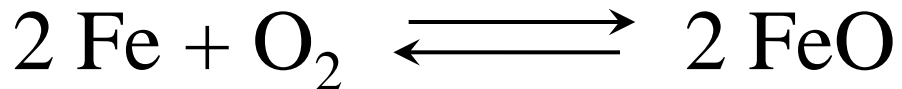
# Ellingham Diagrams for Oxide Formation



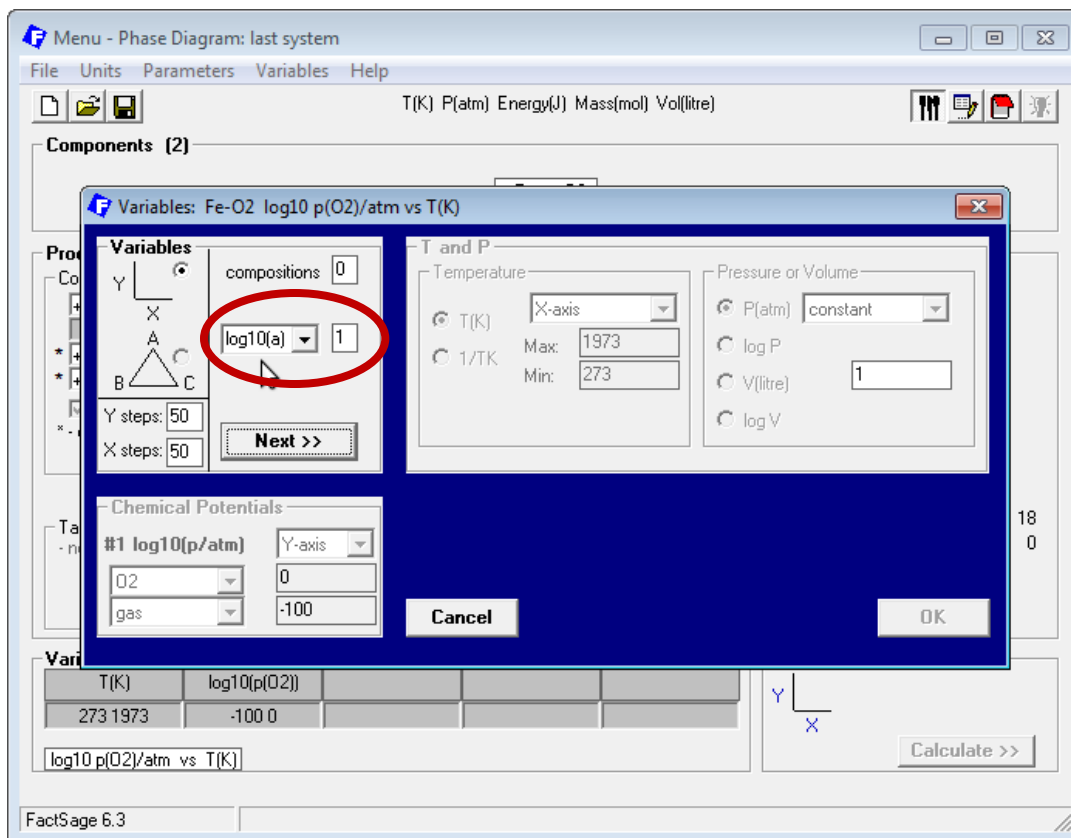
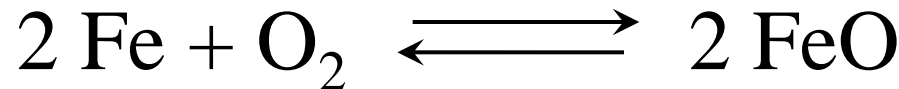
# Ellingham Diagrams for Oxide Formation



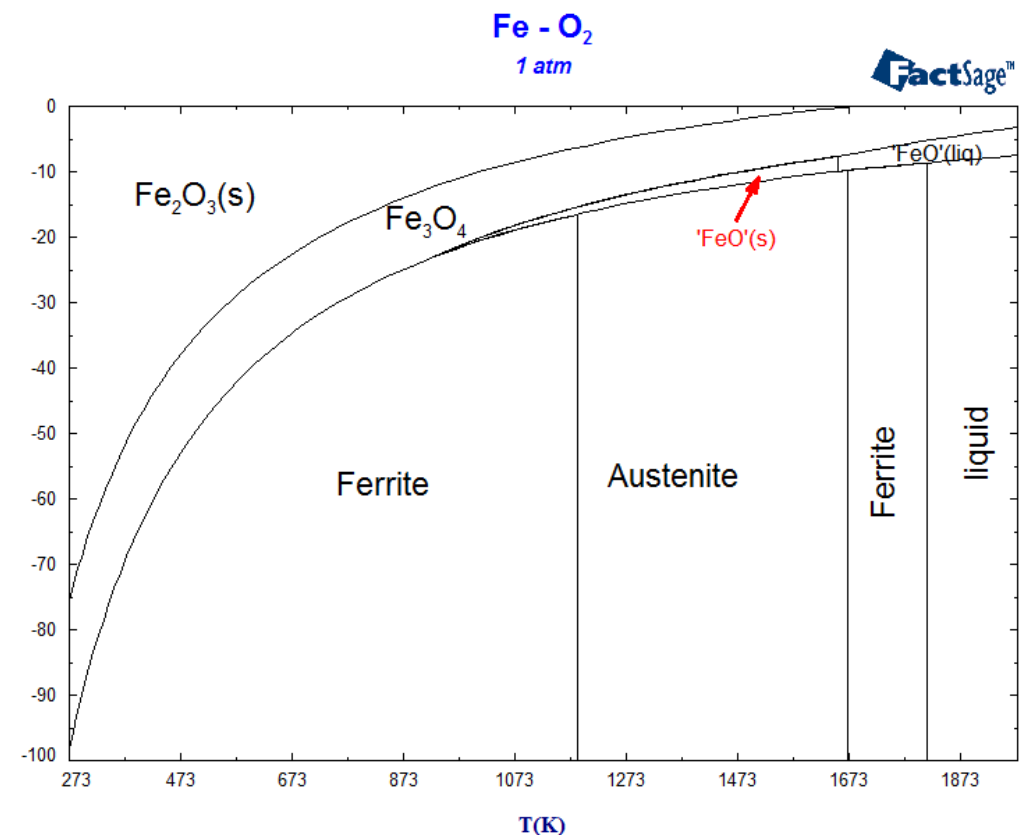
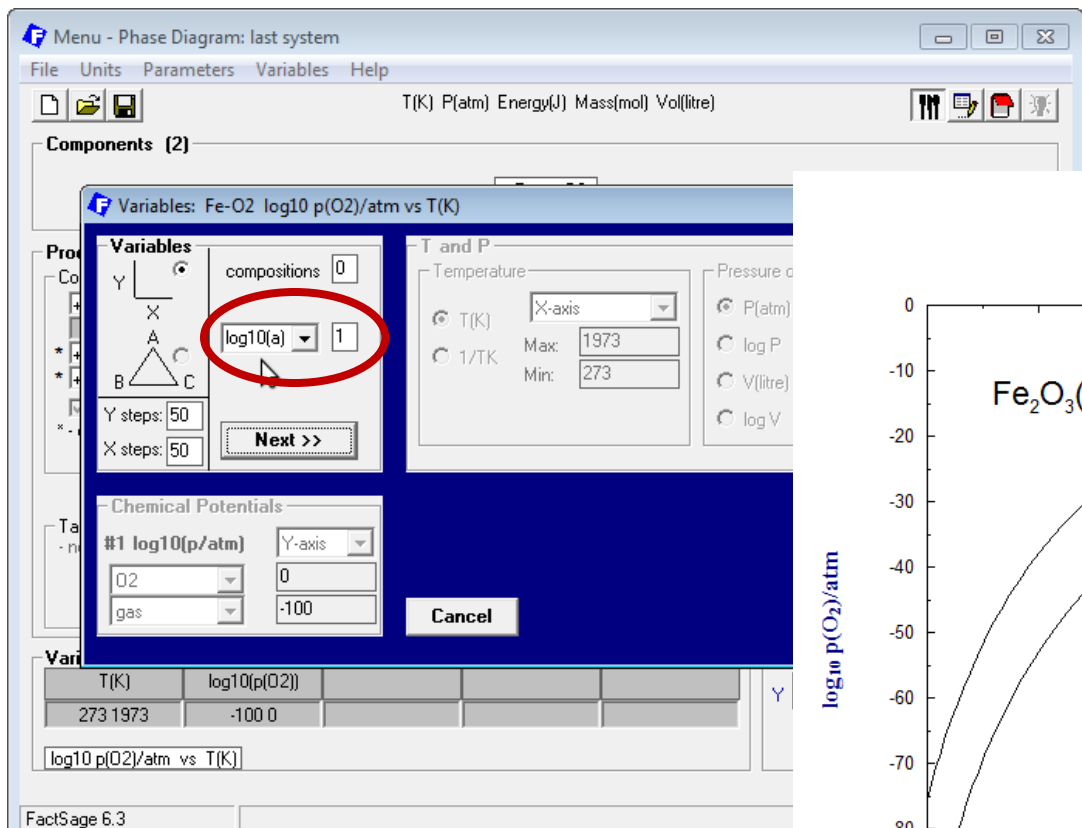
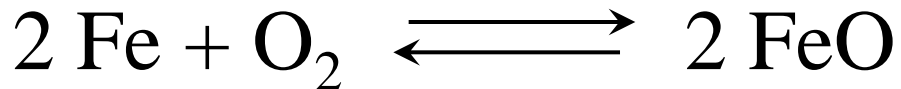
# Ellingham Diagram with FACTSage



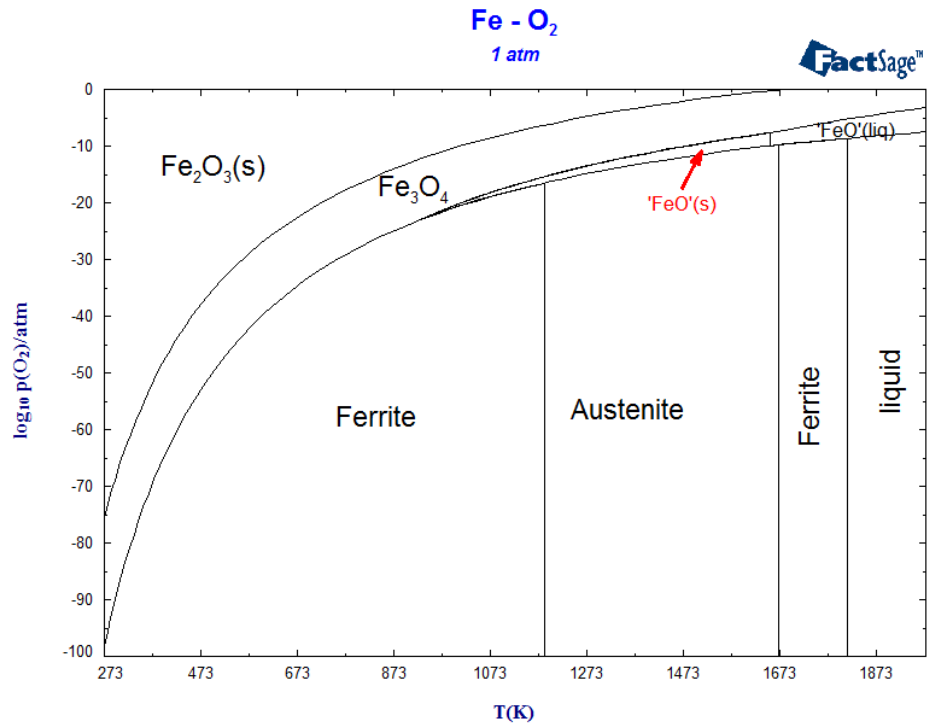
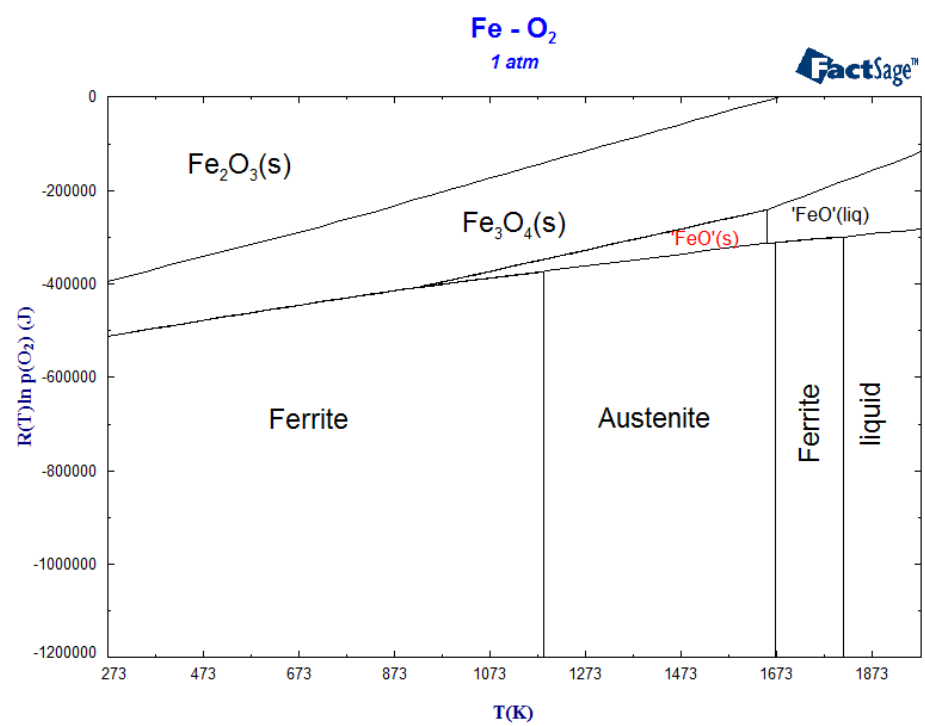
# Stability Diagrams with FACTSage



# Stability Diagrams with FACTSage



# Comparison

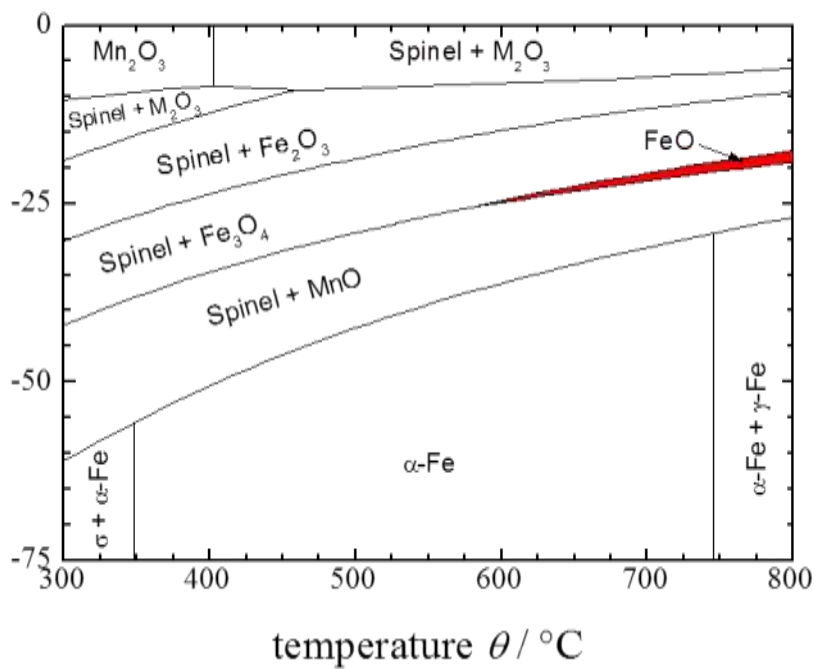
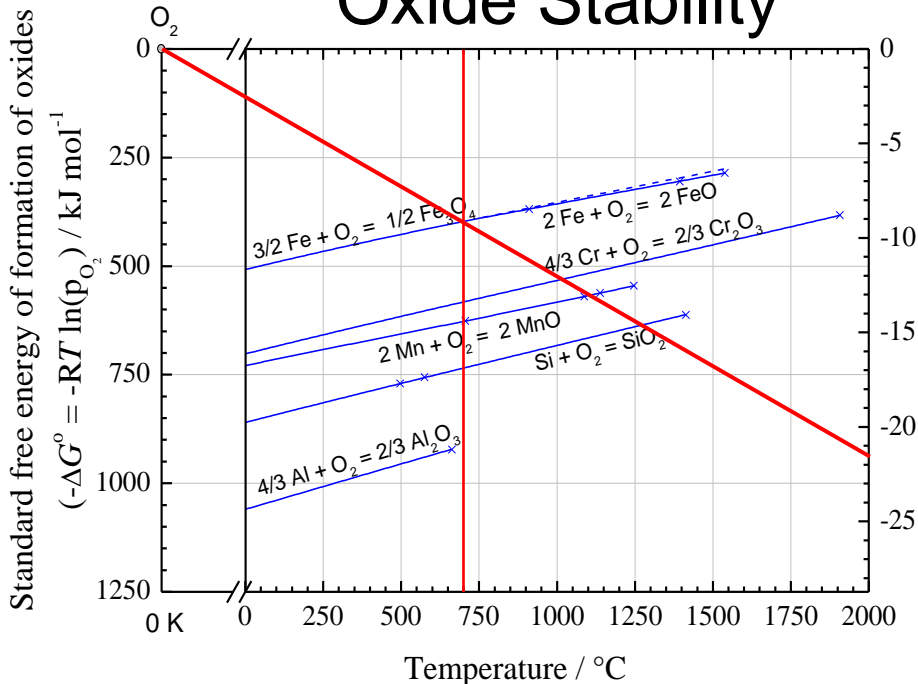


$$-2 G_{(T)}^{o, FeO} + 2 G_{(T)}^{o, Fe} + G_{(T)}^{o, O_2} = -R \ln \left( \frac{p_{O_2}}{p_o} \right) T$$

$$-\frac{2 G_{(T)}^{o, FeO} - 2 G_{(T)}^{o, Fe} - G_{(T)}^{o, O_2}}{RT} = \ln \left( \frac{p_{O_2}}{p_o} \right)$$

# Properties of Oxygen

## Oxide Stability



# Iron – Manganese – Chromium alloy

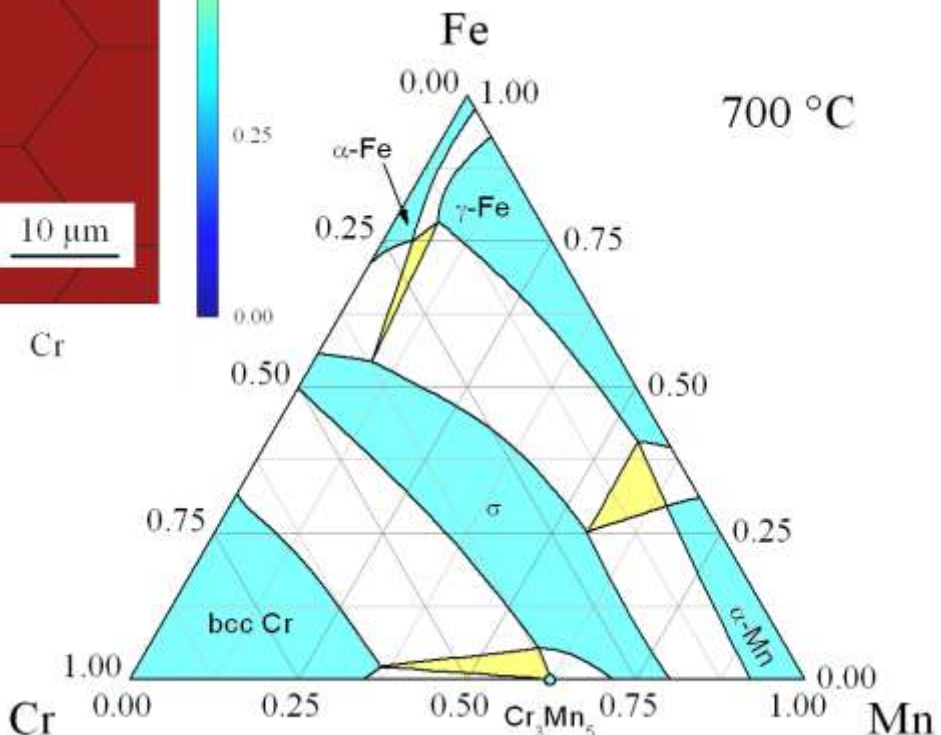
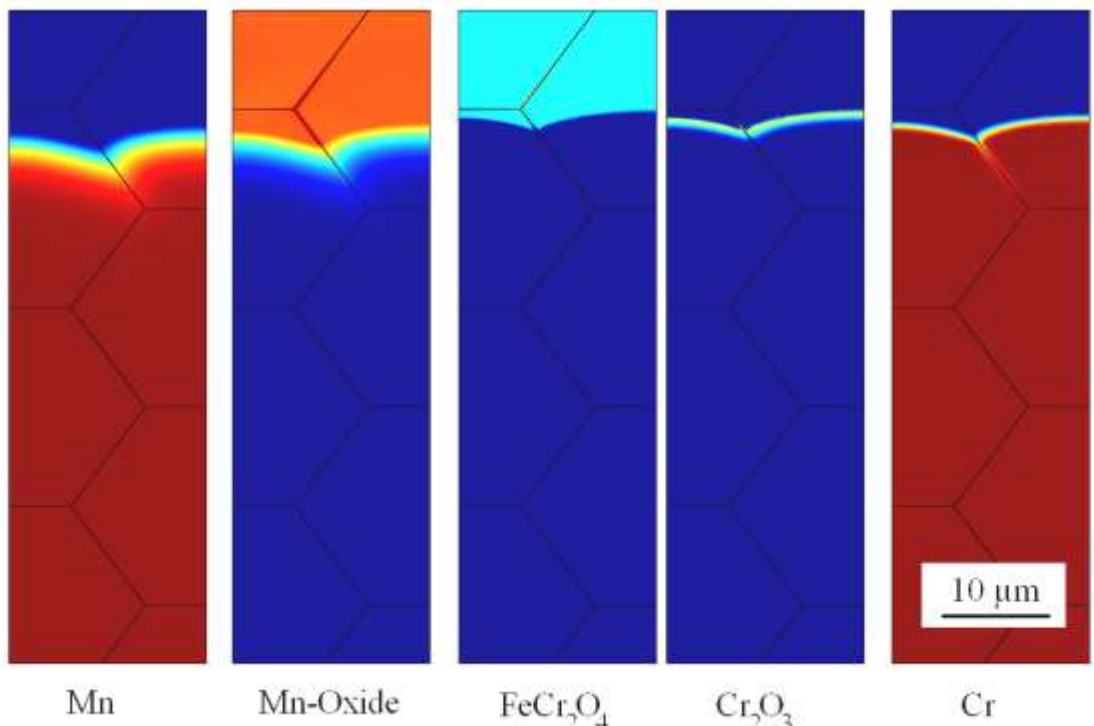


**Figure:** Spatial phase distribution in an Fe, 2 wt-% Mn, 0.8 wt-% Cr alloy after oxidation at  $p(O_2) = 3 \cdot 10^{-22}$  bar and 700 °C for 120 min and ternary phase diagram.

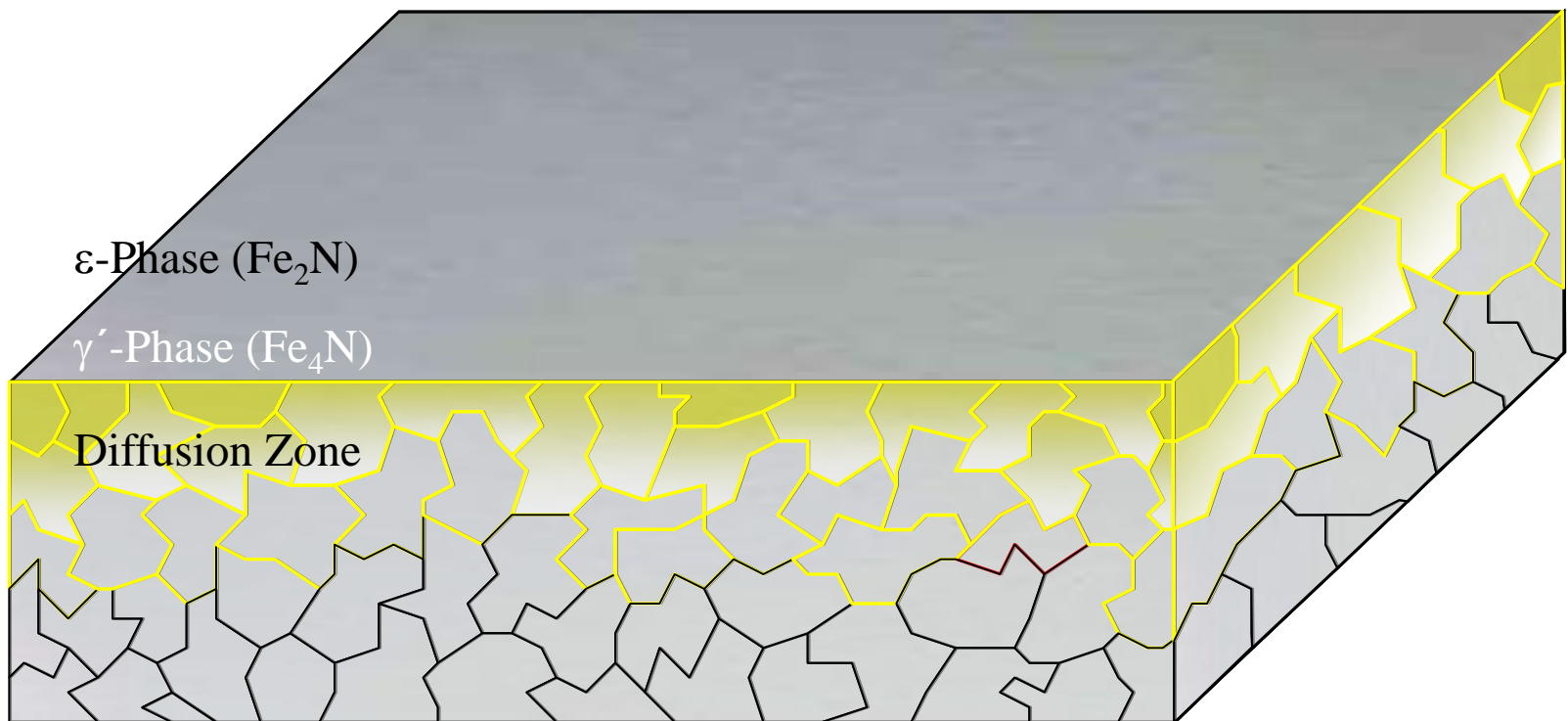
# Part II

## Gaseous Nitriding in the system Fe – Cr – C

Nitriding of      Fe, 1 wt-% Cr, 0.10 wt-% C and

Conditions:    48 h at 500 °C  
                   $p(\text{NH}_3) : p(\text{H}_2) = 100$  ( $K_N = 1\,000$ )

# Gaseous Nitriding Process



# Theoretical Principles

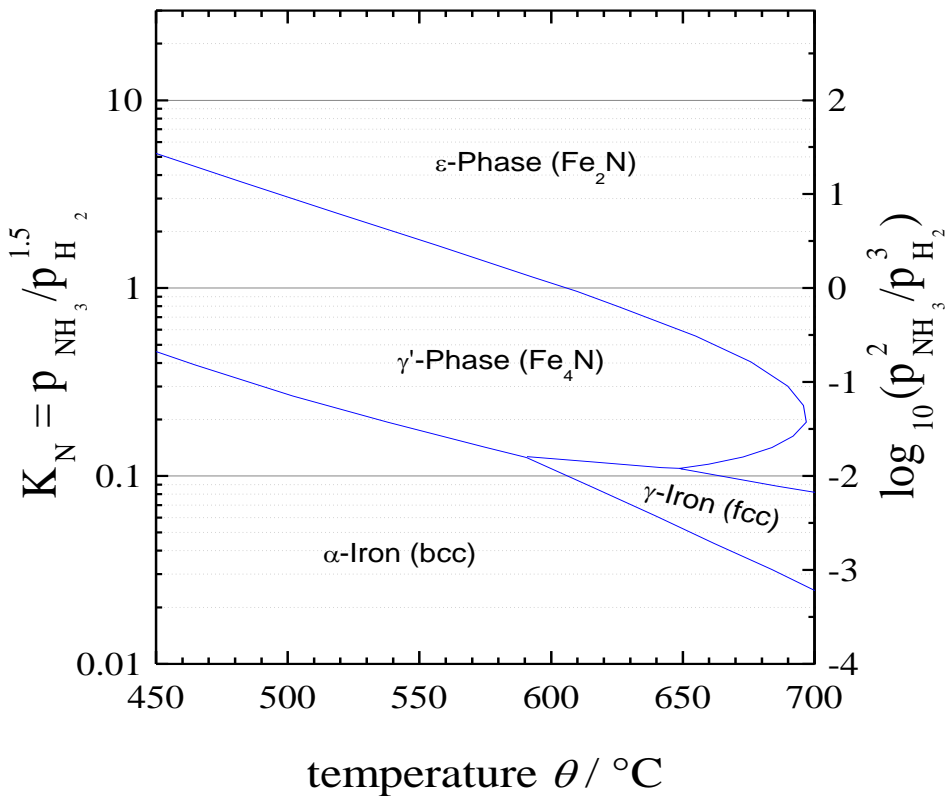
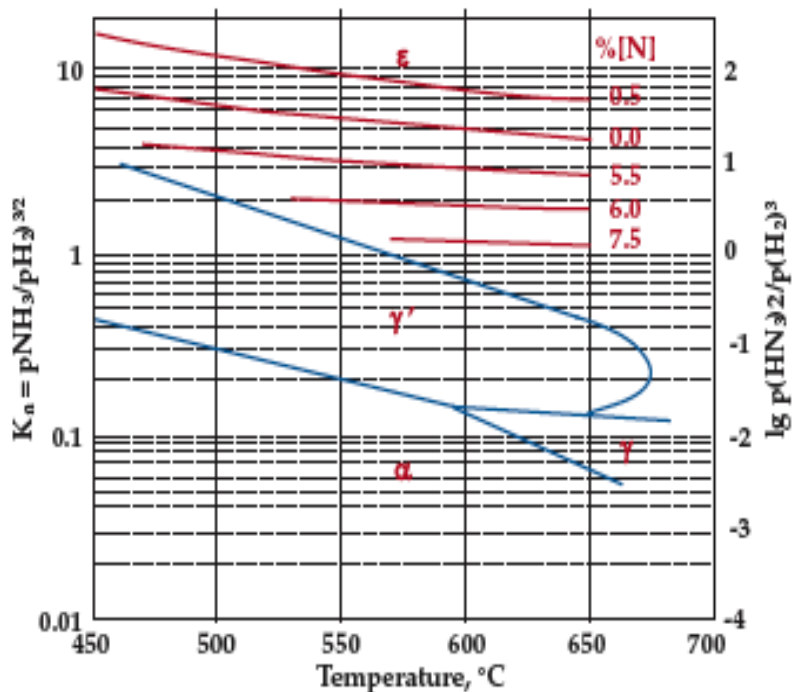


**Figure:** Lehrer-Diagramm of iron nitrides according to literature (left) and calculated with the programme FactSage (right).

# Iron – Chromium – Carbon alloy

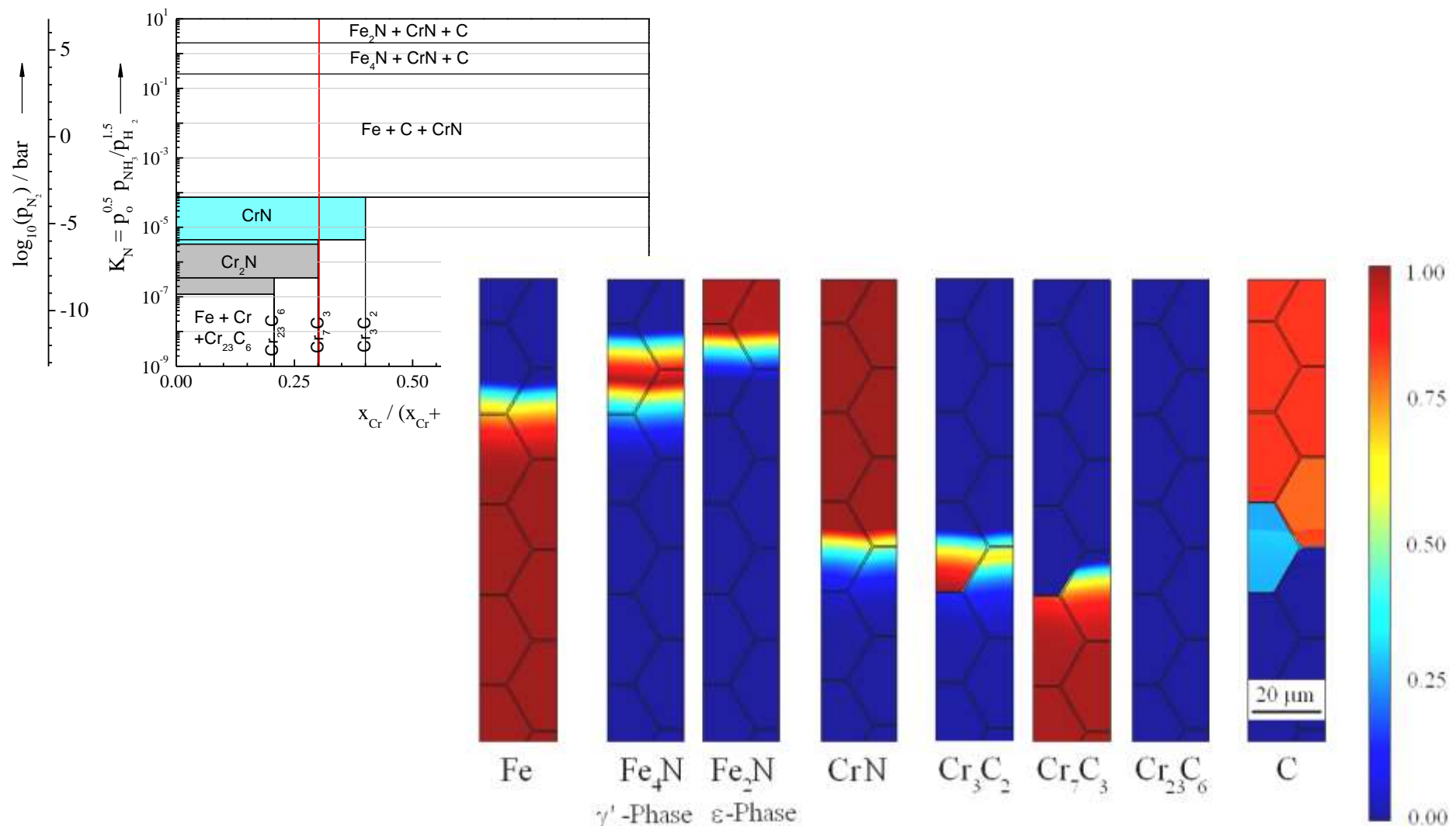
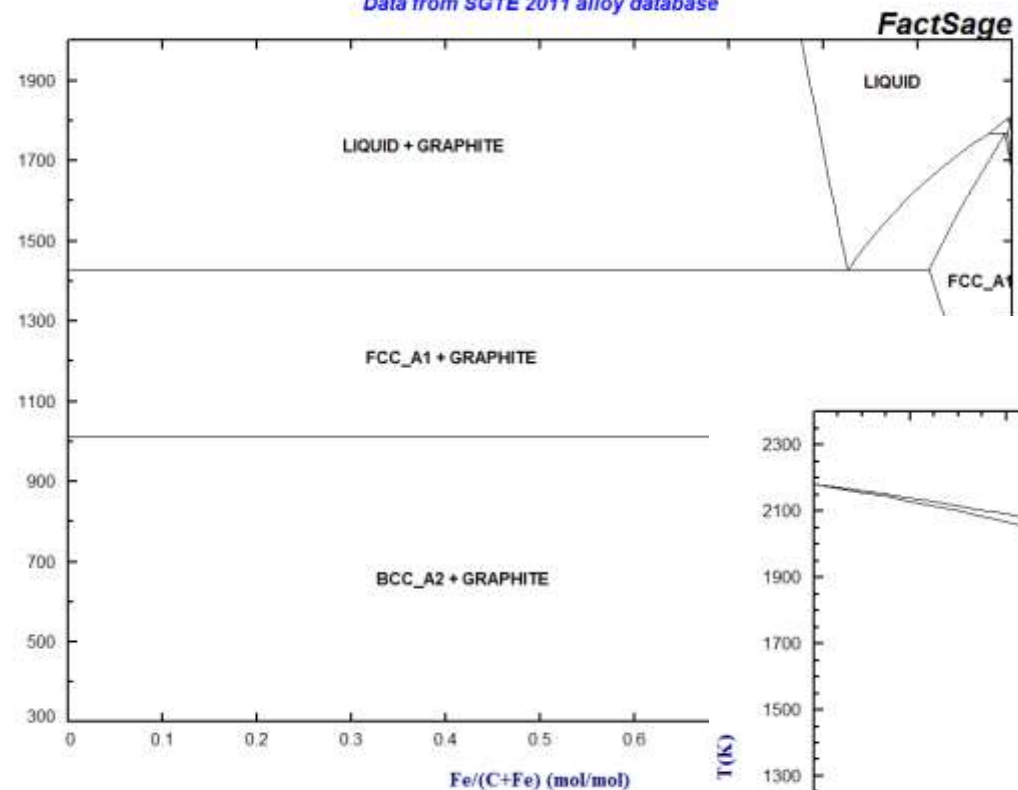


**Figure:** Spatial phase distribution in an Fe, 1 wt-% Cr, 0.1 wt-% C alloy after gas nitriding at  $K_N = 2.4$  and 500 °C for 48 h and phase stability diagram.

# Binary Phase Diagrams

**C - Fe**

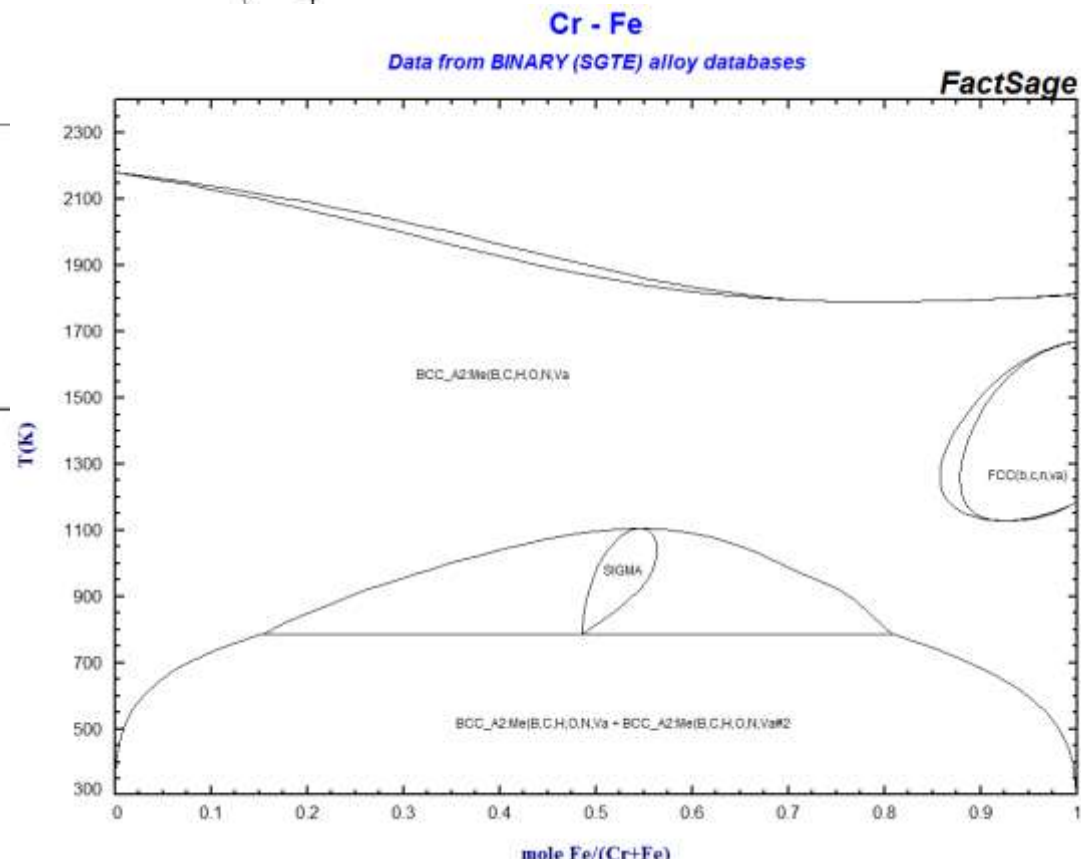
Data from SGTE 2011 alloy database



**FactSage**

**Cr - Fe**

Data from BINARY (SGTE) alloy databases

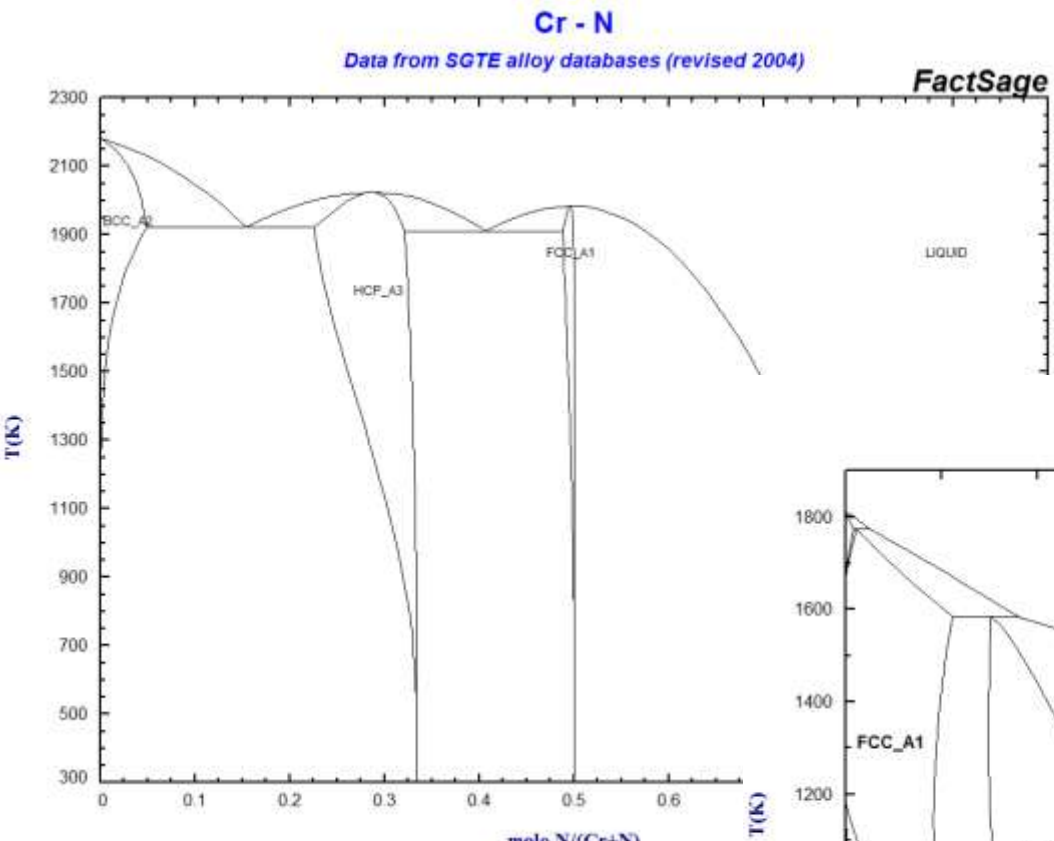


**FactSage**

# Binary Phase Diagrams

**Cr - N**

Data from SGTE alloy databases (revised 2004)

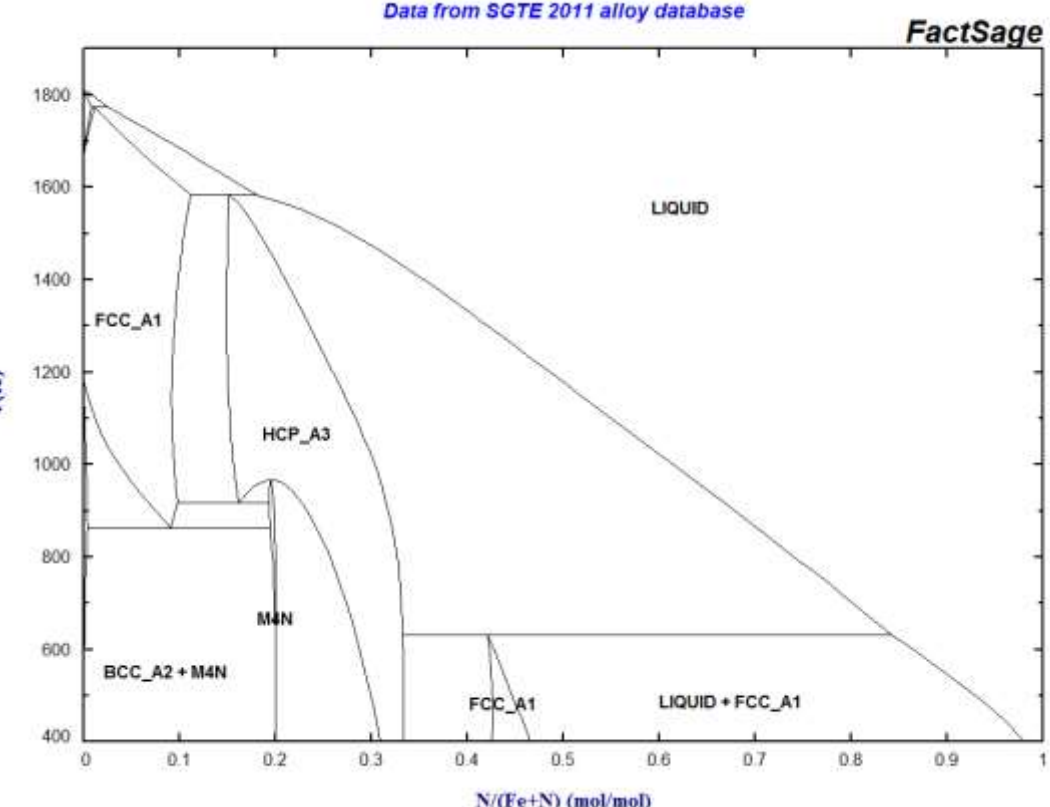


**FactSage**

**Fe - N**

Data from SGTE 2011 alloy database

**FactSage**



# The System Iron – Nitrogen

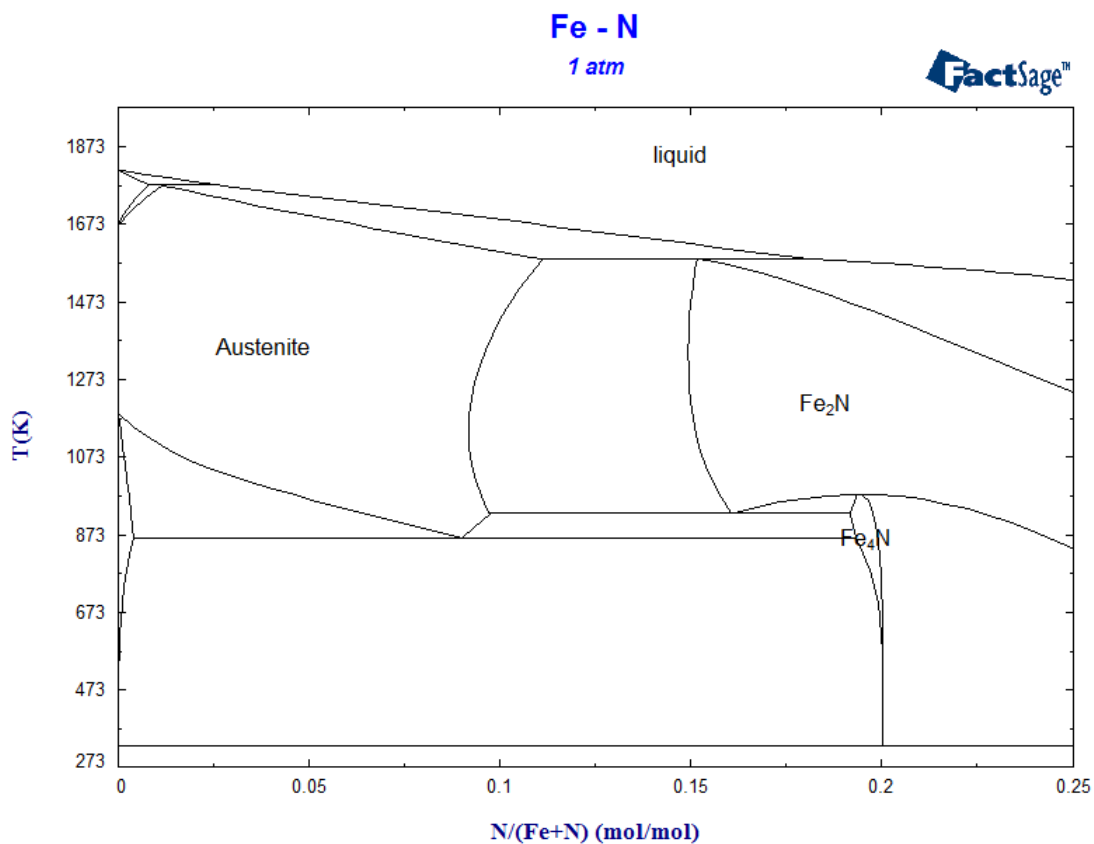
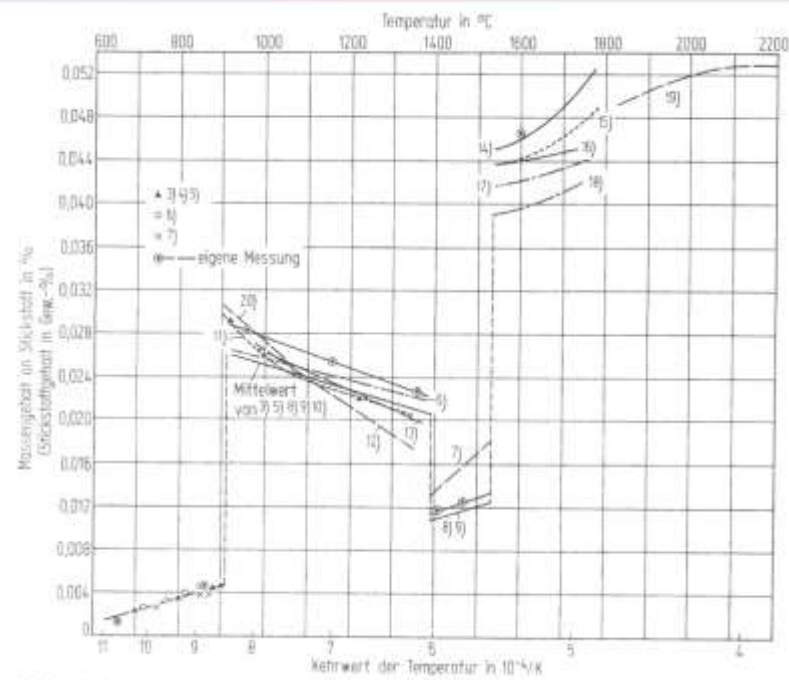


**Figure:** Nitrogen Solubility in Iron at 1 bar (left) and binary Iron-Nitrogen phase diagram, calculated with FACTSage (right).

# The System Iron – Nitrogen

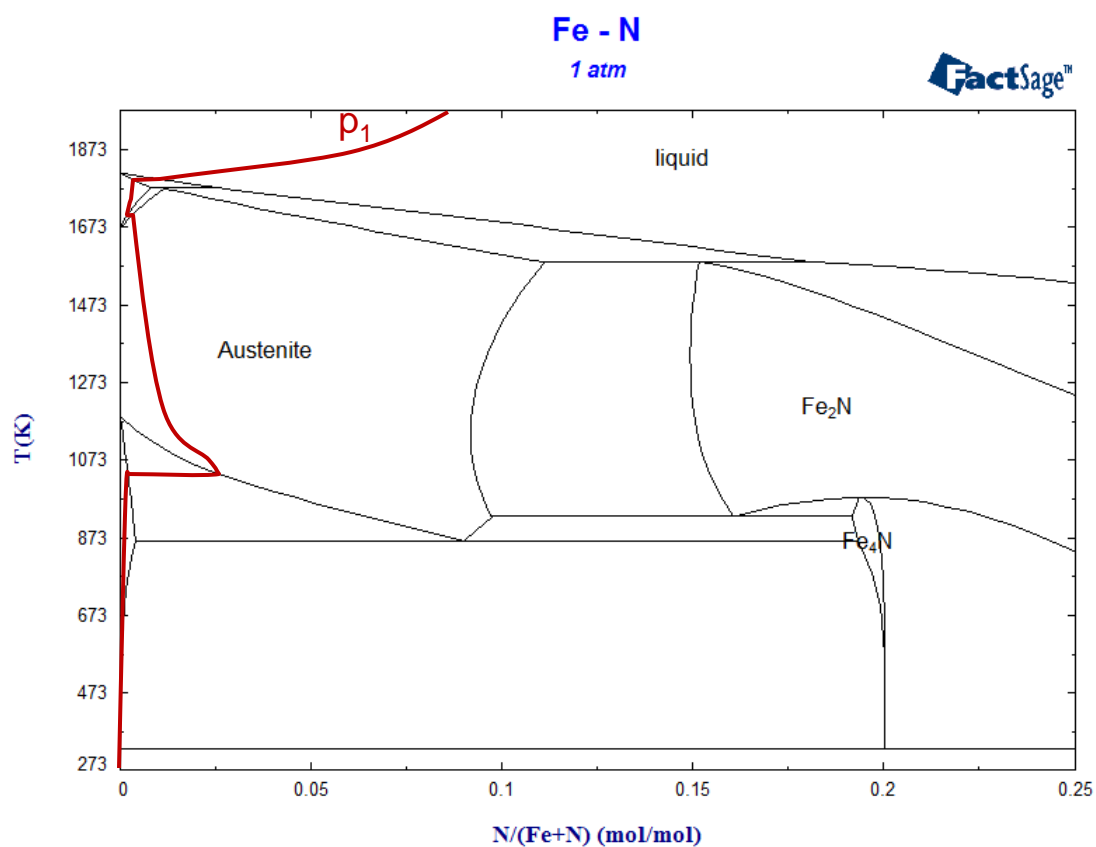
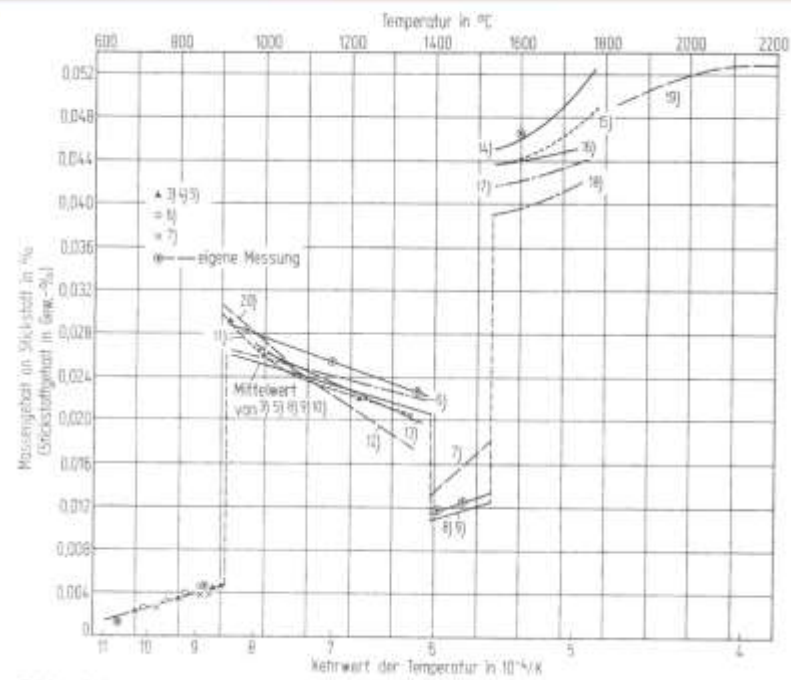


**Figure:** Nitrogen Solubility in Iron at 1 bar (left) and binary Iron-Nitrogen phase diagram, calculated with FACTSage (right).

# The System Iron – Nitrogen

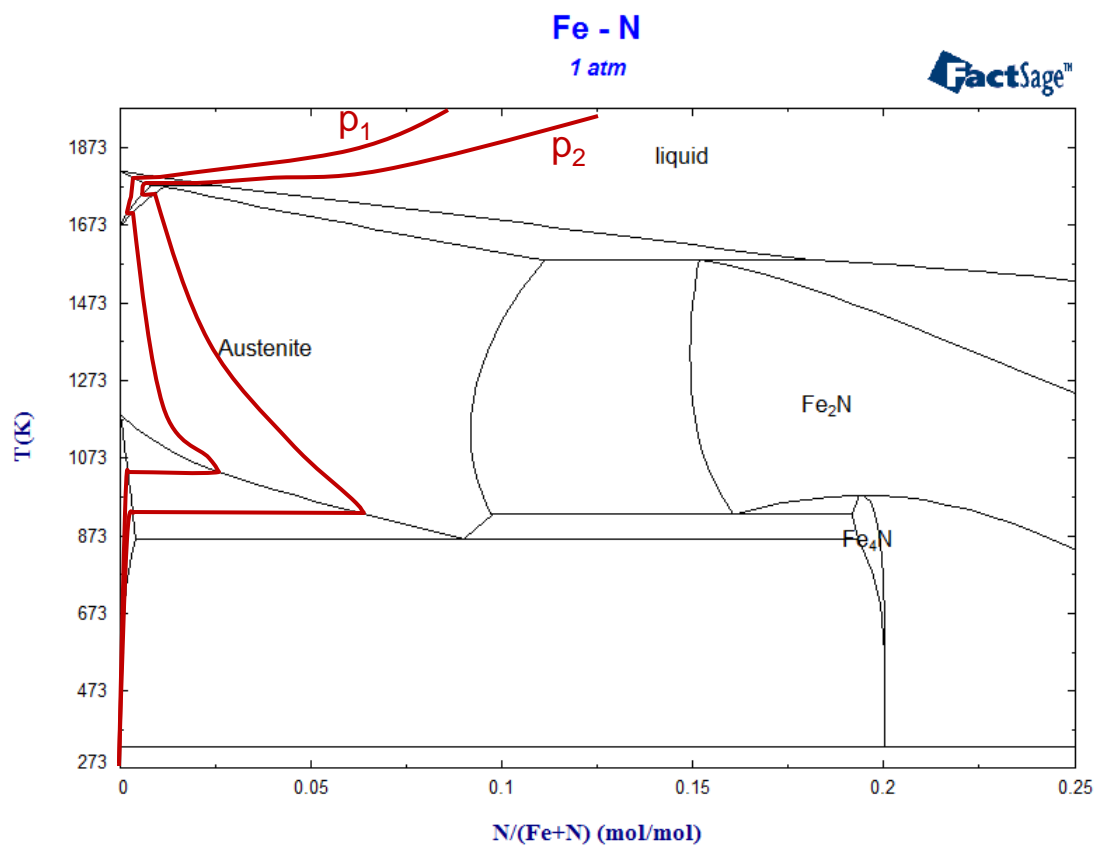
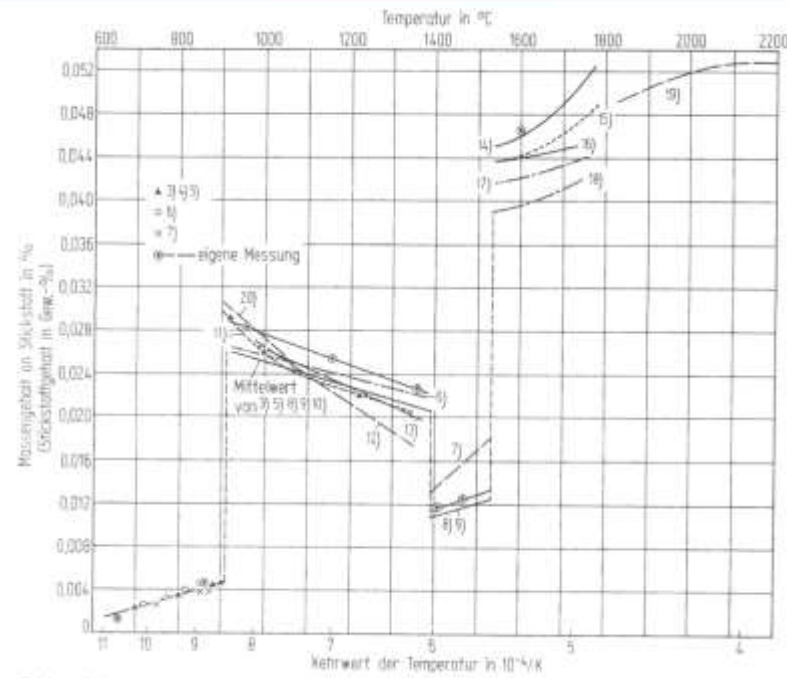


**Figure:** Nitrogen Solubility in Iron at 1 bar (left) and binary Iron-Nitrogen phase diagram, calculated with FACTSage (right).

# Part III

## Gaseous Nitriding and Oxidation in the system Fe – Si

Nitriding of      Fe, 1 wt-% Si

Conditions:      20 h at 550 °C ( $K_N = 1\ 000$ )  
                      4 h at 550 °C ( $K_O \approx 0.01$ )

# Stability Diagram of Iron – Silicon

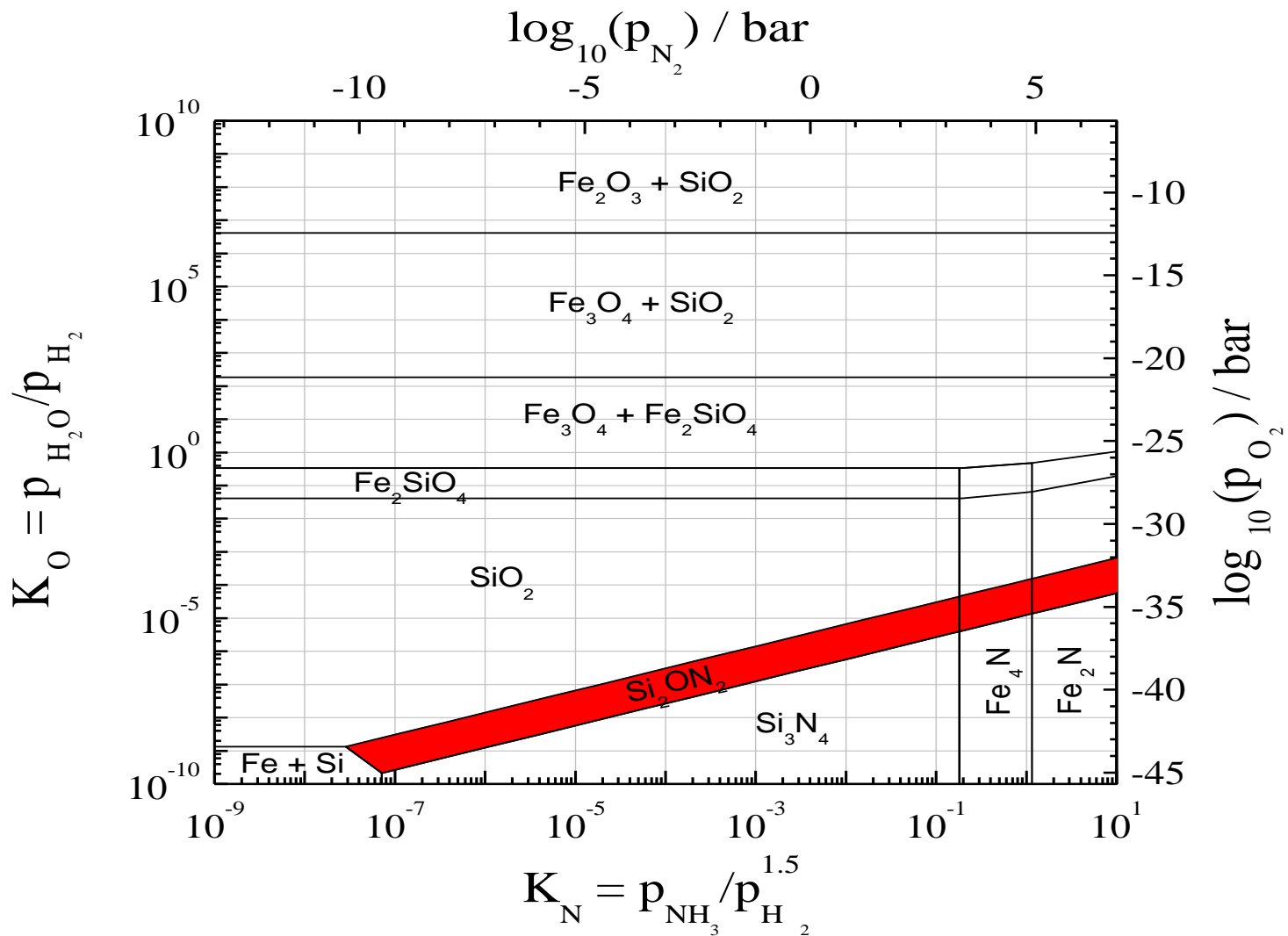


**Figure:** Stability diagram of an Fe, 1 wt-% Si alloy at 550 °C with respect to the partial pressures of nitrogen and oxygen (SGTE Pure Substance Database).

# Simulation Results with ASTRID

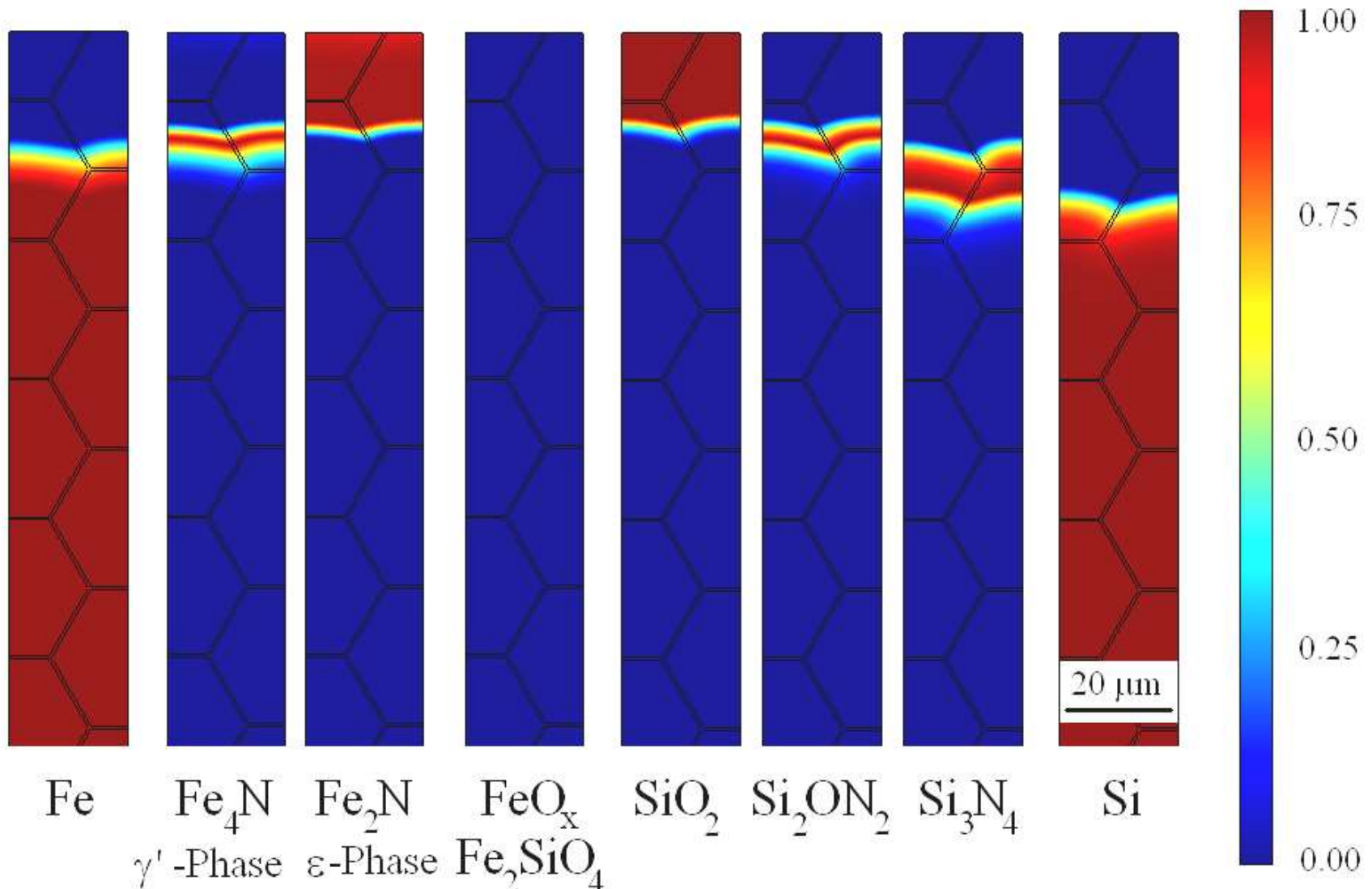
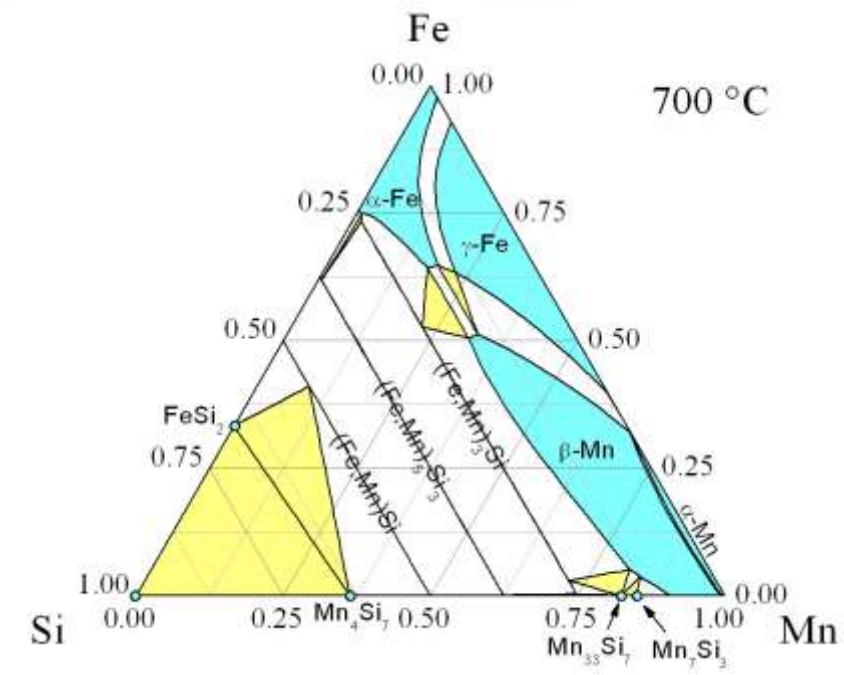
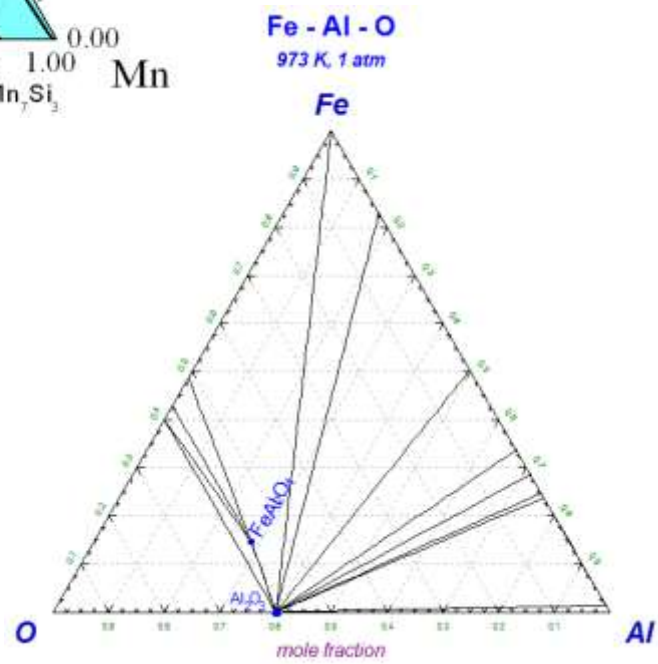
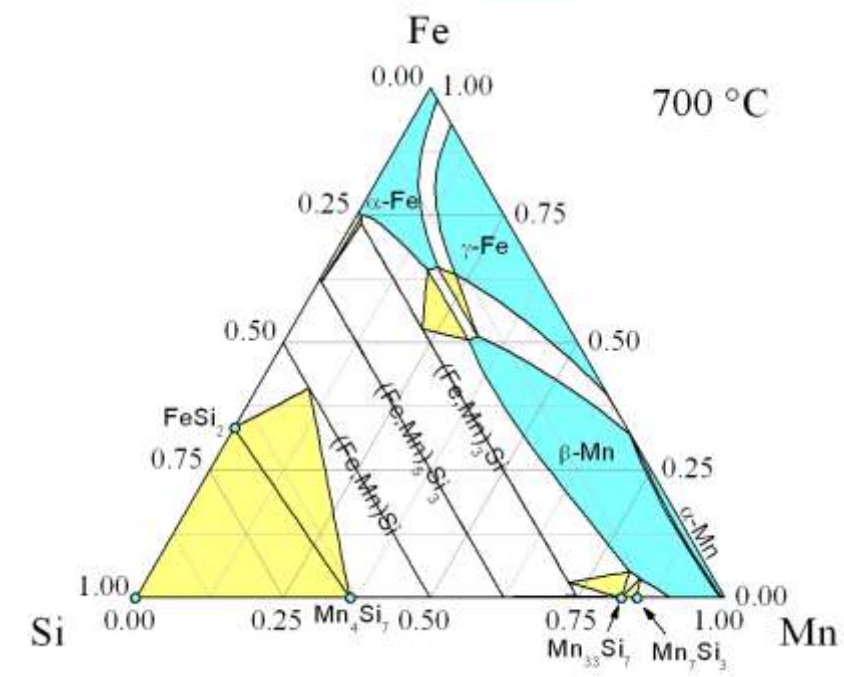


**Figure:** Spatial phase distribution in Fe, 1 wt-% Si after gaseous nitriding for 20 h at  $K_N = 1\ 000$  and oxidation for 4 h and  $K_O \approx 0.01$  ( $p_{\text{tot}} = 1 \text{ atm}$ ,  $550^\circ\text{C}$ ) .

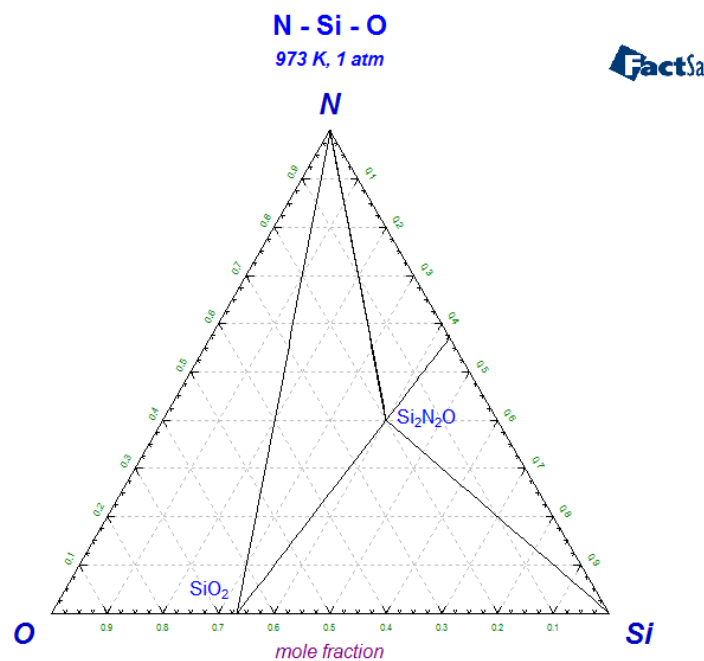
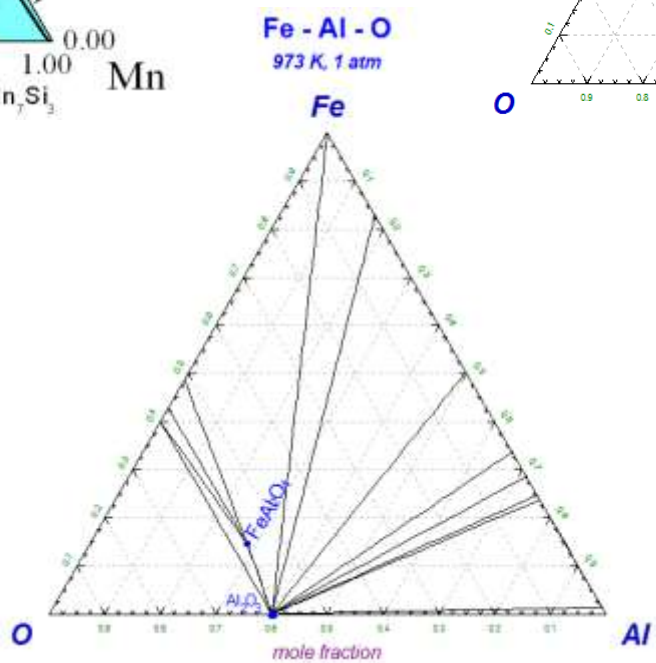
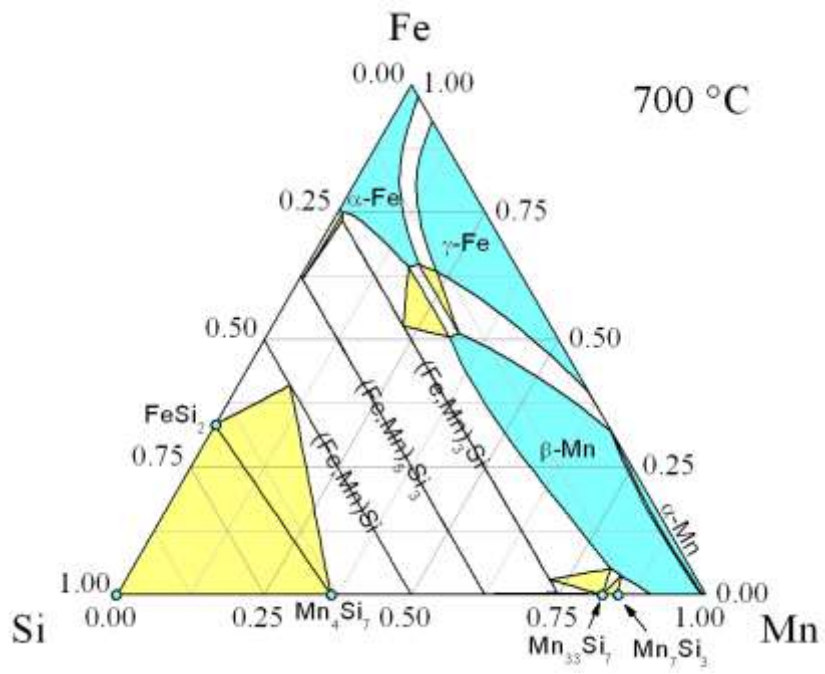
# Ternary Phase Diagrams



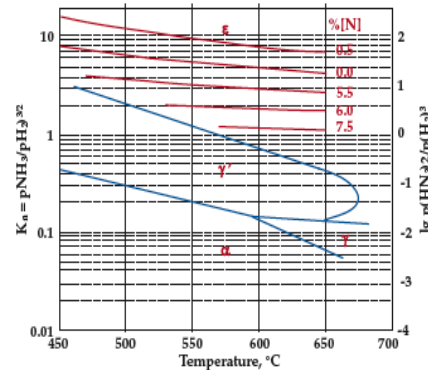
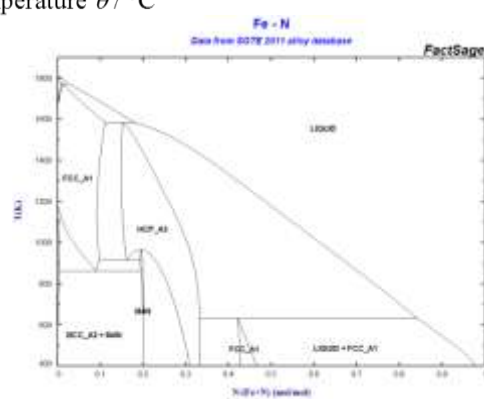
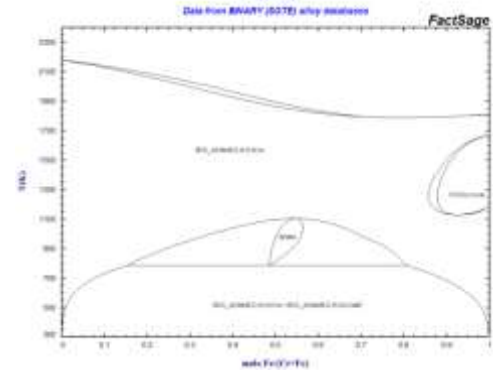
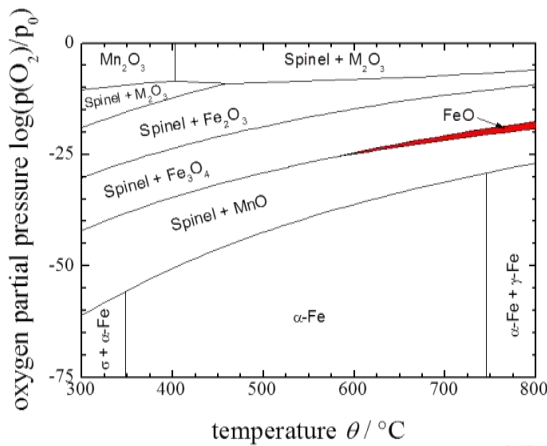
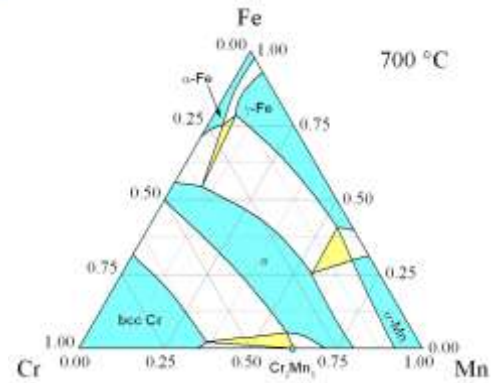
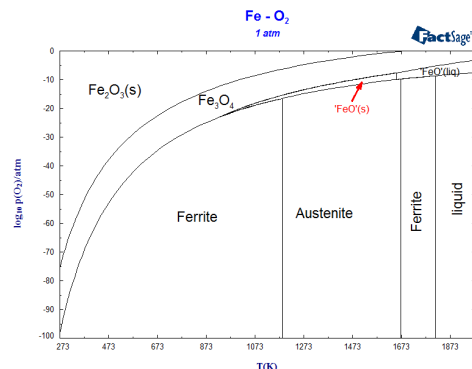
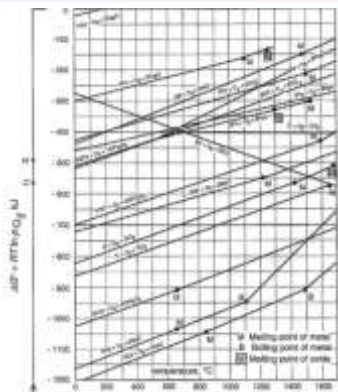
# Ternary Phase Diagrams



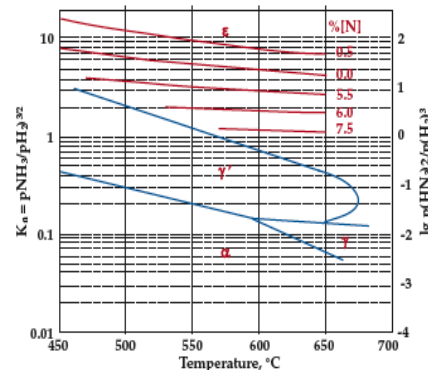
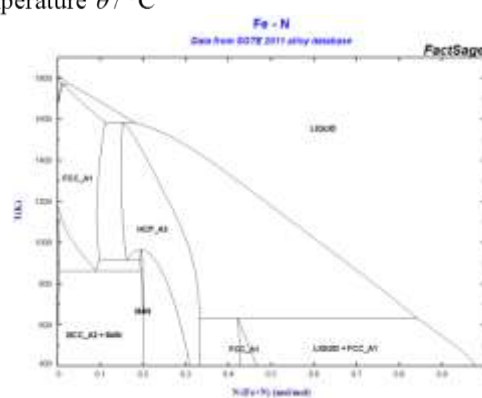
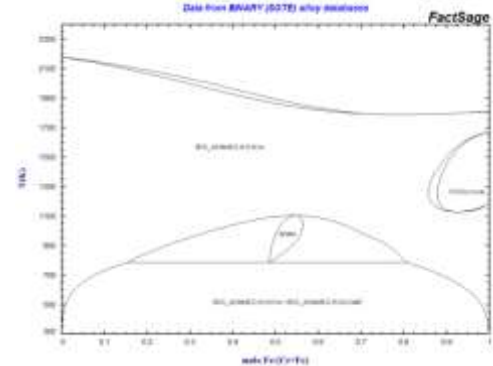
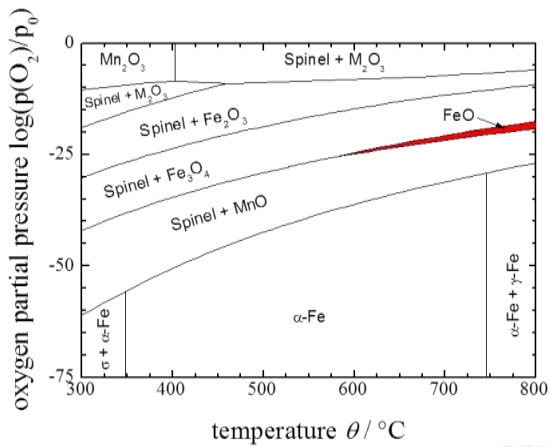
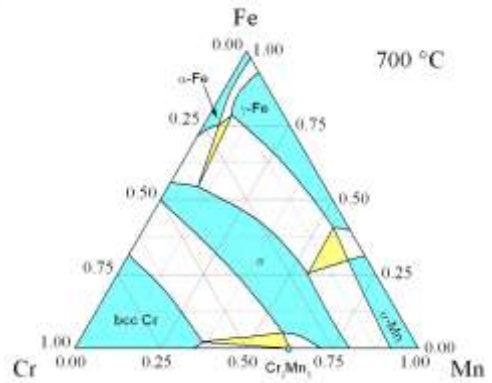
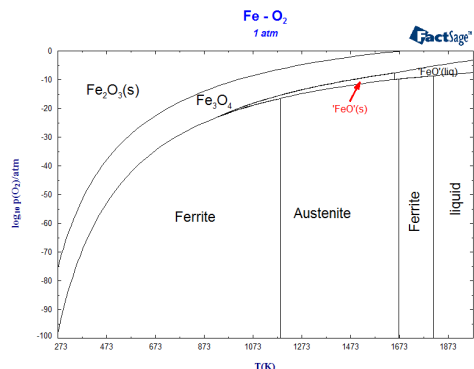
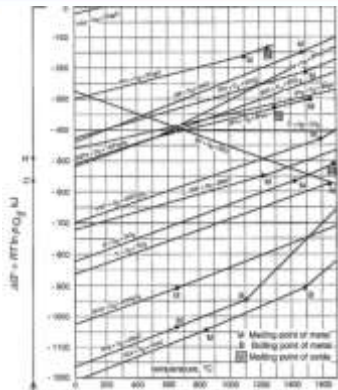
# Ternary Phase Diagrams



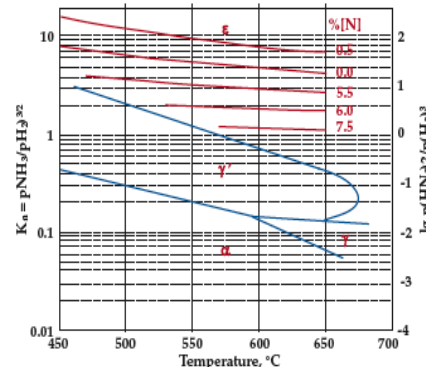
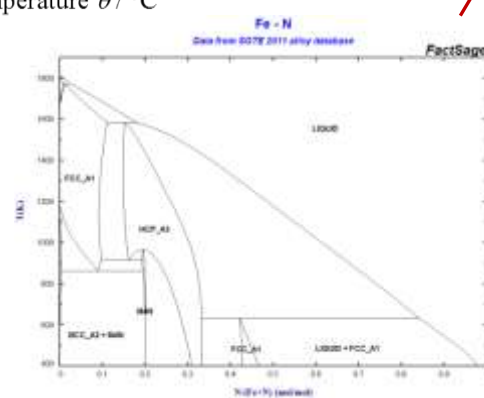
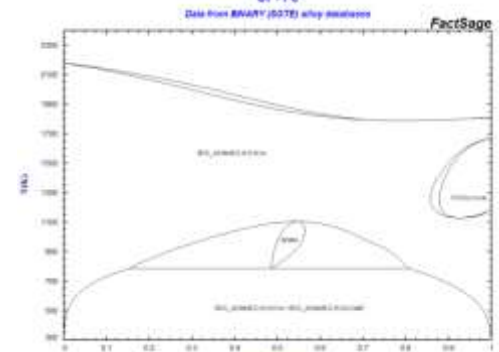
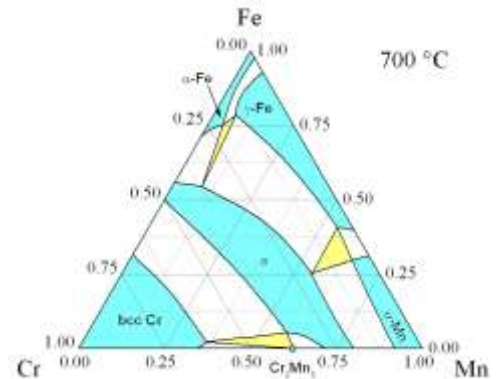
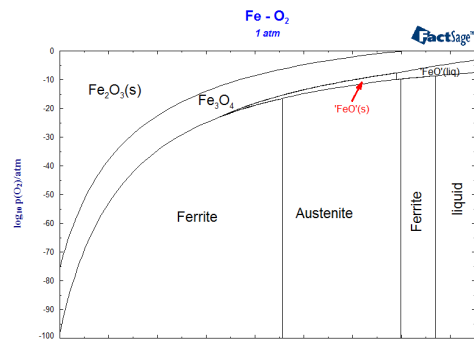
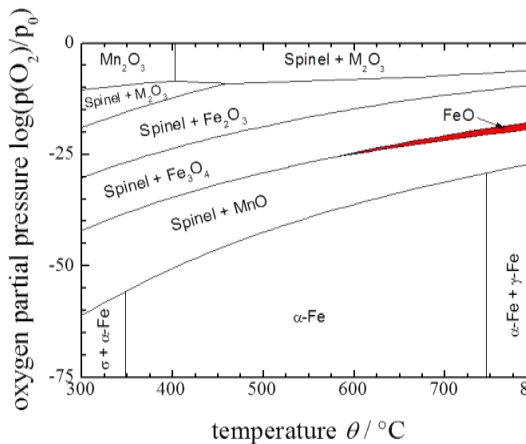
# Conclusions - The Problem



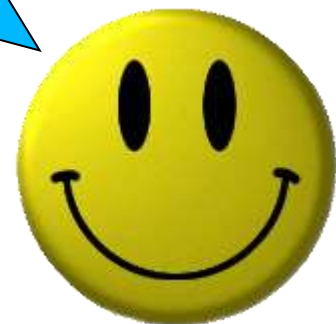
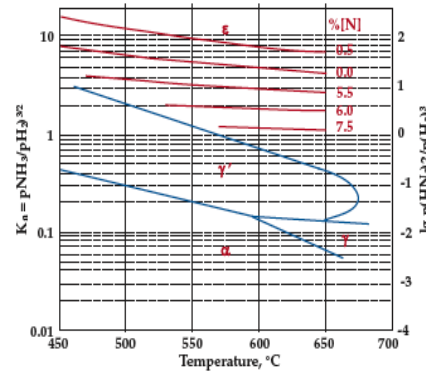
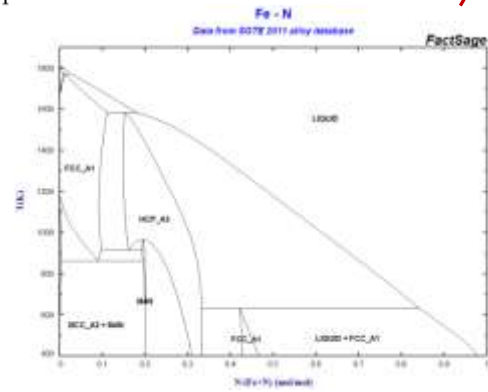
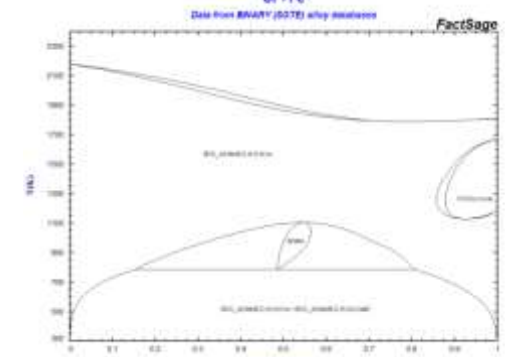
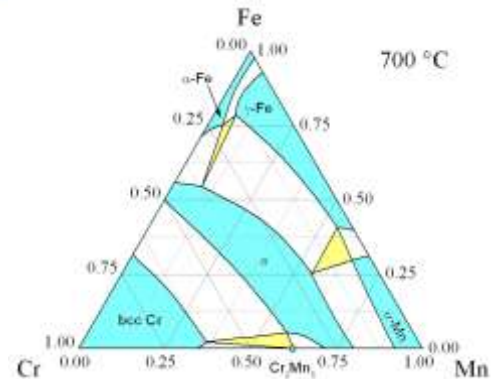
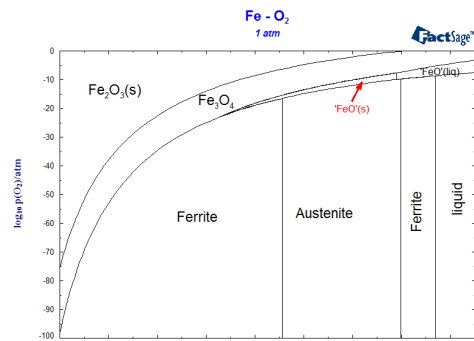
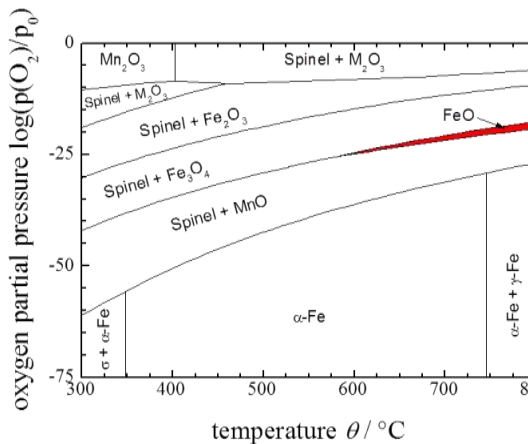
# Conclusions – An Effective Solution



# Conclusions – An Effective Solution



# Conclusions – An Effective Solution





# Acknowledgements



Max-Planck-Institut  
für Eisenforschung GmbH

Dirk and Alexandra Vogel,  
Else-Marie Müller-Lorenz,  
Monika Nellessen



TECHNISCHE  
UNIVERSITÄT  
WIEN  
Vienna University of Technology

Prof. H. Danninger

Vera G. Praig, Markus Holzweber,  
Kurt Piendl

**voestalpine**  
EINEN SCHRITT VORAUS.

Dr. D. Paesold

Bernhard Linder, Klaus Rendl,  
Andreas Muhr

## Funding



Christian Doppler  
Forschungsgesellschaft

**voestalpine**

EINEN SCHRITT VORAUS.





# Backup Slides

Additional Slides for the Presentation



# Where we work...



## **Max-Planck-Institut für Eisenforschung GmbH**

Head: Prof. Dierk Raabe



Founded in 1917 from the “Kaiser Wilhelm Institute”  
by Fritz Wüst.

### 3 Departments:

Computational Materials Design

Interface Chemistry and Surface Engineering

Microstructure Physics and Alloy Design



## Austria

Area: 83 879 km<sup>2</sup>

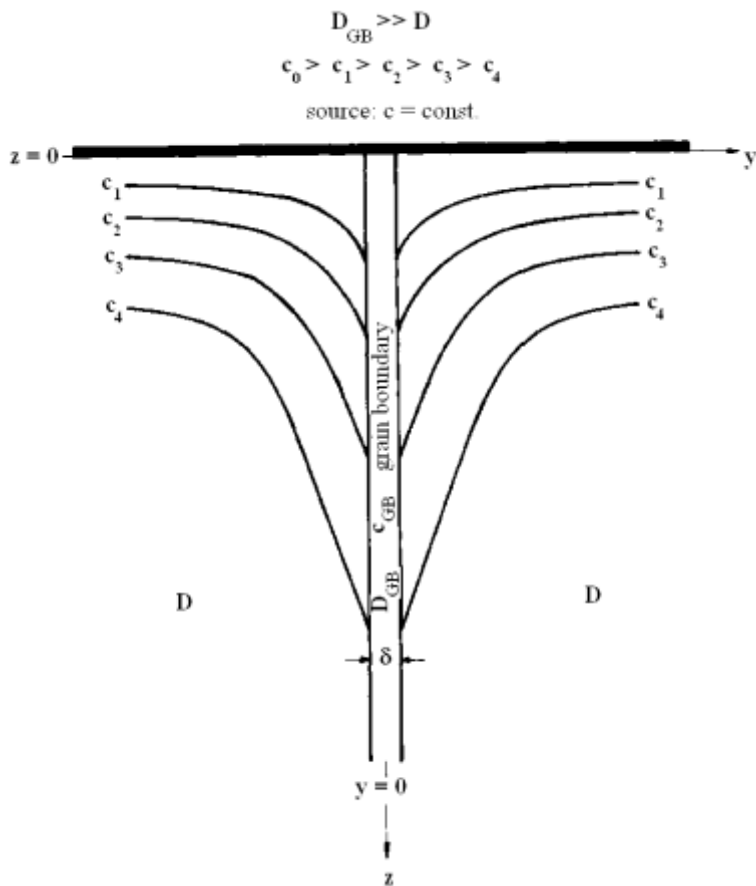
Inhabitants: ~ 8 405 000

Language: German

Capital: Vienna

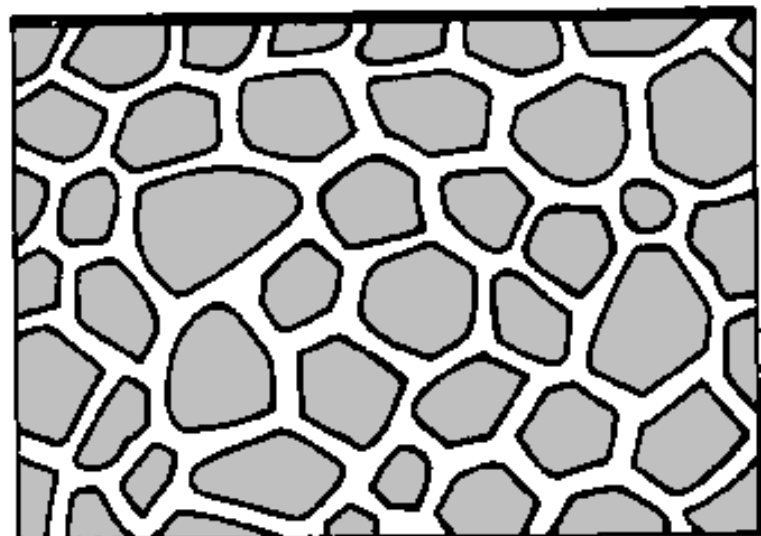


# Fisher's Model of Diffusion



*Whipple – Le Claire* equation

$$s \delta D_{GB} = 0.3292 \sqrt{\frac{D}{t}} \left( \frac{\partial \log \bar{c}}{\partial z^{6/5}} \right)^{-\frac{5}{3}}$$



*Levine – MacCallum* equation

$$s \delta D_{GB} = 0.4704 \sqrt{\frac{D}{t}} \left( \frac{\partial \log \bar{c}}{\partial z^{6/5}} \right)^{-\frac{5}{3}}$$

# Some Published Works on HT-Corrosion



JPEDAV (2005) 26:487-493  
DOI: 10.1361/154770305X66592  
1547-7037/\$19.00 ©ASM International

Basic and Applied Research: Section I

## Internal Corrosion of Engineering Alloys: Experiment and Computer Simulation

Ulrich Krupp and Hans J. Christ

(Submitted July 18, 2005)

High-temperature corrosion is generally known as a material degradation process that occurs at the surface of engineering components. In the case of internal corrosion, the corrosive species penetrates into the material by solid-state diffusion leading to the formation of internal precipitates, for instance, oxides (internal oxidation), nitrides (internal nitridation), and carbides (carburization). It is known from numerous publications and technical failure cases that internal corrosion results in a strong deterioration of the properties of a material (i.e., near-surface embrittlement or the dissolution of strengthening phases). The present article introduces the classic theory of internal oxidation and reviews some recent research on internal corrosion phenomena that are closely related to the failure mechanisms of thermally grown protective oxide scales on several commercial high-temperature alloys (e.g., single-crystalline and polycrystalline Ni-base alloys and Cr steels). The mechanisms and kinetics of internal corrosion processes are determined by the temperature, the local chemical composition of the material, the solubility and diffusivity of the corrosive species, as well as the mechanical loading conditions. These influence factors are taken into account by means of a computer model combining a numerical finite-difference approach to solve the diffusion differential equations with the thermodynamic tool ChemApp. Using several examples, it is shown that the model has been applied successfully to simulate the internal nitridation, carburization, and oxidation of high-temperature alloys.



### ARTICLE IN

#### Article history:

Received 1 December 2004

Accepted 22 February 2005

Available online 26 February 2005

#### Abstract

A coupled phase transformation as well as multiple coexisting phases in a  $\gamma$ -Ni-27%Cr-2%Al-2%Ti-0.5%Nb-0.5%W-0.5%Mo-0.5%Co-0.5%Fe-0.5%Cr<sub>2</sub>O<sub>3</sub> system is observed during the developing oxidation stage, whereas the parabolic oxide-layer growth rate is

© 2005 Acta Materialia Inc. Printed in the United States of America

**Keywords:** Modelling; Thermodynamics; Internal oxidation; Internal nitridation; Alloy 601

#### 1. Introduction

Internal corrosion is a generic kind of material degradation occurring at high temperatures that is driven by the inward diffusion of a corrosive species (i.e., oxygen, nitrogen, carbon, or sulfur), followed by internal precipitation of the respective oxides, nitrides, carbides, and sulfides.<sup>[1]</sup> Contrary to the formation of superficial scales, which in the case of  $\text{Cr}_2\text{O}_3$  and  $\text{Al}_2\text{O}_3$  protect the substrate against excessive corrosion attack,<sup>[2]</sup> internal corrosion may result in a deep deterioration of the physical properties of the material (e.g., creep resistance and high-temperature fatigue strength).<sup>[3,4]</sup> Figure 1 shows an example of internal oxidation (Al<sub>2</sub>O<sub>3</sub>) and nitridation (AlN; penetration depth  $\xi = 600 \mu\text{m}$ ) underneath a thin  $\text{Cr}_2\text{O}_3$  scale.

The mechanism of internal corrosion depends on the local concentrations and the diffusivities of the corrosive species and the metallic elements in the substrate. For the example shown in Fig. 1, a low oxygen partial pressure,  $p(\text{O}_2)$ , relative to the nitrogen partial pressure  $p(\text{N}_2)$  in the combustion gas leads to conditions in the material interior, for

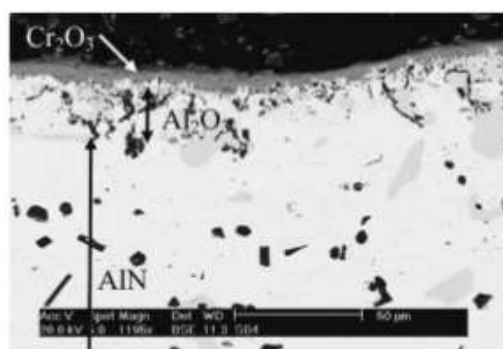


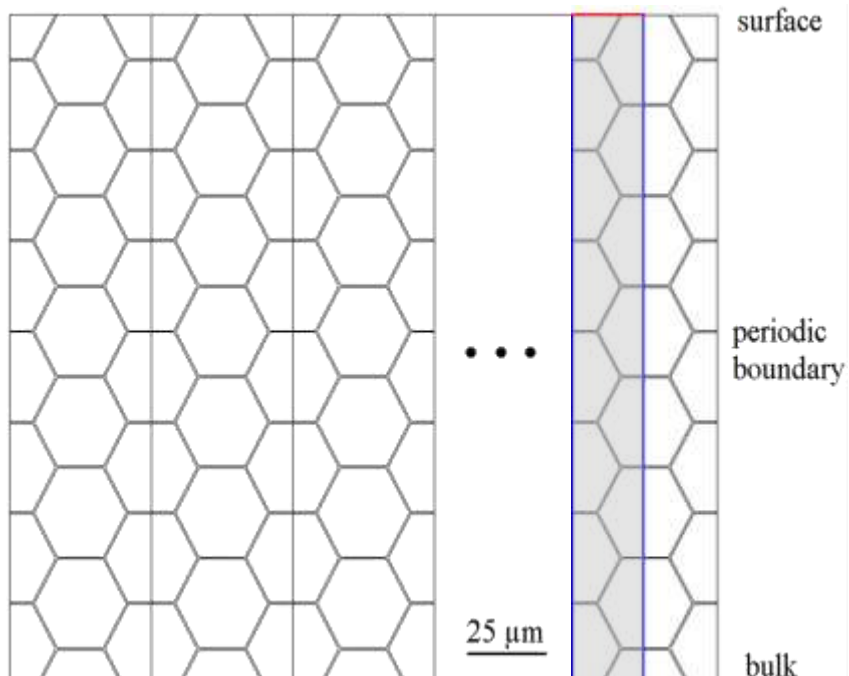
Fig. 1 Internal oxidation and nitridation attack of a failed natural gas burner tube of alloy 601 operated at  $T = 1100^\circ\text{C}$

which AlN instead of  $\text{Al}_2\text{O}_3$  is the thermodynamically most stable compound.\*

Even in the case of  $\text{Al}_2\text{O}_3$ -scale-forming Ni-base super-

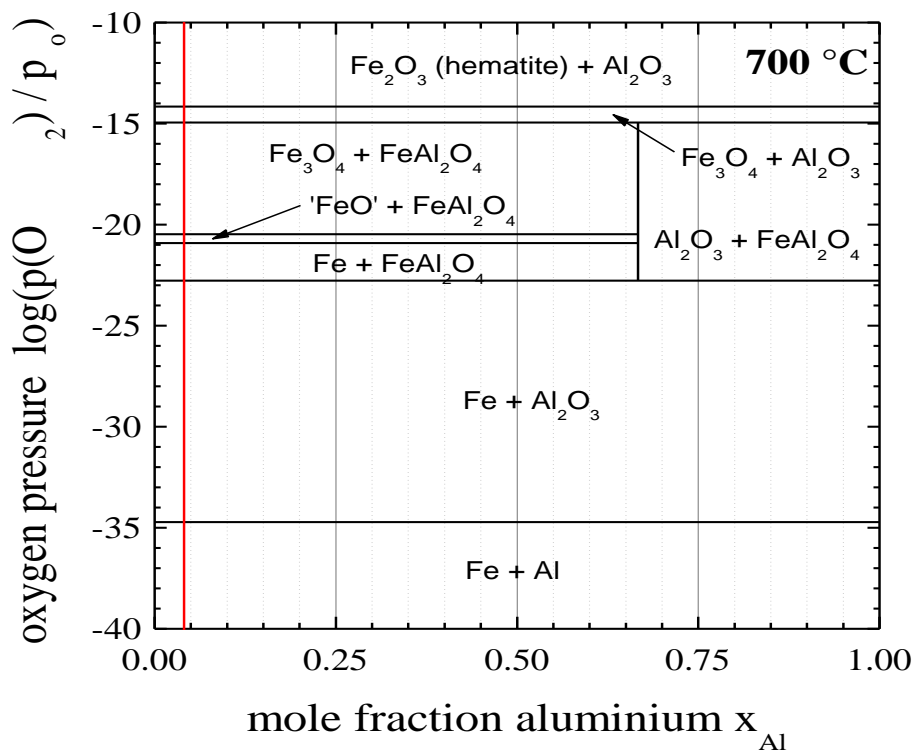
## element migration

$$\frac{dc_{i(x,t)}}{dt} = \operatorname{div}(D_{i(x,T)} \cdot \nabla c_{i(x,t)})$$



## chemical reaction

 **CHEMAPP**



# Data Handling

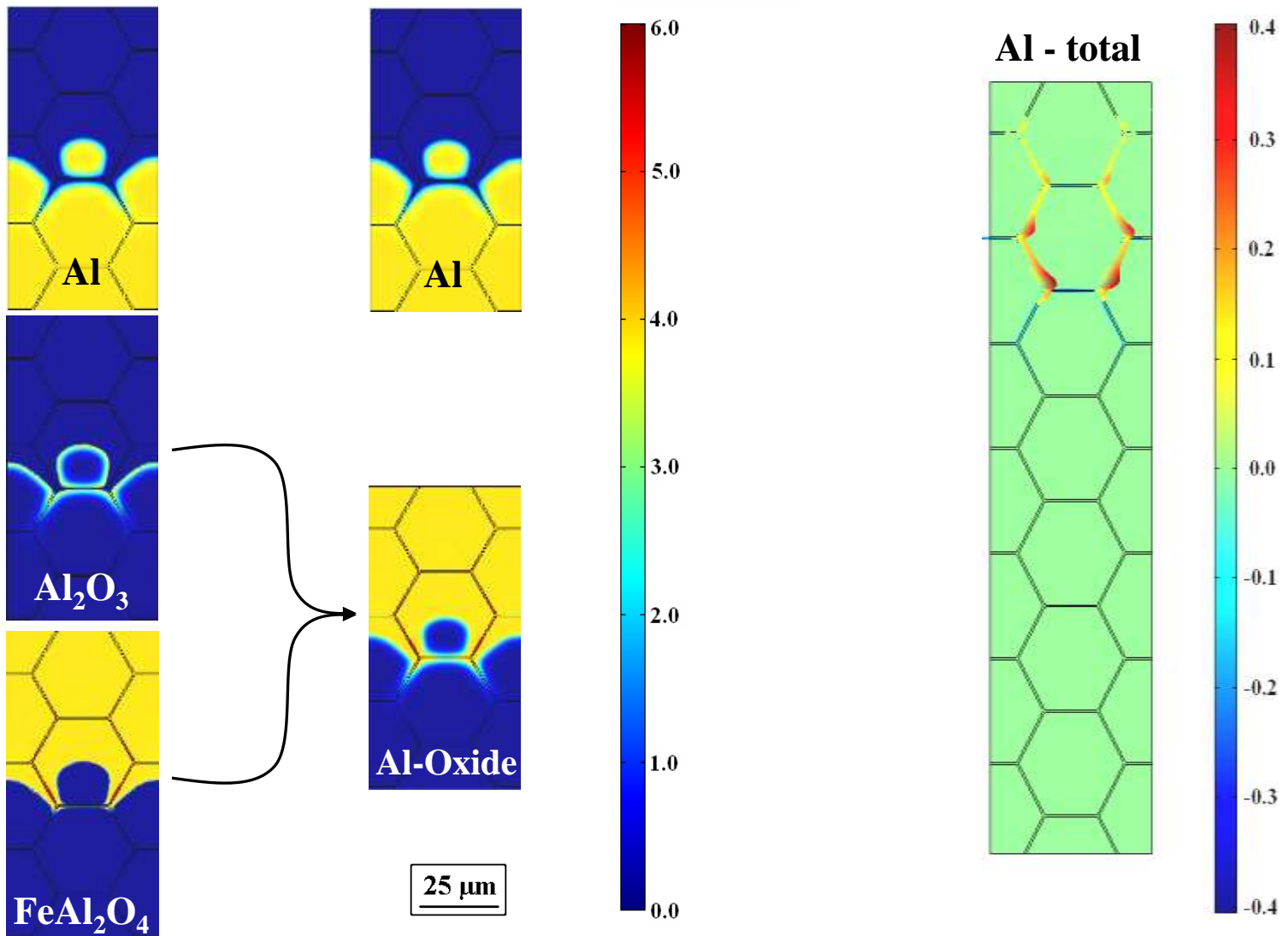


**Figure:** Spatial phase distributions of Fe, 2 wt-% Al (4.05 mol-% Al) after oxidation at  $p(\text{O}_2) = 10^{-22}$  bar for 60 min at 700 °C.

# Detail of a Grain Boundary

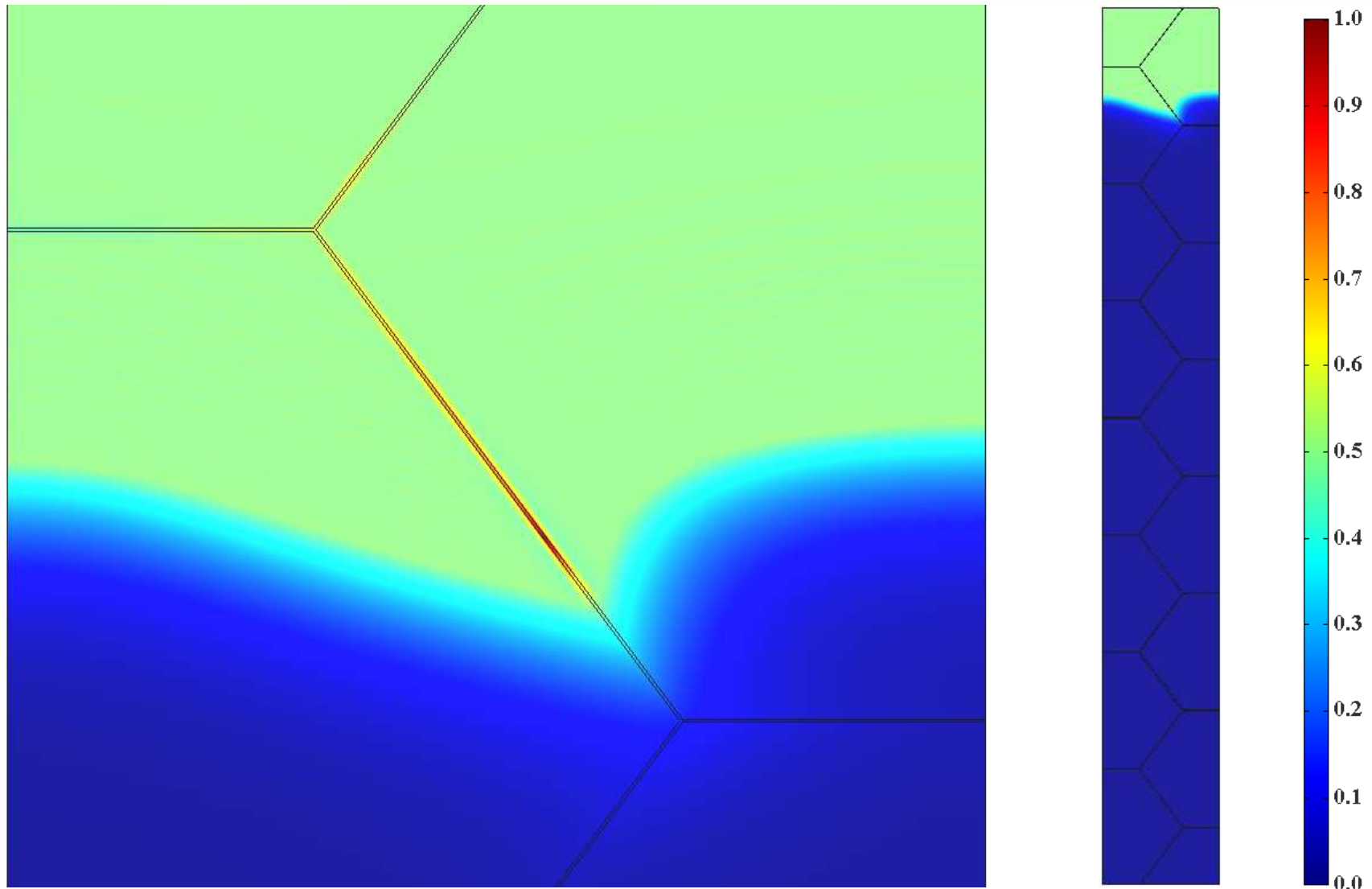


**Figure:** Spatial distribution of chromium oxides  $\text{Cr}_2\text{O}_3$  and  $\text{FeCr}_2\text{O}_4$  along a grain boundary in Fe, 3 wt-% Cr after finished cooling from 650 °C.

# Diffusion between different Phases



$$J_A = -D \nabla c$$

$$J_A = -L \nabla \mu$$

$$J_A = -L \nabla \mu = -L \frac{\partial \mu}{\partial c} \nabla c = \dots = -L \underbrace{\frac{RT}{c}}_D \nabla c - L \underbrace{\left( \nabla \mu^o + \frac{RT}{\gamma} \nabla \gamma \right)}_{}$$

**Figures:** Shibuya (渋谷) crossing in Tokyo with green and red pedestrian lights.

# Modelling Segregation

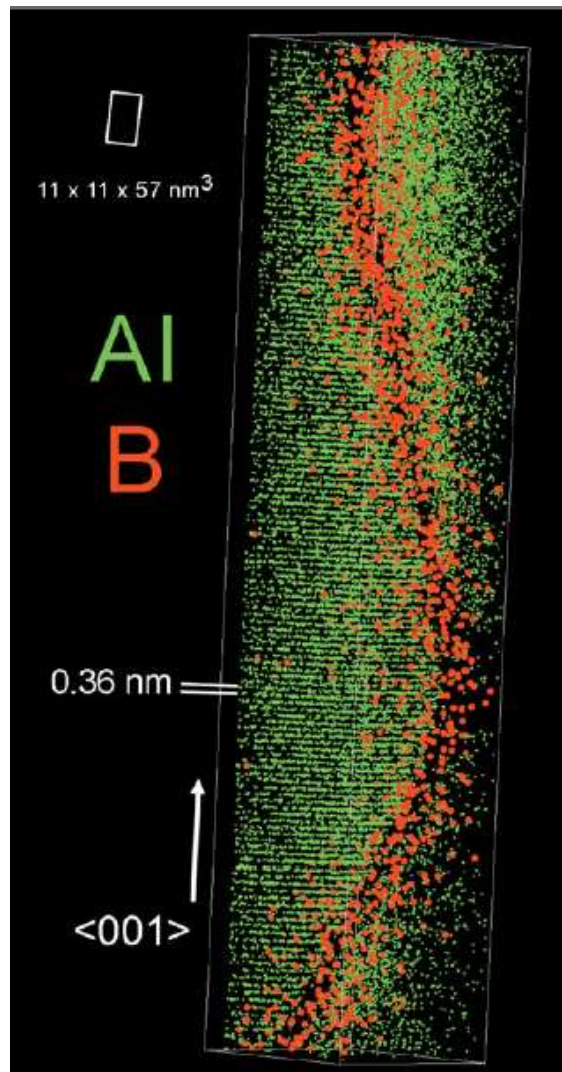
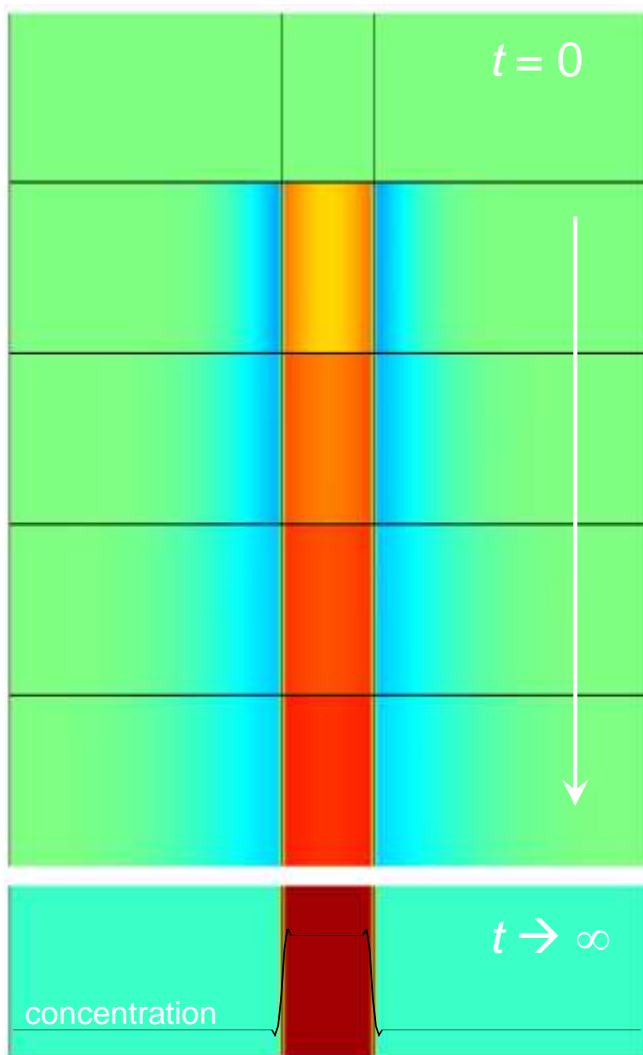
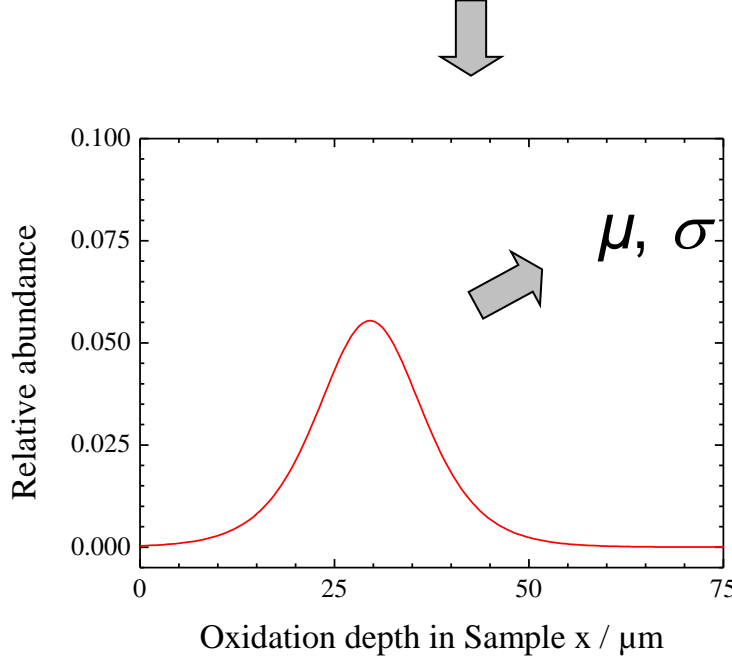
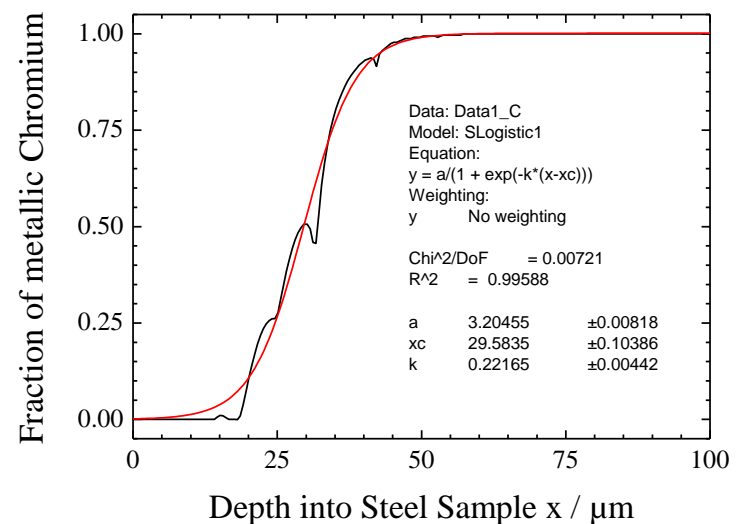
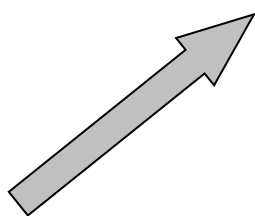
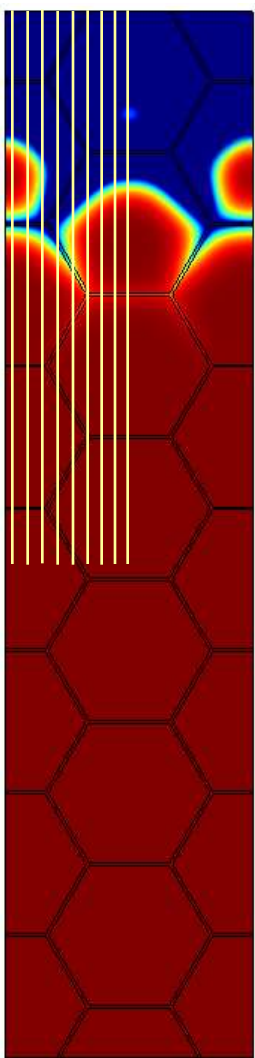
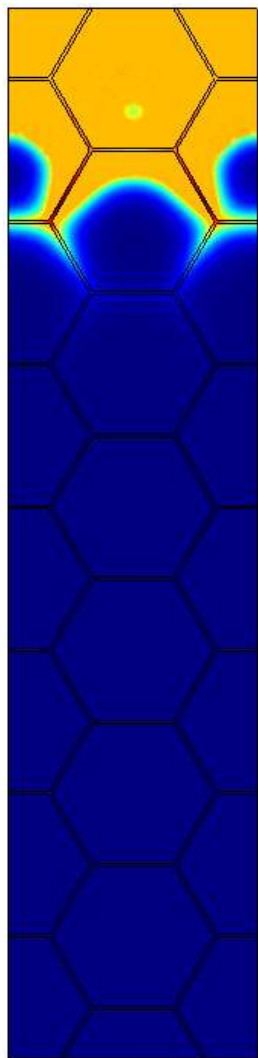


**Figure:** Numerical simulation of segregation (left) and 3D atom probe tomography of segregated boron atoms along the grain boundary in a NiAl superalloy [1] (right).

# Calculation of the Oxidation Depth



# Multikomponentensysteme

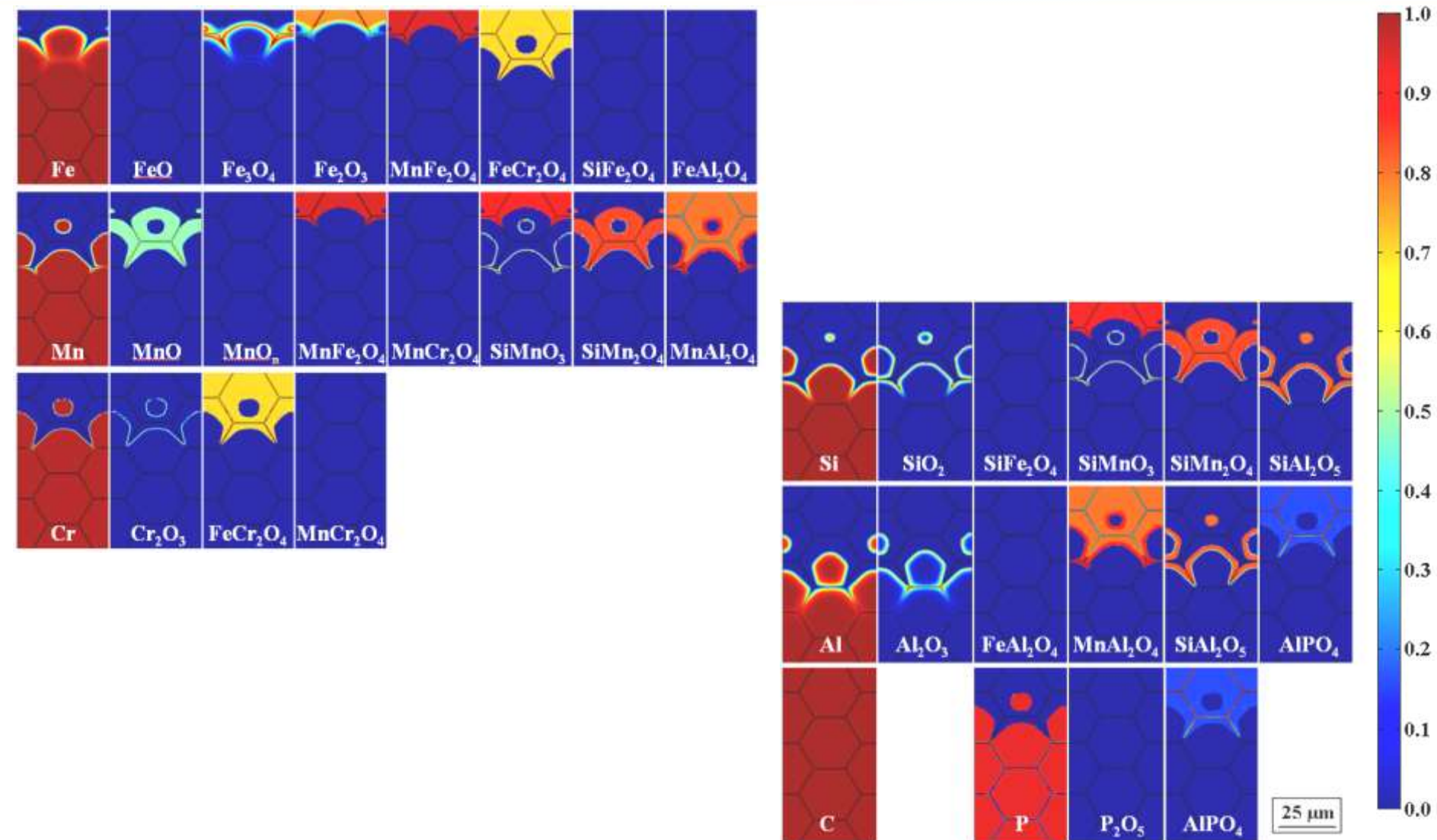
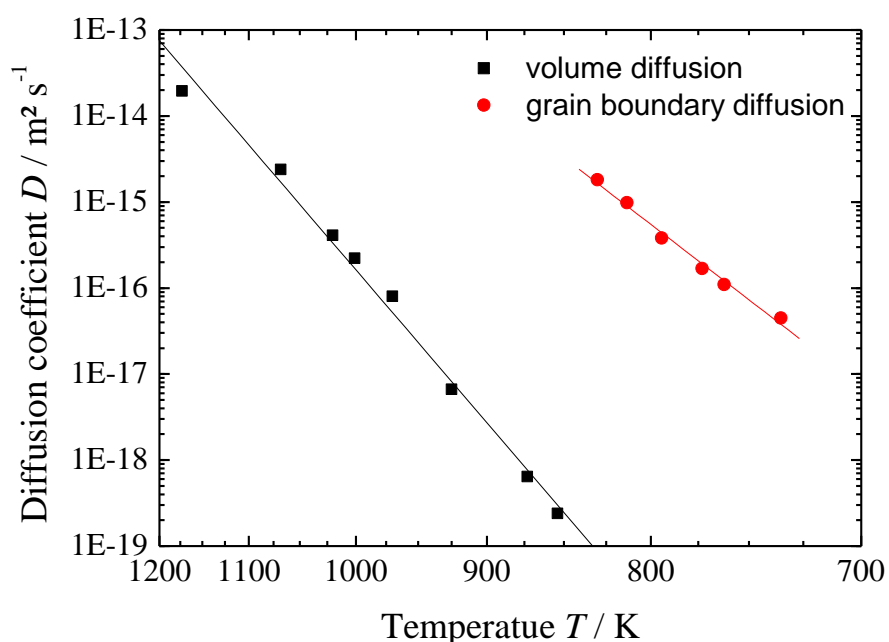


**Abbildung:** Phasenverteilung einer industrienahen Legierungszusammensetzung nach erfolgter Oxidation bei  $p(O_2) = 10^{-22}$  bar und einer technischen Abkühlkurve.

# Temperature Dependence

$$\frac{dc_{i(x,t)}}{dt} = \operatorname{div}\left(D_{i(x,T)} \cdot \nabla c_{i(x,t)}\right) + f_{(x,T,c_i(x,t))}$$

Diffusion equation



$$D_i(T) = D_i^o e^{-\frac{Q}{RT}}$$

**Figure:** Temperature dependence of phosphorous diffusion in iron.

# Thermodynamic Principles

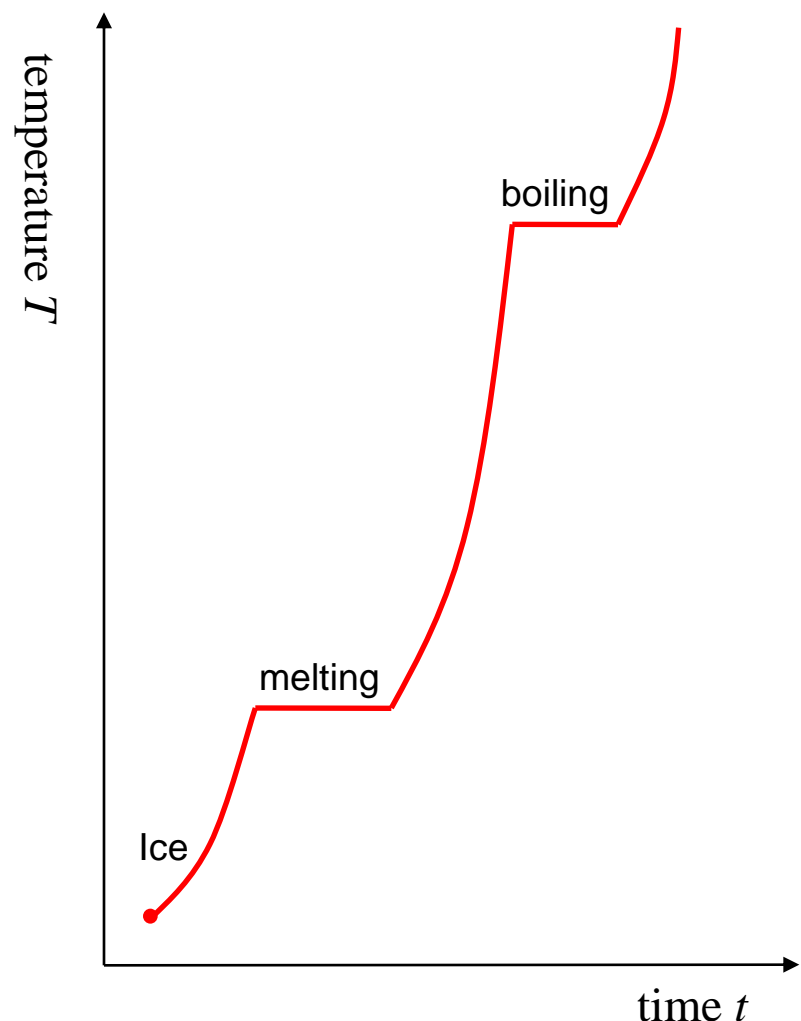
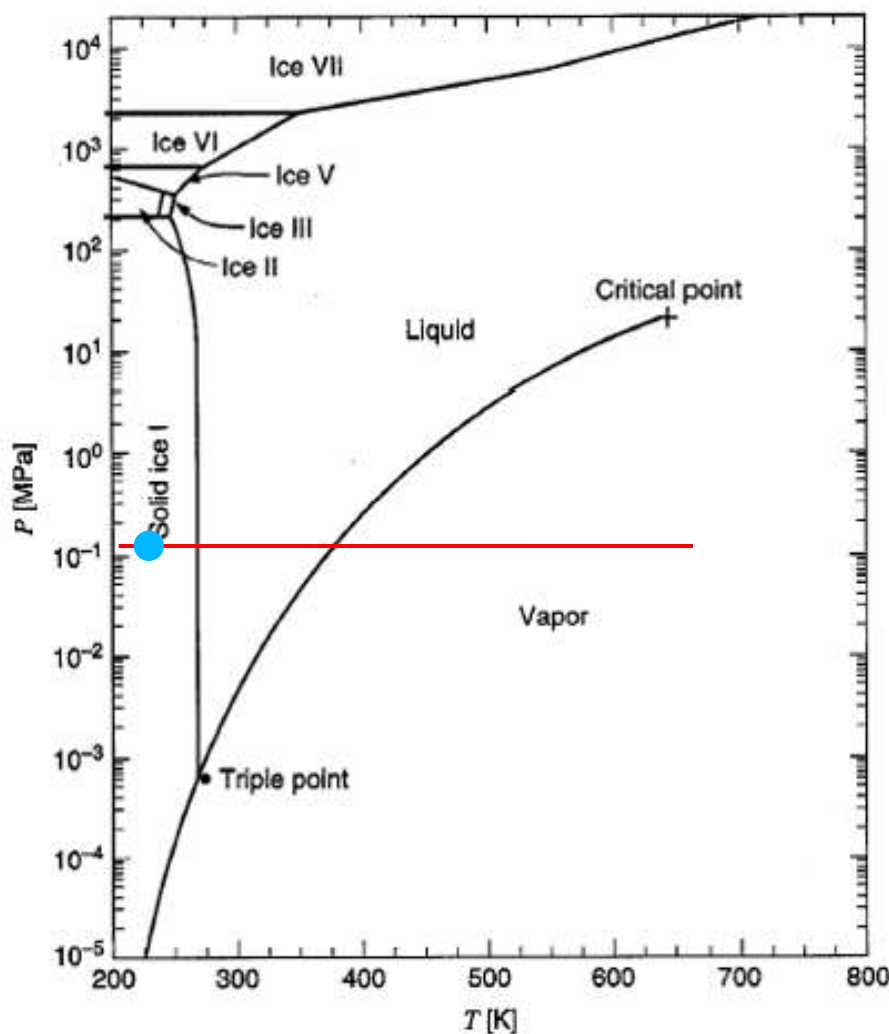
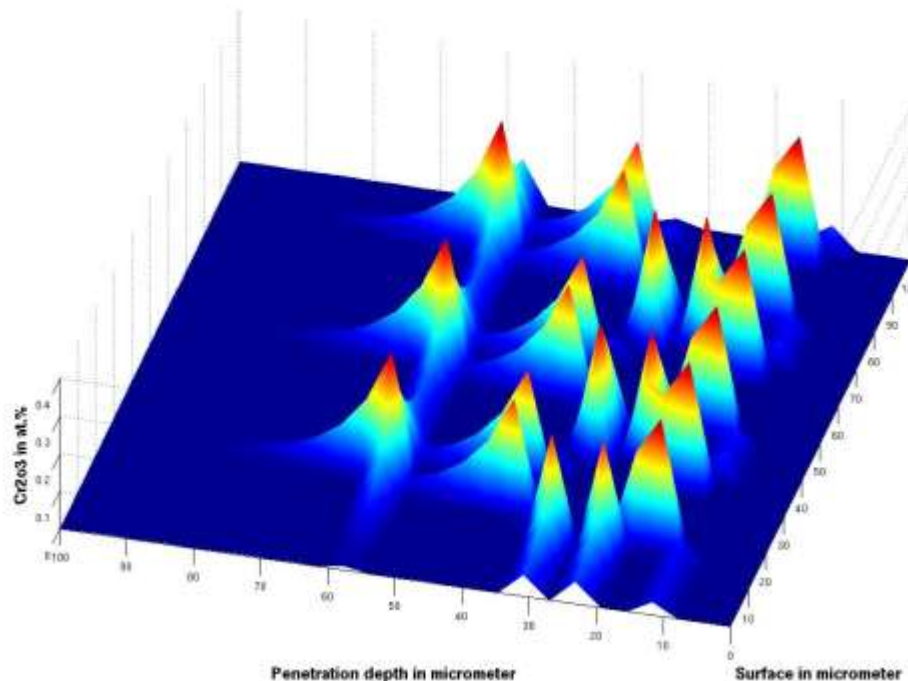
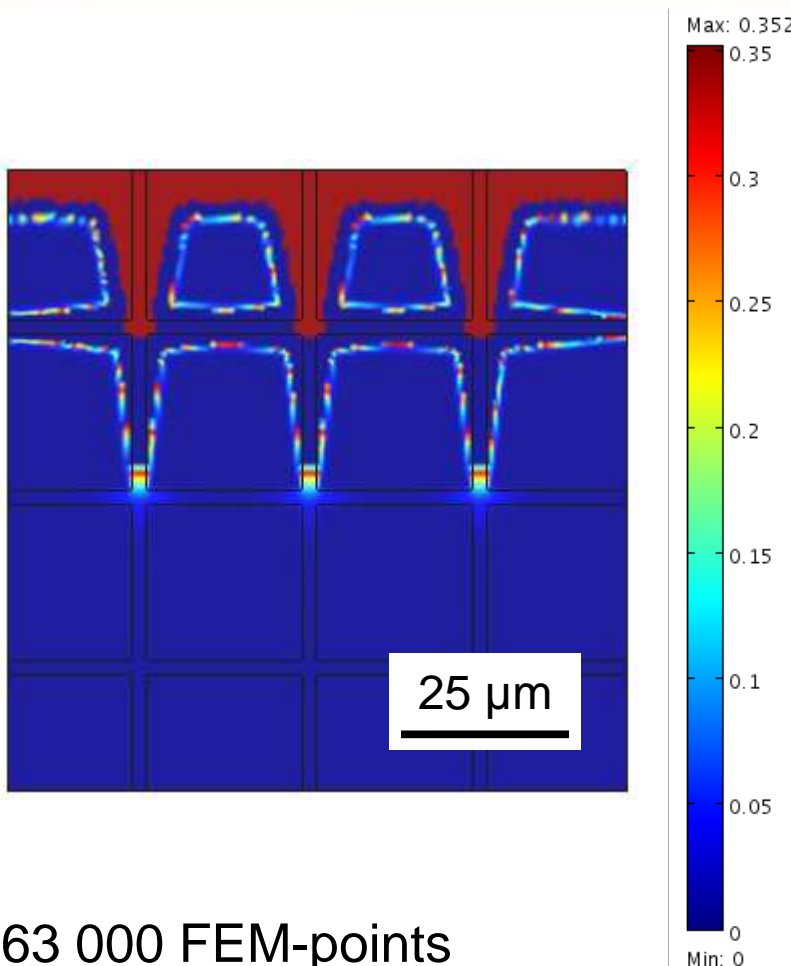


**Figure:** State diagram of water [2] (left) and schematic temperature evolution with constant heating (right).

# Efficiency of the Calculation



300 FEM-points  
Calculation time: 90 min



63 000 FEM-points  
Calculation time: 120 min

**Figure:** Distribution of  $\text{Cr}_2\text{O}_3$  in Fe, 0.67 wt-% Cr at 700 °C after 90 min. Simulation with InCorr (left) and with self-written programme (right).

# Berechnungsaufwand

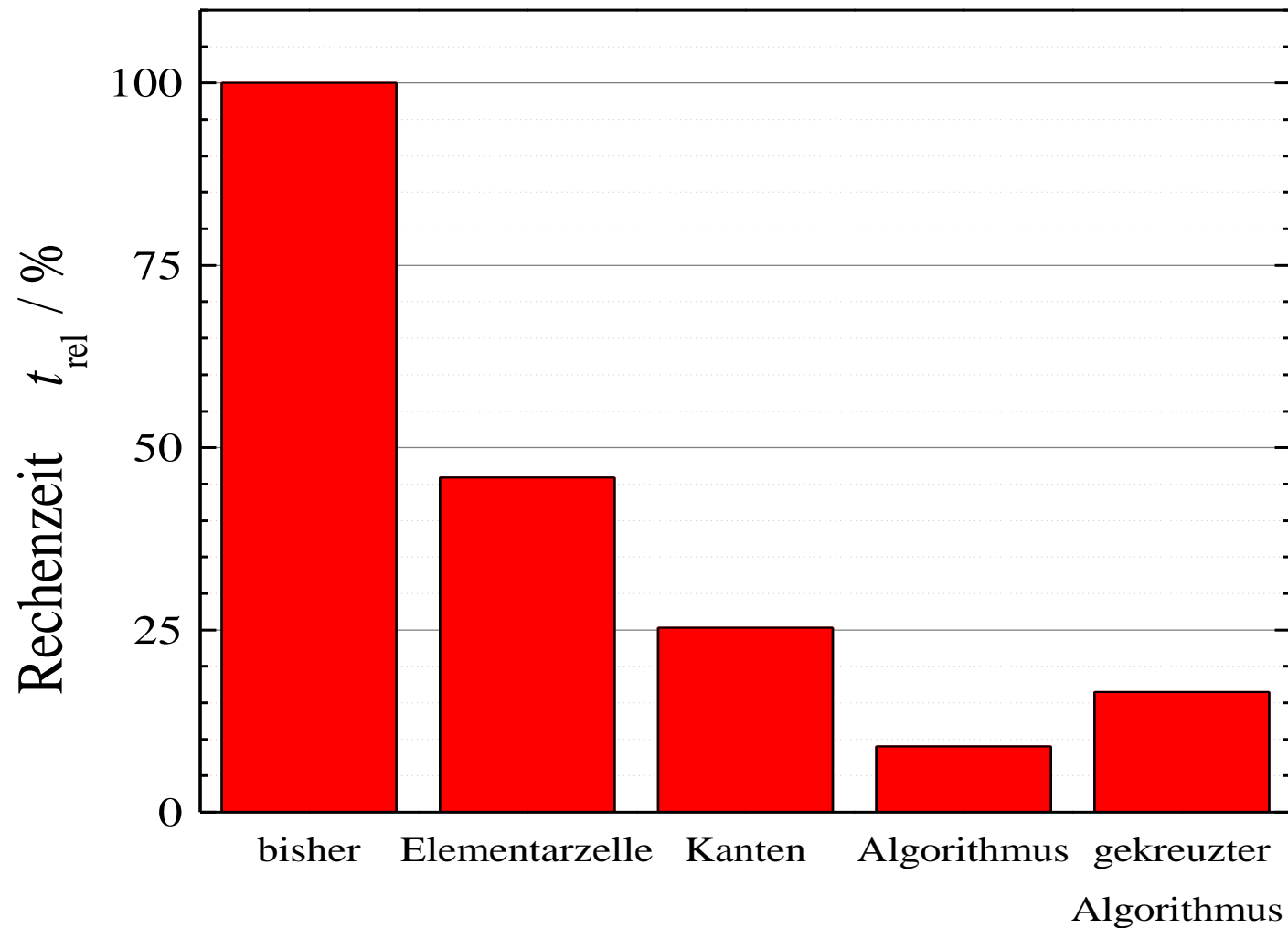


**Abbildung:** Abhangigkeit der Rechenzeit zur Simulation des Oxidationsverhaltens von Fe, 3 wt-% Cr bei verwendetem Kuhlprogramm ab 650 °C (B).

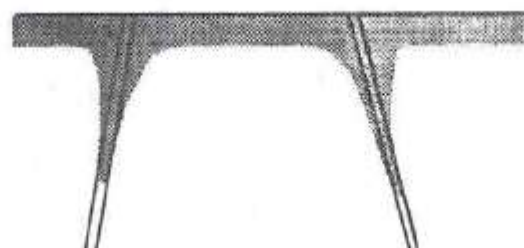
# Grain Boundary Diffusion Regimes



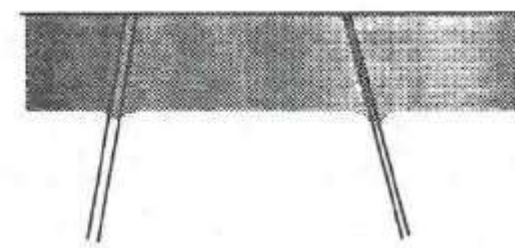
Coarse grained



C – regime

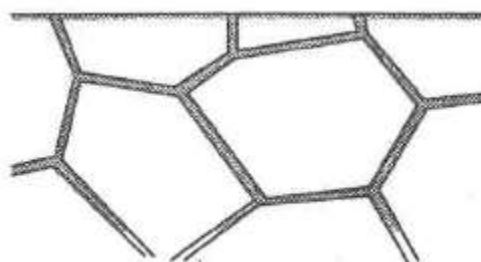


B – regime

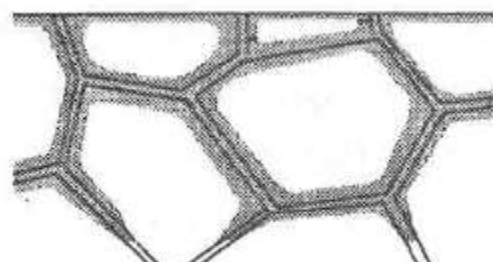


A – regime

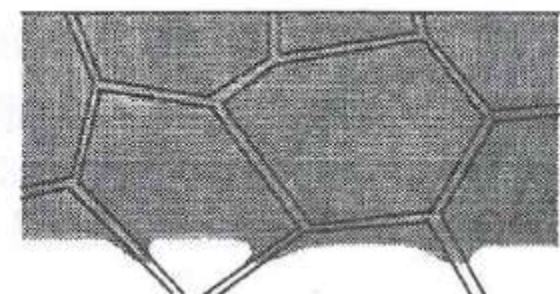
Fine grained



C' – regime



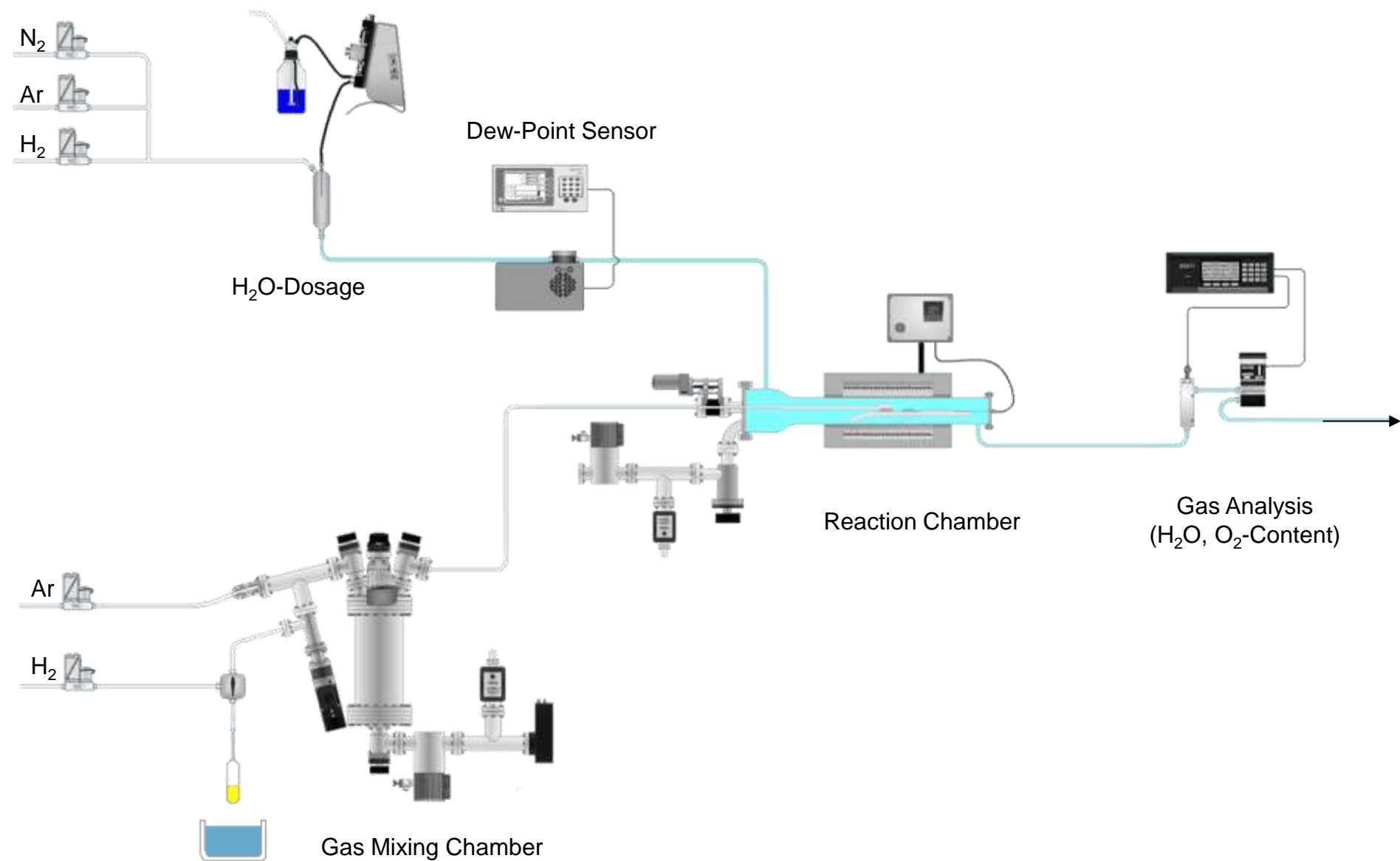
B' – regime



A' – regime

**Figure:** Illustration of different diffusion regimes, depending on total diffusion time and ratio of  $D_{GB}/D$ .

# Experimental Set-up





# Selective Decarburisation at 800 °C

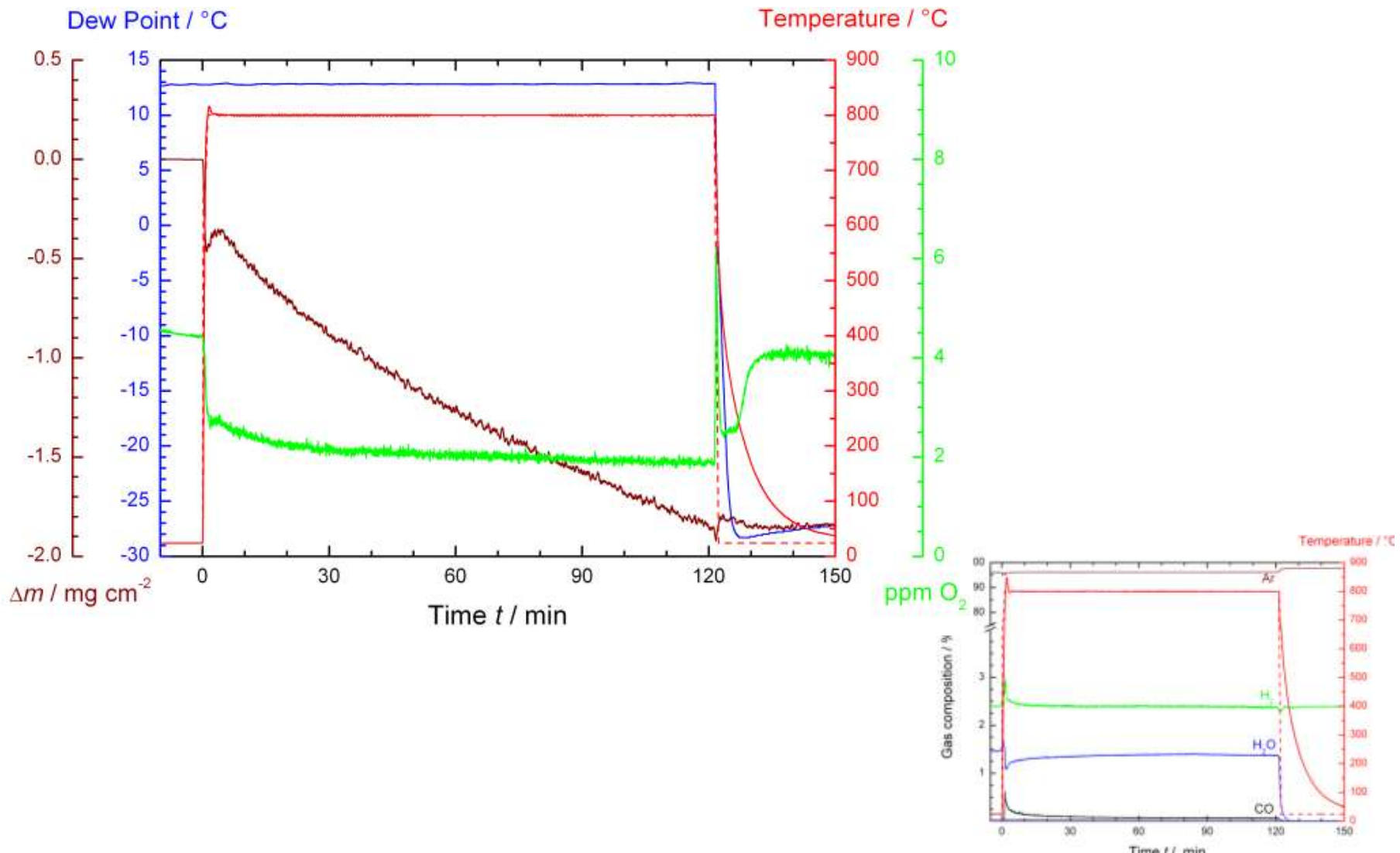


**Figure:** Experimental parameters during selective decarburisation of Fe, 0.8 wt-% C at 800°C in Ar / 2.5 vol-% H<sub>2</sub> / H<sub>2</sub>O.

# Selective Decarburisation at 800 °C

Fe, 0.8 wt-%C, 800 °C, Ar/2.5% H<sub>2</sub>, DP+13°C

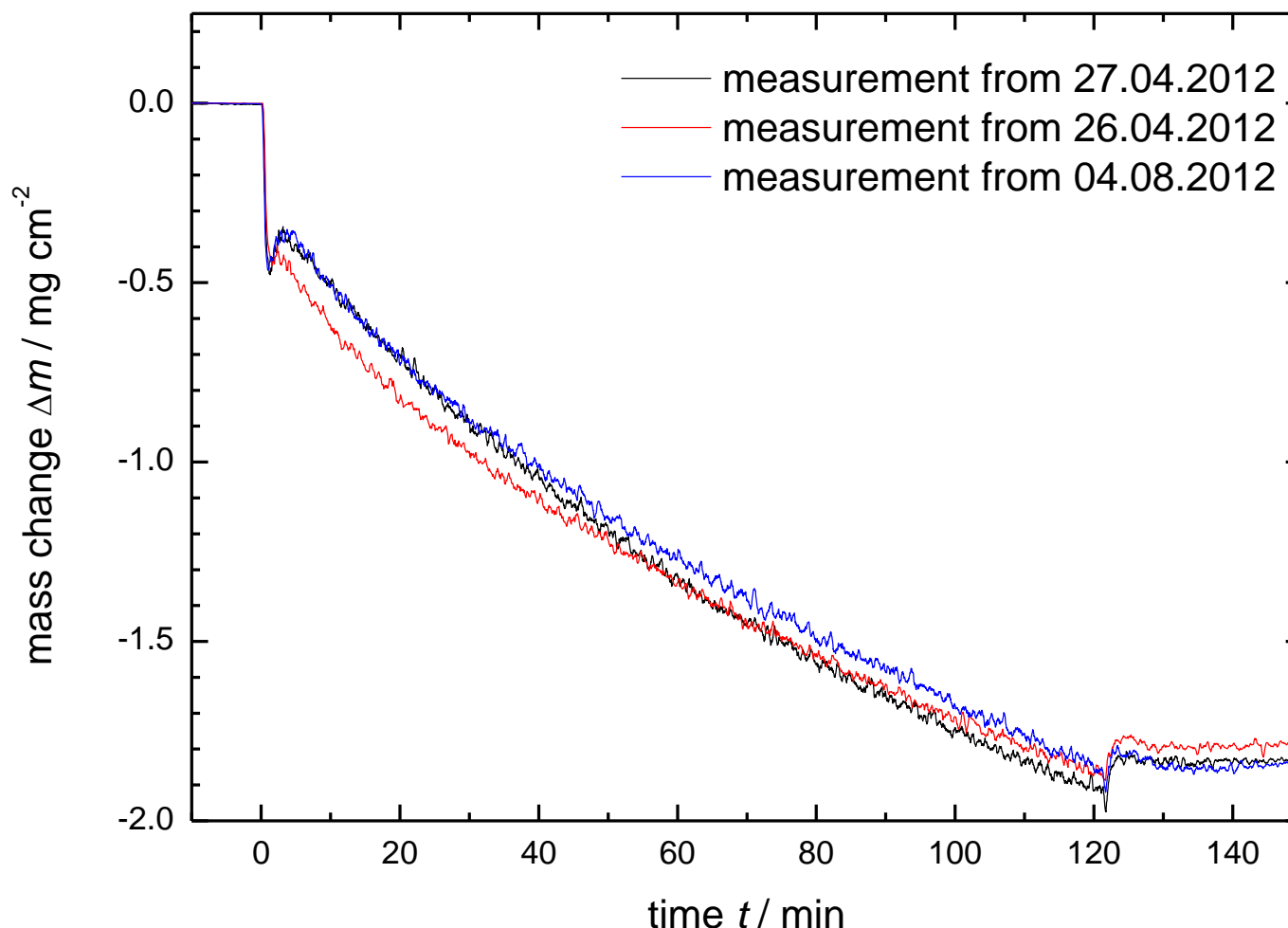


**Figure:** Mass change during selective decarburisation of Fe, 0.8 wt-% C at 800°C in Ar / 2.5 vol-% H<sub>2</sub> / H<sub>2</sub>O.

# Selective Decarburisation at 800 °C

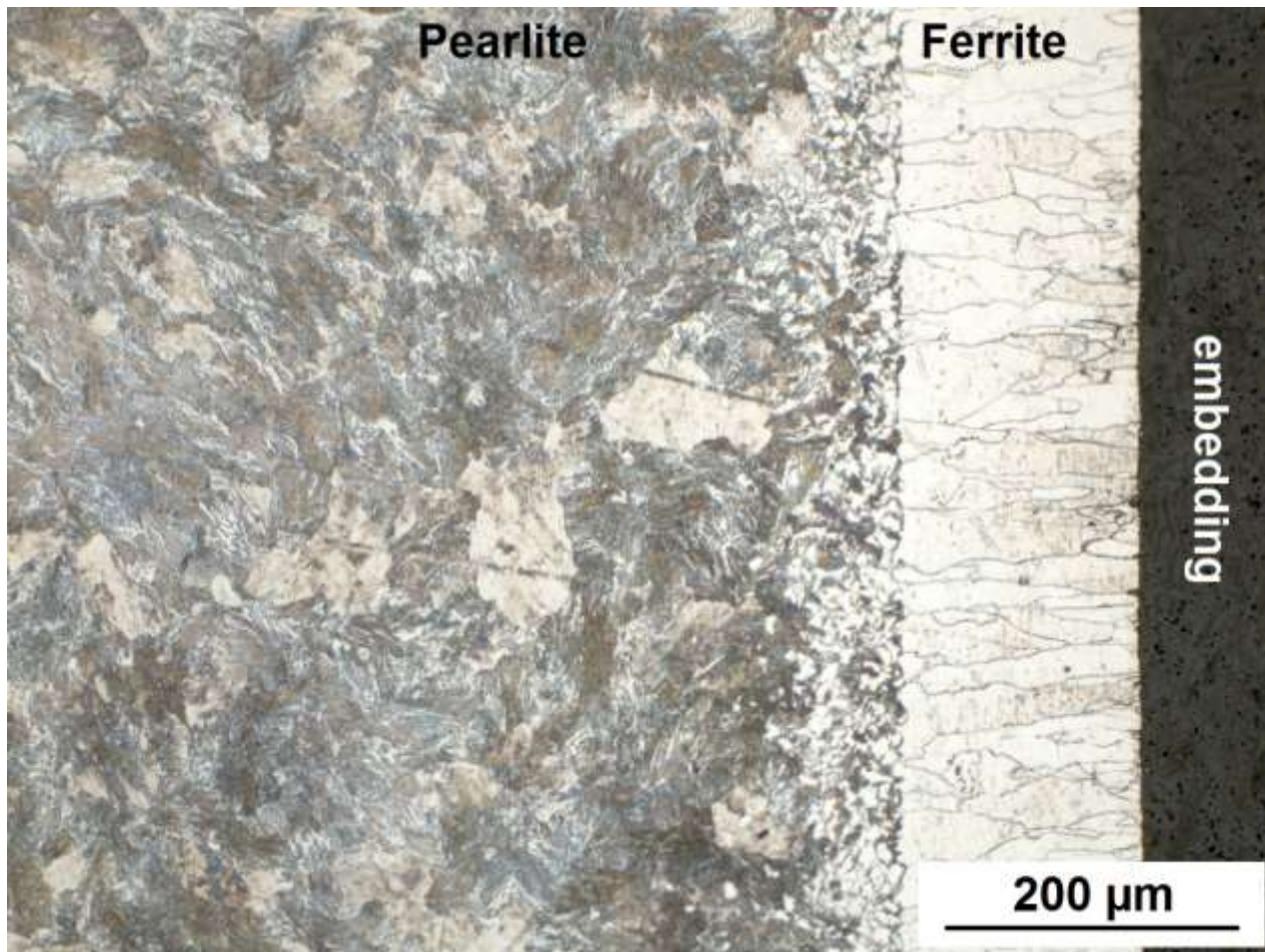


**Figure:** Cross section of Fe, 0.8 wt-% C after oxidation at 800 °C in Ar / 2.5 % H<sub>2</sub> / H<sub>2</sub>O for 60 min. The cross section was etched with 1 % HNO<sub>3</sub> / Ethanol for 15 s.

# Selective Decarburisation at 800 °C

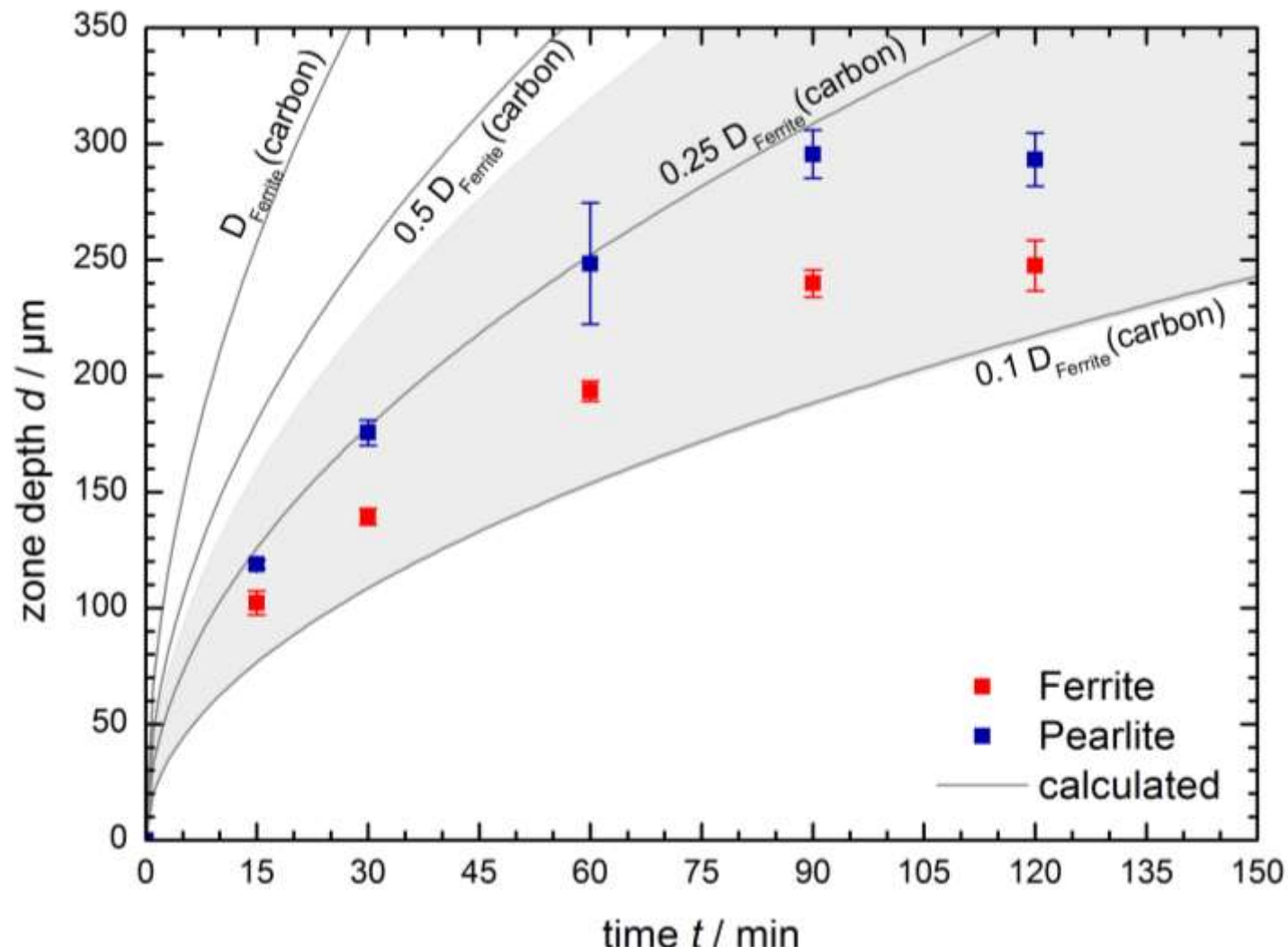


**Figure:** Evolution of the decarburised zone depth in Fe, 0.8 wt-% C after oxidation at 800 °C in Ar / 2.5 % H<sub>2</sub> / H<sub>2</sub>O. The solid lines represent theoretical results.

# Selective Decarburisation at 800 °C

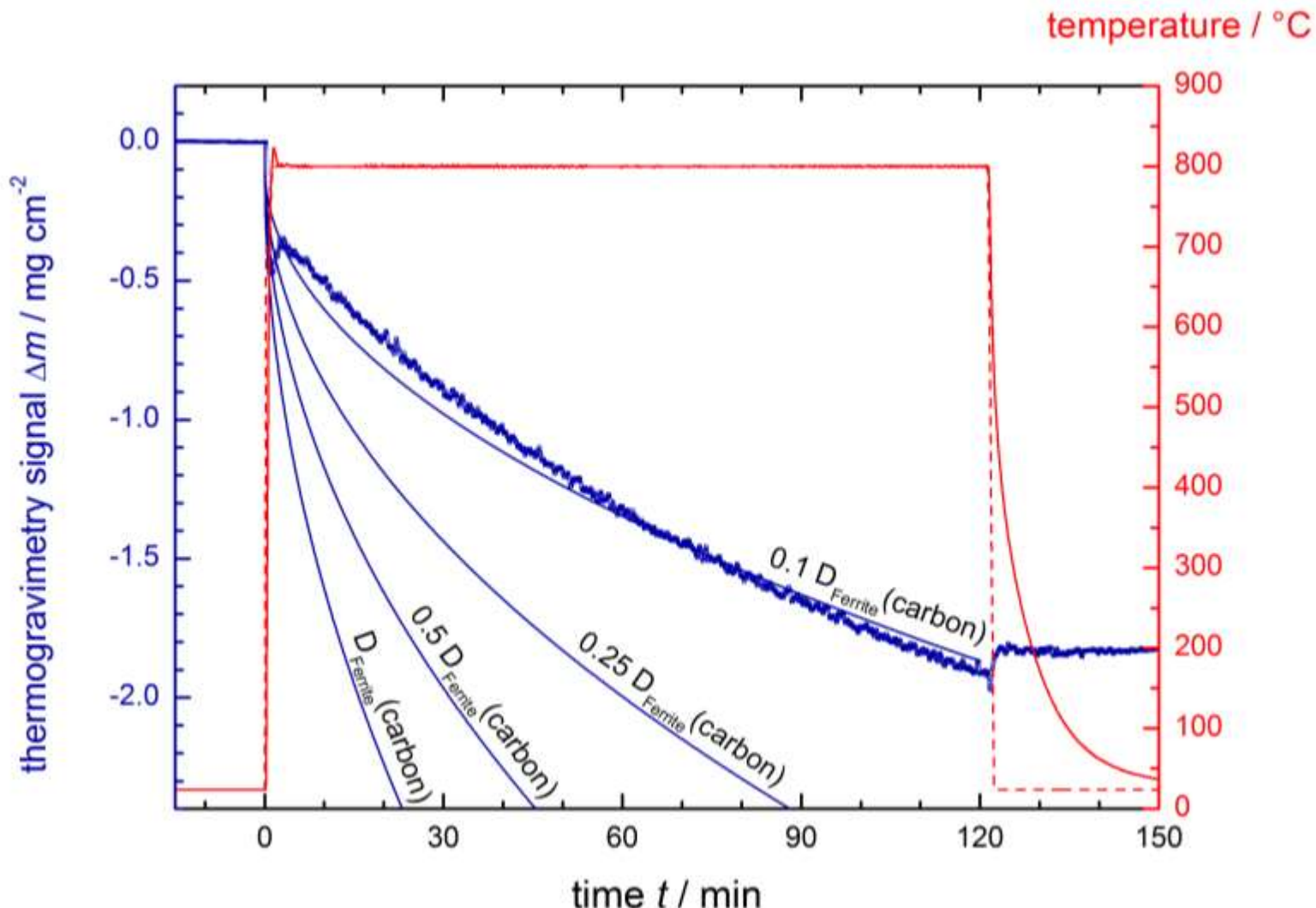
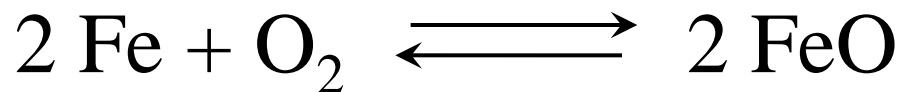


**Figure:** Evolution of the mass change in Fe, 0.8 wt-% C during oxidation at 800 °C in Ar / 2.5 % H<sub>2</sub> / H<sub>2</sub>O. The solid lines represent the theoretical results.



$$\Delta G_{(T)}^{\text{Formation}} \approx 2 \mu_{(T)}^{\text{FeO}} - 2 \mu_{(T)}^{\text{Fe}} - \mu_{(T)}^{\text{O}_2} = 0$$

$$0 = 2 G_{(T)}^{o, \text{FeO}} + 2 RT \ln(a_{\text{FeO}}) - 2 G_{(T)}^{o, \text{Fe}} - 2 RT \ln(a_{\text{Fe}}) - G_{(T)}^{o, \text{O}_2} - RT \ln\left(\frac{p_{\text{O}_2}}{p_o}\right)$$

$$\Delta G_{(T)}^{o, \text{Formation}} = 2 G_{(T)}^{o, \text{FeO}} - 2 G_{(T)}^{o, \text{Fe}} - G_{(T)}^{o, \text{O}_2} = -RT \ln\left(\frac{p_{\text{O}_2}}{p_o}\right) + 2(RT \ln(a_{\text{FeO}}) - RT \ln(a_{\text{Fe}}))$$

$$2 G_{(T)}^{o, \text{FeO}} - 2 G_{(T)}^{o, \text{Fe}} - G_{(T)}^{o, \text{O}_2} = -R \ln\left(\frac{p_{\text{O}_2}}{p_o}\right) T + 0$$

\_\_\_\_\_ \_\_\_\_\_  
 y d

# Properties of Nitrogen

## Nitride Stability

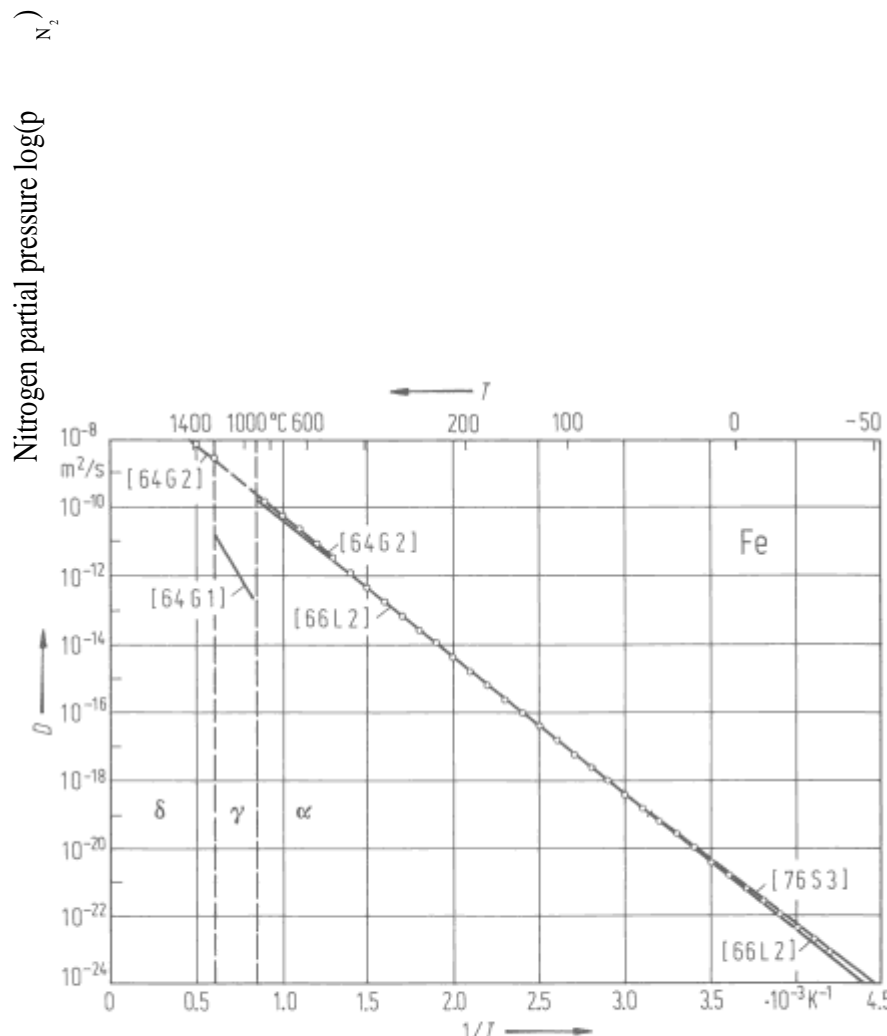
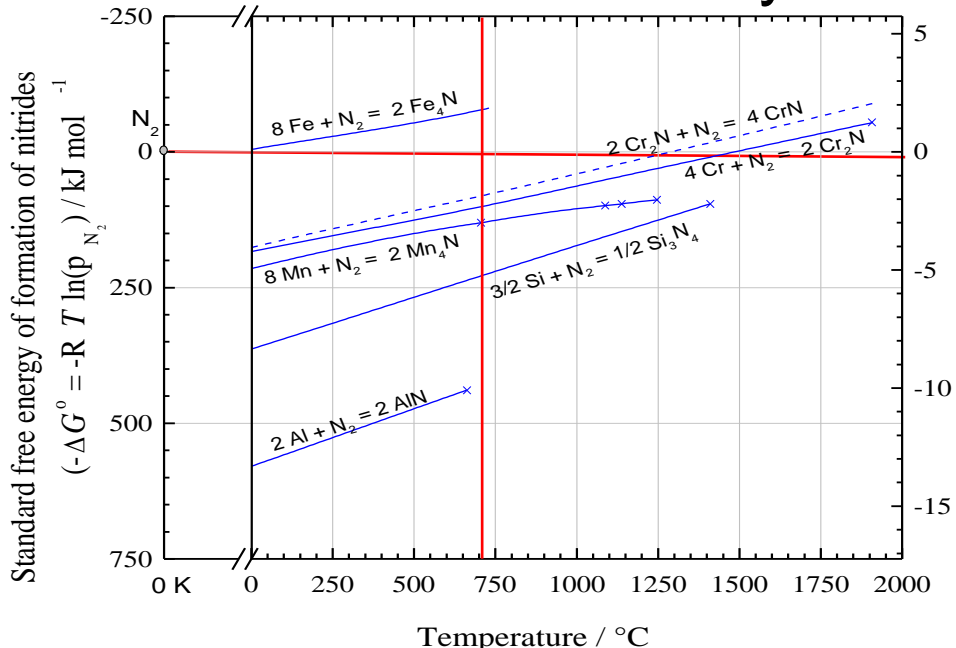
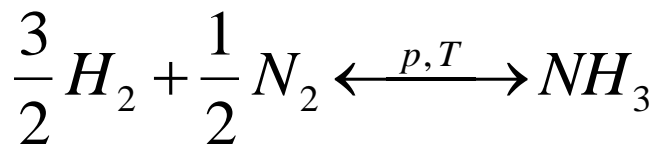


Fig. 22. Fe. Diffusion coefficient for N diffusion in  $\alpha$ ,  $\gamma$  and  $\delta$ -phase Fe vs. (reciprocal) temperature. Circles: calculated from equation quoted from [76S3].

# Theoretical Principles



$$G_{(T)}^{NH_3} - \frac{3}{2}G_{(T)}^{H_2} - \frac{1}{2}G_{(T)}^{N_2} \stackrel{!}{=} 0$$

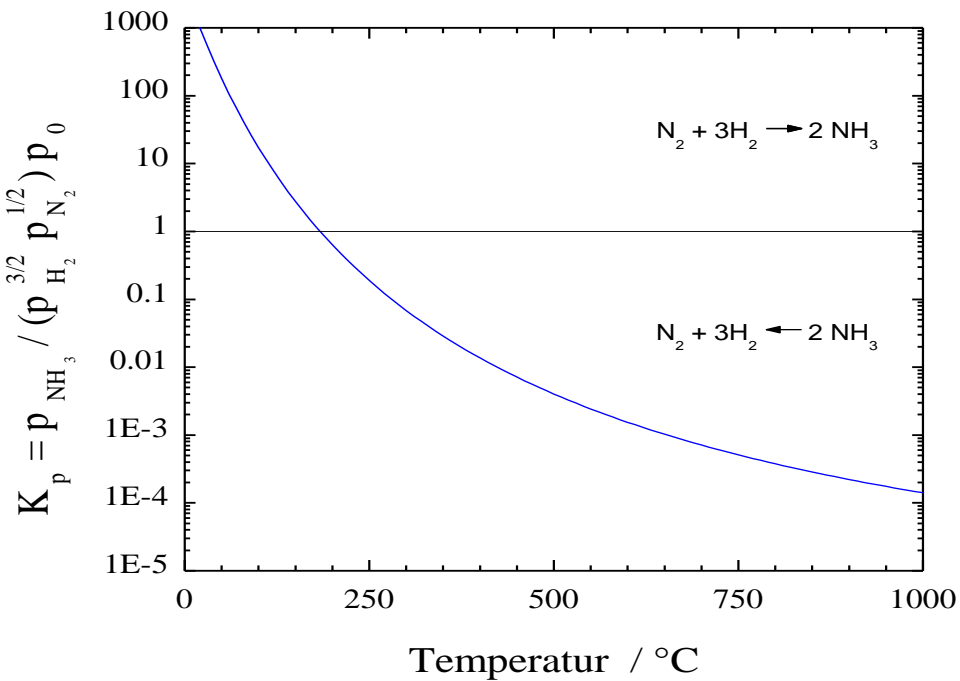
$$K_{p(T)} = e^{\frac{G_{NH_3,(T)}^o - \frac{3}{2}G_{H_2,(T)}^o - \frac{1}{2}G_{N_2,(T)}^o}{RT}}$$

$$K_{p(T)} = \frac{p_{NH_3}}{p_{H_2}^{1.5} p_{N_2}^{0.5}} p_0$$

$$K_N \stackrel{!}{=} \frac{p_{NH_3}}{p_{H_2}^{1.5}} \sqrt{p_0}$$

$$K_N = \sqrt{p_{N_2}} \frac{K_{p(T)}}{\sqrt{p_0}}$$


---



# Theoretical Principles

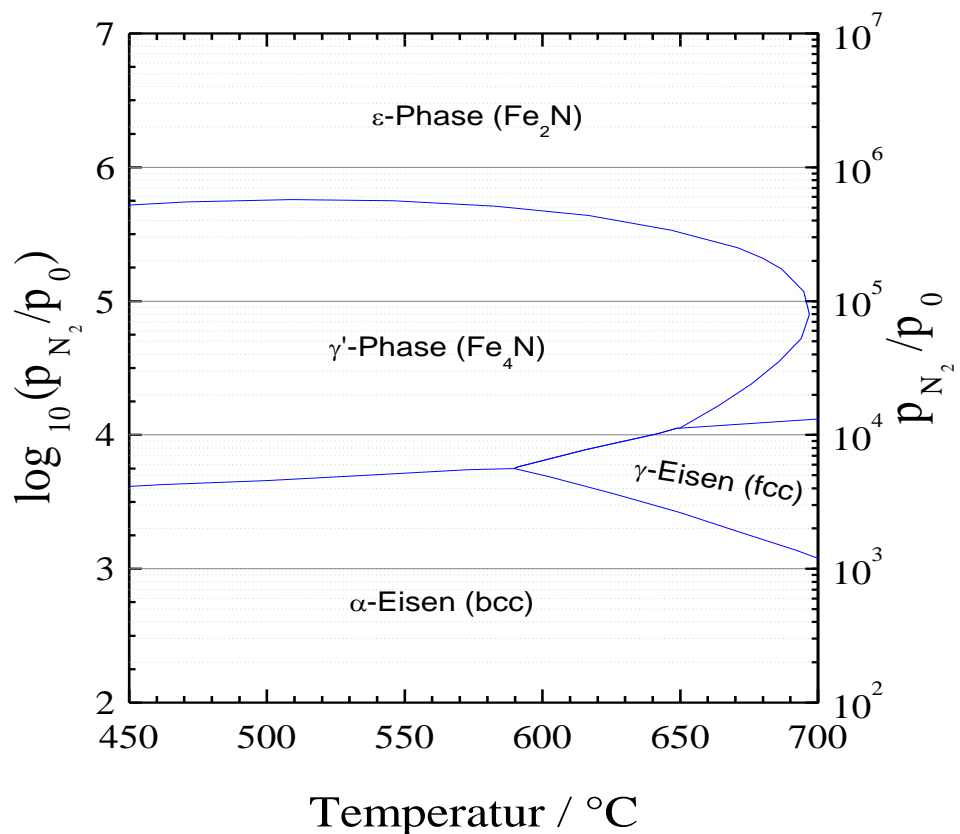
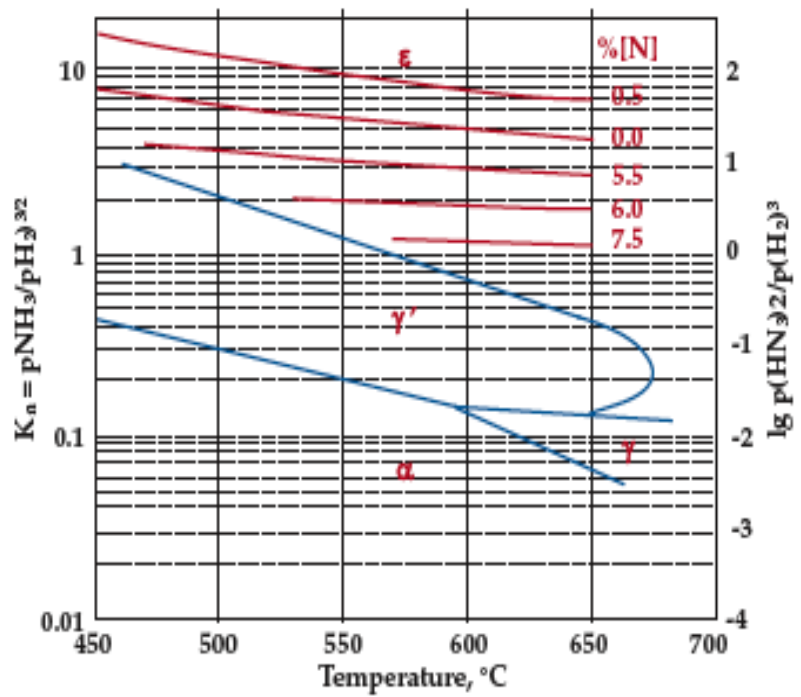


**Figure:** Lehrer-Diagramm of iron nitrides according to literature (left) and stability diagram calculated with the programme FactSage (right).